Unlocking keystone structures: Opening the door to new uses of airborne and handheld lidar for remote characterization of standing dead trees and nest cavities in closed-canopy conifer forests

A Dissertation
Presented in Partial Fulfillment of the Requirements for the
Degree of Doctor of Philosophy
with a
Major in Natural Resources
in the
College of Graduate Studies
University of Idaho
by
Jessica M. Stitt

Major Professor: Kerri T. Vierling, Ph.D.
Committee Members: Andrew T. Hudak, Ph.D.; Tracey N. Johnson, Ph.D.;
Lee A. Vierling, Ph.D.
Department Administrator: Kerri T. Vierling, Ph.D.

May 2022

Abstract

In closed-canopy conifer forests, standing dead trees (known as snags) serve as keystone structures, supporting disproportionate amounts of biodiversity. Their reduced woody structure, as well as their decaying wood, make snags different enough from live trees to provide unique habitat features for wildlife. One such feature of snags in northwestern conifer forests is that they are the preferred sites for woodpeckers to excavate nest cavities, which are also considered keystone structures in this system. Woodpecker cavities are essential to multiple species of birds and mammals for nesting and roosting–and this habitat feature makes locating snags all the more valuable. Using remote sensing to map where snags occur across the landscape is of great benefit in multiple ecological contexts but is made difficult due the sparse, cryptic, and variable nature of standing deadwood throughout a forest.

This dissertation tests novel methodologies to evaluate whether one type of remote sensing, light detection and ranging (known as lidar), applied at different spatial scales is sensitive enough to discern structural characteristics pertaining to: (1) tree cavity entrance dimensions; (2) snags versus live trees; and (3) variation among snags. I evaluated lidar at the individual tree scale for (1) to determine the accuracy of smartphone lidar in measuring cavity entrance dimensions under controlled conditions. I evaluated lidar at the landscape scale for (2) and (3) to explore the capabilities of airborne lidar for snag detection and characterization in conifer stands of the Idaho Panhandle National Forest.

I found that smartphone lidar (1) was very accurate in measuring at least one dimension of cavity entrance size, enabling discernment among species of cavity excavators. I found airborne lidar to be (2) effective at distinguishing between snags and live trees at the individual tree level using the proportion of open space surrounding each, but (3) airborne lidar was not high enough resolution to reliably characterize multiple snag classes.

Acknowledgements

This body of work would never have been possible without the tremendous support of my mentors and peers at the University of Idaho and beyond. I would especially like to thank my major advisor, Kerri Vierling, for her tireless assistance and enthusiastic encouragement from the beginning. I would also like to thank each of my committee members for their invaluable input, mentorship, and guidance throughout the years: Andy Hudak, Tracey Johnson, and Lee Vierling. My lab mates have been fantastic and invaluable assets, improving the quality of my thinking and presenting with their feedback and friendship. The faculty, staff, and my fellow graduate students in the College of Natural Resources and the Department of Fish and Wildlife Sciences have been remarkable sources of help and guidance throughout my time in the doctoral program. The compassionate support provided by the staff of the College of Graduate Studies and the U of I Library was instrumental for countless steps along the way.

I want to thank my coauthors for their contributions and insights for each manuscript found within this dissertation; in addition to my committee, I thank Leona Svancara for Chapter 2, and Carlos Silva for Chapters 3 and 4. I would also like to thank the anonymous reviewers who provided input to strengthen each manuscript found within this dissertation. Further I want to acknowledge those who helped me on projects that did not make it into this dissertation but still contributed greatly to my skills of analysis and sophistication of thinking during my doctoral program, including Teresa Lorenz, Phil Fischer, and Michelle Jusino.

I wish to thank the USFS RMRS for providing the ALS data of the Idaho Panhandle National Forests, as well as mentorship and assistance from Ben Bright, Patrick Fekety, John Byrne, and Andy Hudak – both in the field and with their help in lidar data analysis. I also appreciate the time and effort given by the University of Idaho Logger Sports Club in assisting with my experimental setup for Chapter 2, climbing the logger pole and belaying. This dissertation was funded in part by the NSF Idaho EPSCoR Program, the NASA Idaho Space Grant Consortium, and by a NASA Carbon Monitoring Systems (CMS) Program Award (NNH15AZ06I).

Table of Contents

List of Tables

List of Figures

Chapter 1: Introduction

Biodiversity indicators are ecosystem components that serve as useful proxies for monitoring a community across many taxonomic levels, and likely reduce the time or effort needed to evaluate the community. The ability to use biodiversity indicators that are measurable via remote sensing techniques can enable wildlife and biodiversity assessment across broad spatial scales (Michel and Winter, 2009; Paillet et al., 2017; Asbeck et al., 2020). One type of remote sensing that is useful in assessing biodiversity indicators is light detection and ranging (known as lidar), as lidar has applications for wildlife modeling at multiple scales (Vierling et al., 2008; Martinuzzi et al., 2009; Vogeler et al., 2013; Casas et al., 2016; Vogeler and Cohen, 2016). This dissertation focuses on exploring new ways lidar data can be incorporated in assessing biodiversity indicators within forested systems.

One valuable indicator of biodiversity in forested systems is standing dead trees. When a tree dies in the forest, sometimes it falls right away and other times it will remain standing long after death. Standing dead trees are known as snags, and they are important structural elements in forest ecosystems (Thomas et al., 1979; Bull et al., 1997). Snags are keystone structures for wildlife, meaning they play a disproportionately large role in community composition and dynamics (Tews et al., 2004). Though they comprise a relatively small portion of the biomass, snags serve valuable and unique roles in closed-canopy conifer forests of northwestern North America (Miller and Miller, 1980; Michel and Winter, 2009; Larrieu et al., 2018). One key feature of snags is that they are distinct from live trees in several ways: exposing open spaces, supporting unique functions and niches for wildlife that live trees cannot, and providing deadwood for decomposition and use by fungi and animals. In particular, this deadwood is used by woodpeckers to excavate cavities for nesting and roosting (Thomas et al., 1979; Davis, 1983; Martin and Eadie, 1999).

The tree cavities created by woodpeckers serve outsized roles within closed-canopy conifer forest communities as keystone structures in their own right (Bull et al., 1997; Martin and Eadie, 1999; Blanc and Walters, 2008). Having access to a sizeable hole high above the ground which is relatively hard to reach is something desirable for many species of wildlife beyond woodpeckers. Cavities can be safer for nesting, protecting eggs and young from

predators and providing more stable microclimates, with the inside buffered from temperature swings (Wiebe, 2001; Vierling et al., 2018). Cavities can also provide shelter during rain or snowstorms (Wiebe, 2001; Vierling et al., 2018). Species that use cavities for nesting or roosting but cannot create them directly are known as secondary cavity users (Martin and Eadie, 1999; Martin et al., 2004). The number of cavities available for secondary cavity users is limited by cavity excavator densities and the number of trees available to excavate.

Taken together, all of the snags available to excavate, all of the cavity excavators, and all of the secondary cavity users found within a closed-canopy conifer forest are linked through a diverse network of connections known as a cavity nest web (Martin and Eadie, 1999). The cavity nest web can be viewed hierarchically, with three levels dependent on the ones below: secondary cavity users comprise the top level stacked upon cavity excavators which are stacked upon the snags that form the foundation of the cavity nest web. Each level of the nest web contains multiple species, and each species has different relationships and interaction strengths with the species in the other levels (Martin and Eadie, 1999; Martin et al., 2004; Aitken and Martin, 2007; Manley and Tarbill, 2012).

Cavity nest webs can become complicated quickly, with increasing species diversity driving greater complexity and interactions at each level. Understanding these connections in cavity nest webs takes a great amount of effort and time in the field spent locating cavities and observing occupancy by woodpeckers and secondary cavity users across multiple years (Martin et al., 2004; Aitken and Martin, 2007; Manley and Tarbill, 2012). One way to tease apart these complex relationships among cavities and wildlife species is to look more closely at cavity entrance sizes.

Cavity nest webs can be approached with a focus on the body size of each animal involved and its relationship with cavity entrance size. When a woodpecker excavates a cavity, it will only make it as big as needed, in terms of both cavity entrance dimensions and interior volume (Wiebe, 2001; Martin et al., 2004; Gentry and Vierling, 2008; Bunnell, 2013). When secondary cavity users are looking for a suitable cavity, many may take the Goldilocks approach with regard to entrance size: too small and they cannot access the

cavity; too big and it may take excessive energy to stay warm inside (Pyle, 1918; Martin et al., 2004). Cavity entrance size also limits which predators can access a nest, so finding a fit closest to a cavity user's body size is beneficial (Martin et al., 2004; Vierling et al., 2018).

Multiple species of cavity excavators can coexist in the same space; within the closed-canopy conifer forests of northern Idaho four woodpecker species (all within order Piciformes) coexist on the landscape and excavate cavities in snags. The four differ in body size and thus excavate cavities of differing sizes. This diversity of cavity sizes increases accessibility for secondary cavity users with access determined by body size. Many secondary cavity users are obligate cavity nesters, meaning they need cavities to breed (Martin and Eadie, 1999). Should there not be any suitable cavities available in an area for a given species, that secondary cavity user may not be able to inhabit the space and thus will not be present on the landscape.

Having a diversity of sizes in keystone structures is important for biodiversity and thus important to quantify. Being able to measure the cavity entrance size dimensions found in an area could tell about the presence or absence of woodpecker species on the landscape, as well as the potential habitat suitability for secondary cavity users, stratified by body size. However, remote measurement of tree cavities can be tricky, as direct measurement is frequently dangerous and difficult due to the location of cavities often high above the ground in snags. Snags are inherently unstable structures, which makes directly accessing cavities located more than few meters above the ground very challenging. Developing an approach to remotely measure cavity entrance dimensions would need to be safe, rapid, and accurate.

While measuring tree cavities in the field is useful for mapping cavity nest webs, it is equally important to locate where the snags are that these cavities can be built in. Unlike cavities, snags have the potential to be detected remotely from far above. Knowing how snags are distributed across the landscape can inform where woodpeckers will occur and where cavities can be created, thus also informing where cavity-dependent species occur. Having reliable maps of snags across a landscape could lead to better spatial representations of the potential footprint for cavity nest webs in conifer forests of the northwest.

However, mapping snags within closed-canopy conifer forests via remote sensing is challenging, as snags are difficult to detect both spatially and temporally (Falkowski et al., 2009; Wing et al., 2015). Therefore, the value of snags as biodiversity indicators cannot be fully realized until snags can be better characterized across broad spatial scales. Some challenges in characterizing snags remotely include their sparse and sporadic distributions across the landscape, their lack of data stemming from their lesser structure, and the highly variable set of shapes included within the "snag" category.

This dissertation focuses on challenges in using lidar tools to better map keystone structures, specifically by paying attention to their diversity of sizes, spaces, and shapes. First, a diversity of cavity sizes supports greater biodiversity so I will look at ways to measure tree cavities from the ground using handheld lidar (Chapter 2). Next, I will look at how a diversity of spaces within the forest canopy benefits wildlife and can benefit snag mapping efforts via airborne lidar (Chapter 3). Then I will look at how a diversity of shapes among snags matters to wildlife and may hold untapped potential for modeling (Chapter 4). Finally, I will wrap things up by explaining how these novel approaches can be applied at broader scales for a variety of disciplines and suggest future applications (Chapter 5).

Literature Cited

Aitken, K. E. H., & Martin, K. (2007). The importance of excavators in hole-nesting communities: availability and use of natural tree holes in old mixed forests of western Canada. *Journal of Ornithology, 148(S2)*, 425–434. https://doi.org/10.1007/s10336-007-0166-9

Asbeck, T., Basile, M., Stitt, J., Bauhus, J., Storch, I., & Vierling, K. T. (2020). Tree-related microhabitats are similar in mountain forests of Europe and North America and their occurrence may be explained by tree functional groups. *Trees, 34*(6), 1453–1466. https://doi.org/10.1007/s00468-020-02017-3

Blanc, L. A., & Walters, J. R. (2008). Cavity excavation and enlargement as mechanisms for indirect interactions in an avian community. *Ecology, 89(2)*, 506–514. https://doi.org/10.1890/07-0219.1

Bull, E. L., Parks, C. G., & Torgersen, T. R. (1997). *Trees and logs important to wildlife in the Interior Columbia River Basin* (PNW-GTR-391). U.S. Department of Agriculture, Forest Service, Pacific Northwest Research Station. https://doi.org/10.2737/PNW-GTR-391

Bunnell, F. L. (2013). Sustaining cavity-using species: patterns of cavity use and implications to forest management. *International Scholarly Research Notices*. https://doi.org/10.1155/2013/457698

Casas, Á., García, M., Siegel, R. B., Koltunov, A., Ramírez, C., & Ustin, S. (2016). Burned forest characterization at single-tree level with airborne laser scanning for assessing wildlife habitat. *Remote Sensing of Environment, 175*, 231–241. https://doi.org/10.1016/j.rse.2015.12.044

Davis, J. W. (1983). *Snags are for wildlife*. In Proceedings of the Symposium on Snag Habitat Management. USDA Forest Service General Technical Report RM-99 4–9.

Falkowski, M. J., Evans, J. S., Martinuzzi, S., Gessler, P. E., & Hudak, A. T. (2009). Characterizing forest succession with lidar data: An evaluation for the Inland Northwest, USA. *Remote Sensing of Environment, 113*(5), 946–956. https://doi.org/10.1016/j.rse.2009.01.003

Gentry, D. J., & Vierling, K. T. (2008). Reuse of woodpecker cavities in the breeding and non-breeding seasons in old burn habitats in the Black Hills, South Dakota. *The American Midland Naturalist, 160*(2), 413–429. https://doi.org/10.1674/0003-0031(2008)160[413:ROWCIT]2.0.CO;2

Larrieu, L., Paillet, Y., Winter, S., Bütler, R., Kraus, D., Krumm, F., Lachat, T., Michel, A. K., Regnery, B., & Vandekerkhove, K. (2018). Tree related microhabitats in temperate and Mediterranean European forests: A hierarchical typology for inventory standardization. *Ecological Indicators, 84*, 194–207. https://doi.org/10.1016/j.ecolind.2017.08.051

Manley, P. N., & Tarbill, G. (2012). *Ecological succession in the Angora fire: The role of woodpeckers as keystone species*. Final Report to the South Nevada Public Lands Management Act.

Martin, K., Aitken, K. E. H., & Wiebe, K. L. (2004). Nest sites and nest webs for cavity-nesting communities in interior British Columbia, Canada: Nest characteristics and niche partitioning. *The Condor*. https://doi.org/10.1650/7482

Martin, K., & Eadie, J. M. (1999). Nest webs: A community-wide approach to the management and conservation of cavity-nesting forest birds. F*orest Ecology and Management, 115*(2), 243–257. https://doi.org/10.1016/S0378-1127(98)00403-4

Martinuzzi, S., Vierling, L. A., Gould, W. A., Gould, W. A., Gould, W. A., Falkowski, M. J., Evans, J. S., Hudak, A. T., & Vierling, K. T. (2009). Mapping snags and understory shrubs for a LiDAR-based assessment of wildlife habitat suitability. *Remote Sensing of Environment, 113*(12), 2533–2546. https://doi.org/10.1016/j.rse.2009.07.002

Michel, A. K., & Winter, S. (2009). Tree microhabitat structures as indicators of biodiversity in Douglas-fir forests of different stand ages and management histories in the Pacific Northwest, U.S.A. *Forest Ecology and Management, 257*(6), 1453–1464. https://doi.org/10.1016/j.foreco.2008.11.027

Miller, E., & Miller, D. R. (1980). *Snag use by birds*. Management for Non-Game Birds. Gen. Tech. Rep. INT-GTR-86. Ogden, UT: Intermountain Forest and Range Experiment Station, Forest Service, US Department of Agriculture, 337–356.

Paillet, Y., Archaux, F., Boulanger, V., Debaive, N., Fuhr, M., Gilg, O., Gosselin, F., & Guilbert, E. (2017). Snags and large trees drive higher tree microhabitat densities in strict forest reserves. *Forest Ecology and Management, 389*, 176–186. https://doi.org/10.1016/j.foreco.2016.12.014

Pyle, K. (1918). Goldilocks and the three bears. In *Mother's Nursery Tales* (pp. 207–213). Project Gutenberg: https://www.gutenberg.org/files/49001/49001-h/49001-h.htm#Page_207

Tews, J., Brose, U., Grimm, V., Tielbörger, K., Wichmann, M. C., Schwager, M., & Jeltsch, F. (2004). Animal species diversity driven by habitat heterogeneity/diversity: the importance of keystone structures: Animal species diversity driven by habitat heterogeneity. *Journal of Biogeography, 31*(1), 79–92. https://doi.org/10.1046/j.0305-0270.2003.00994.x

Thomas, J. W., Anderson, R. G., & Maser, C. (1979). Snags. In Wildlife habitats in managed forests: the Blue Mountains of Oregon and Washington. *Agricultural Handbook, 553*, 60-77.

Vierling, K. T., Lorenz, T. J., Cunningham, P., & Potterf, K. (2018). Thermal conditions within tree cavities in ponderosa pine (*Pinus ponderosa*) forests: potential implications for cavity users. *International Journal of Biometeorology, 62*(4), 553–564. https://doi.org/10.1007/s00484-017-1464-4

Vierling, K. T., Vierling, L. A., Gould, W. A., Martinuzzi, S., & Clawges, R. M. (2008). Lidar: shedding new light on habitat characterization and modeling. *Frontiers in Ecology and the Environment, 6*(2), 90–98. https://doi.org/10.1890/070001

Vogeler, J. C., & Cohen, W. B. (2016). A review of the role of active remote sensing and data fusion for characterizing forest in wildlife habitat models. *Revista de Teledetección (45),* 1–14. https://www.fs.usda.gov/treesearch/pubs/57106

Vogeler, J. C., Hudak, A. T., Vierling, L. A., & Vierling, K. T. (2013). Lidar-derived canopy architecture predicts brown creeper occupancy of two western coniferous forests. *The Condor, 115*(3), 614–622. https://doi.org/10.1525/cond.2013.110082

Wiebe, K. L. (2001). Microclimate of tree cavity nests: Is it important for reproductive success in northern flickers? *The Auk, 118*(2), 412–421. https://doi.org/10.1093/auk/118.2.412

Wing, B. M., Ritchie, M. W., Boston, K., Cohen, W. B., & Olsen, M. J. (2015). Individual snag detection using neighborhood attribute filtered airborne lidar data. *Remote Sensing of Environment, 163*, 165–179. https://doi.org/10.1016/j.rse.2015.03.013

Chapter 2: Smartphone LIDAR can measure tree cavity dimensions for wildlife studies

Stitt, J.M., Svancara, L.K., Vierling, L.A., & Vierling, K.T. (2019) Smartphone LIDAR can measure tree cavity dimensions for wildlife studies. *Wildlife Society Bulletin*, *43*(1), 159–166. https://doi.org/10.1002/wsb.949

Abstract

Remote sensing technologies are increasingly able to measure environmental characteristics important for wildlife, but remain limited in measuring small-scale structures like tree cavities. Tree cavities are essential structures in many systems, including use for breeding and roosting by multiple animal species that vary in size. However, obtaining cavity dimensions directly is often difficult, dangerous, or impossible. During September–October 2017 at the University of Idaho Experimental Nursery in Moscow (ID, USA), we tested a handheld Light Detection and Ranging (LIDAR) device that interfaces with smartphones and tablets called Spike® by IkeGPS (Wellington, New Zealand) to determine whether it could be used to remotely measure tree cavity entrance dimensions. The Spike laser range-finding device pairs with a mobile app to allow users to photograph a target (i.e., a tree cavity) on their phone or tablet and measure dimensions of that target onscreen. We designed an experiment to test the accuracy of Spike across 4 cavity entrance sizes ranging from 8.25 cm^2 to 80.11 cm^2, based on average cavity dimensions of Pacific Northwest woodpecker (Picidae) species. We varied height of target off the ground, obliqueness of the viewing angle (i.e., offset from target azimuth), and distance from target. Correlations between Spike measurements and cavity dimensions were high (r > 0.91 across 3 dimensions; n = 294). Measurement error for both vertical and horizontal diameters of cavity entrances was < 1 cm on average. Accuracy was most influenced by taking photos from a large oblique viewing angle, high target height, and large distance from the target combined, based on results from generalized linear models. Spike proved to be a low-cost, portable technology that can noninvasively measure structures that are small and difficult to access. Because of the ease with which it can be used, handheld LIDAR likely has potential future applications in wildlife research as well as citizen science education and outreach efforts.

Introduction

Tree cavities are used for breeding and roosting by multiple animal species that vary in size from small bats to large raptors (Martin et al., 2004; Aitken and Martin, 2007; Blanc and Walters, 2008; Gentry and Vierling, 2008; Bunnell, 2013; see Table A1 in Appendix A). Quantifying cavity-entrance size dimensions has implications for the management of cavity-using communities because cavity entrance size can limit accessibility by different cavity users, many of whom are sensitive species of management concern (Appendix A Table A1). Although it is recognized that cavity entrance dimensions might be important for multiple species and communities, measuring tree cavity characteristics can be challenging because woodpeckers (Picidae), especially in the Pacific Northwest of the United States, often excavate nests in standing dead trees (known as snags), and select sites located high above the ground (Bull and Jackson, 2011; Wiebe and Moore, 2017; Jackson and Ouellet, 2018; Jackson et al., 2018). Snags are inherently unstable structures, often dangerous or difficult to access, which makes many cavities unreachable when located more than a few meters above the ground. Those cavities that can be directly accessed require the use of ladders, poles, or other systems for reaching the cavity entrances (e.g., Martin et al., 2004; Jusino et al., 2014; Lorenz et al., 2015; Vierling et al., 2018). Although these techniques afford a much richer assortment of information (including degree of excavation, internal cavity dimensions, and the opportunity to collect samples, band individuals, and monitor occupancy), they further compound the costs of time, funds, and experience required to obtain data.

Developing a safe, accurate, and rapid approach to remotely measure cavity entrance dimensions would benefit ecologists studying cavity-using communities. There have been no studies to our knowledge that explore tools that would allow for the measurement of such small features in inaccessible sites. Recent developments with laser-based approaches (i.e., Light Detection and Ranging [LIDAR]) have expanded our ability to characterize forest structures and processes in new ways (e.g., Eitel et al., 2016). Although multiple vegetation features can be detected with combinations of satellite imagery, airborne LIDAR, and terrestrial laser scanning (TLS), these tools are more appropriate at the plot, stand, or landscape scale (O'Neil et al., 2012). With technology rapidly advancing the capabilities of field tools and techniques, we have identified handheld LIDAR as a cost-effective tool that

may remotely determine cavity dimensions safely, quickly, and accurately. We believe that this approach may fill a gap in obtaining measurements for structures with small spatial extents (defined here as 1–100 cm), which are not detectable via satellite, airborne LIDAR, or TLS methods.

Our study goal was to test whether a handheld LIDAR device (Spike®; IkeGPS 2018, Wellington, New Zealand) could be used to collect accurate data on cavity entrance dimensions across various conditions. Our specific objectives were to (1) determine the accuracy of the Spike device for measurement of cavity entrance dimensions as a function of size of the cavity entrance, distance from the tree, height of the cavity above the ground, and obliqueness of viewing angle (i.e., offset from cavity entrance azimuth); (2) model the factors that most influence measurement error; and (3) discuss the benefits and drawbacks associated with this tool.

Methods and Materials

Study area

For cavity experiments, we collected all measurements on a wooden logger climbing pole (55 cm in diameter, 19.7 m tall) at the University of Idaho Experimental Nursery in Moscow, Idaho, USA. We took all measurements in September–October 2017.

Manufacturer Specifications for the Spike Handheld LIDAR Device

The Spike device is manufactured by IkeGPS (2018). It is a small Class 1 laser range-finder unit that attaches to the back of a smartphone or tablet computer. The device pairs with the phone or tablet via Bluetooth (Bluetooth Special Interest Group International, Bellevue, WA, USA) and is controlled through a mobile app ("Spike" by IkeGPS, available for iOS and Android platforms) to access the smartphone or tablet's camera, accelerometer, and Global Positioning System information. When a photo is taken of a target through the mobile app, it uses the laser-derived distance to the target to calculate lengths and areas within the photo, on a 2-dimensional plane (Appendix B Figure B1). It has an internal lithium-ion battery charged via micro–Universal Serial Bus, with an estimated battery life of 4 hours

with continuous use. The manufacturer specifies that the accuracy of the range finder for the device is 5 cm between 2 m and 200 m, and accuracy of the photo measurements is 1% of the object being measured. The minimum unit of measure for the Spike device is 1 cm. The Spike device was originally intended for architectural applications, measuring dimensions of large manmade structures such as industrial windows and building facades (IkeGPS, 2018). It is important to note that a clear line of sight to the target is required to get accurate distances and subsequent length and area measurements.

Cavity characteristics

To test how well the Spike device could discern among cavity sizes, we created dummy cavity entrances in the form of ovals cut out of black felt that represented the average cavity-entrance dimensions of 4 woodpecker species: downy woodpecker (*Dryobates pubescens*), hairy woodpecker (*D. villosus*), northern flicker (*Colaptes auratus*), and pileated woodpecker (*Dryocopus pileatus*; Figure 2.1). We selected the range of cavity sizes to test the limits of the Spike device to differentiate between cavity entrance dimensions of these coexisting woodpecker species, with small downy woodpecker cavities at one end of the continuum and large pileated woodpecker cavities at the other (Martin et al., 2004; Figure 2.1). We used a logger climbing pole as a dummy snag to establish 3 replicate sets of dummy cavities (in the form of the 4 felt ovals representing the differently sized cavity entrances), affixed to the pole with duct tape at 3 heights above ground, all in the same orientation. We set up an experimental design to test multiple interacting conditions: size of the target (i.e., size of the felt ovals), distance from target (standing 10 m, 20m, and 30m away), height of target (1 m, 10 m, and 15 m above-ground); and oblique viewing angle (standing at 0º, 25º, and 45º offset from target azimuth; Figure 2.1). The vertical diameter of cavity entrances ranged from 3 cm to 12 cm, whereas the horizontal diameter of cavity entrances ranged from 3.5 cm to 8.5 cm (Figure 2.1). For each combination of distance, height of target above-ground, and viewing angle, we took 3 replicate Spike photos of the target cavity set and used the Spike mobile app to measure the vertical and horizontal diameters for each of the 4 dummy-cavity entrance sizes.

Data analyses

We used Program R (Version 3.4.1, www.R-project.org, accessed 9 May 2018) and R Studio (Version 1.0.143, www. rstudio.com, accessed 9 May 2018) to conduct all statistical analyses. For each of the cavity sizes, we measured the vertical diameter of cavity entrance and horizontal diameter of cavity entrance using the Spike device and mobile app. We then calculated cavity entrance area as (vertical diameter/2) × (horizontal diameter/2) × π (Figure 2.1). We used these 3 cavity dimensions (vertical diameter, horizontal diameter, and entrance area) as response variables in 3 separate tests of analysis of variance (ANOVA) to determine whether Spike measurements of the 4 woodpecker cavity sizes were distinguishable from one another across all conditions.

To determine how variable conditions affected the accuracy of Spike measurements, we calculated error rates for vertical diameter of cavity entrance, horizontal diameter of cavity entrance, and cavity entrance area (difference of the Spike measurement minus the reference). This value (error) was used as the response variable in subsequent univariate analyses, where predictor variables included cavity size, distance from target, height of target above ground, and viewing angle. We used ANOVA followed by Tukey honestly significant difference (HSD) tests on all pairwise comparisons and obtained correlation coefficients for paired samples.

We used generalized linear models from the stats package in R to model the error rates for the vertical diameter of cavity entrance, horizontal diameter of cavity entrance, and cavity entrance area as a function of 3 continuous variables (distance from target, height of target above ground, viewing angle) to test the possible interactions driving error rates across our cavity measurements. We tested 9 models: a null model, models with a single variable (distance only, height of target above ground only, viewing angle only), models with 2-way interactions (distance × height of target above ground, distance × viewing angle, viewing angle × height of target above ground), an additive model that included all 3 variables with no interactions, and a global model with all 3 variables interacting. We ranked models by calculating the value of Akaike's Information Criterion corrected for small sample sizes (AIC_c), and Akaike weight (w_i) for each model (Anderson and Burnham, 2002). We included only models with $\Delta AIC < 2$. We set $\alpha = 0.05$ for all statistical tests.

Results

Cavity measures across various conditions

We measured 294 vertical diameters and horizontal diameters of cavity entrances across all combinations of distance, height, angle, and cavity size. For a small number of instances, repeated measures of combinations were limited because of discarded samples (inaccurate laser distances as a result of interference or missed targets at large distances). We found that the 4 individual cavity sizes were distinguishable from one another ($p < 0.001$ for all comparisons; Table 2.1), regardless of response variable used (vertical diameter, horizontal diameter, or area). Correlation coefficients between known cavity dimensions and Spike-derived vertical diameter, horizontal diameter, and area were 0.95, 0.91, and 0.95, respectively ($p < 0.001$ for each correlation). Error rates for Spike measurements differed across univariate ANOVAs, and the importance of each predictor variable varied by cavity dimension (Table 2.2; Figure 2.2). The average error for vertical diameter of cavity entrance was 0.7 ± 0.7 cm, with a significant increase in error positively correlated with height above ground. The average error for horizontal diameter of cavity entrance was 0.6 ± 0.5 cm, with a significant increase in error positively correlated with oblique viewing angle. The average error for cavity entrance area was 6.0 ± 6.2 cm^2.

Multiple models of the accuracy of Spike measurements showed that predictor variables influenced error rates differently by response variable (Table 2.3). For vertical diameter of cavity entrance, the best model characterizing error rates included height of the target above ground and distance from target as parameters, with an interaction between these 2 factors. Error rates were positively associated with height of cavity above ground and distance individually, but interactions were negatively associated (Table 2.4). For horizontal diameter of cavity entrance, the best model characterizing error rates was the global model, including all 3 variables as parameters, with all interactions between them. The obliqueness of the viewing angle appeared repeatedly as a significant variable across multiple interactions, suggesting error rates for horizontal diameter of cavity entrance were driven by oblique viewing angle (Table 2.4). For cavity entrance area, the best model characterizing error rates included only oblique viewing angle as a parameter, with error rates positively associated with greater angles (Table 2.4).

Discussion

We found that handheld LIDAR can be used to accurately characterize tree-cavity-entrance sizes. Under our experimental conditions, we found that the device could be used to discern among objects 3–12 cm in length from distances up to 30 m with errors of < 1 cm on average (0.6 cm). These lengths corresponded to the average cavity entrance diameter measures for 4 different cavity excavators in the Pacific Northwest. Although there can be overlap in entrance sizes between different woodpecker species in the field, we chose to use the average sizes for this experimental approach.

Error rates for Spike photo measurements increased with the severity of conditions, or combinations thereof, and could predominantly be explained by 2 underlying drivers: extreme perspective (vertical or horizontal foreshortening, defined as the shortening of length in an image where a severe angle distorts the perception of depth) and camera resolution. Errors in vertical diameter of cavity entrance were driven by a negative interaction between distance and height, creating extreme perspective (vertical foreshortening)—standing a short distance away from a target located high above ground predictably leads to underestimation of a vertical length (Figure 2.2, top left plots). Errors in horizontal diameter of cavity entrance were driven by extreme perspective (horizontal foreshortening)—standing at an extreme oblique viewing angle from target azimuth predictably leads to underestimation of horizontal length (Figure 2.2, “45 deg” plots).

Further, quality of a Spike photo is determined by the camera of the smartphone or tablet being used: pixel resolution, level of ambient or external light available, and visibility of all objects to be measured (e.g., visible edges of a cavity entrance) must be taken into account for successful subsequent measurements. Errors in both vertical and horizontal diameters of cavity entrance became more variable at larger distances due to resolution limits of the camera used; identifying cavity edges in a Spike photo taken from 30 m away became difficult because object boundaries blurred at such distances. Blurring mainly led to overestimation for both vertical and horizontal diameters of cavity entrance, though underestimation occurred as well (Figure 2.2, “30 m” plots). Errors in cavity entrance area were greater than the other dimensions, likely due to the compounding nature of

incorporating errors from both vertical diameter and horizontal diameter of cavity entrance into each area calculation.

We support the use of the Spike device for cavity measurements in the field, assuming the baseline conditions of clear line of sight and visibility can be met. For measurements of tree cavity entrance sizes < 15 m in height, we suggest users stand within 30 m and at < 25º oblique angle from the cavity entrance azimuth. We recommend avoiding instances where both types of extreme perspective biases occur (vertical and horizontal foreshortening), to enable the user to obtain an accurate metric for ≥ 1 of the 2 cavity dimensions. Although we used both vertical diameter and horizontal diameter of cavity entrance as dimensions, selecting only one to serve as an indicator of cavity size may be sufficient for field sites with dense vegetation or very high cavities.

Multiple remotely sensed tools assist in the characterization of wildlife habitats, and their use depends largely on the spatial scale and vegetation characteristics of interest. Airborne LIDAR can be used to characterize landscape-scale patterns of structural information and coupled with satellite measurements to address a multitude of questions in wildlife studies (e.g., Vierling et al., 2008; Martinuzzi et al., 2009; Palminteri et al., 2012; Davies and Asner, 2014; Hill and Hinsley, 2015). At finer spatial extents, TLS can be used to calculate tree height, diameter at breast height (DBH), and forest biomass from below the canopy at a plot level (Pirotti et al., 2012; Kankare et al., 2013; Kato et al., 2014; Calders et al., 2015). These systems have also been used to characterize fine-scale understory structure and characteristics in novel ways (Eitel et al., 2013; Bright et al., 2016). Spike differs from both airborne and TLS systems in that it is not generating a collection of laser points (i.e., a point cloud), but 1 point/photo, and extrapolating the distance of that point onto a 2-dimensional plane. We consider Spike to be a precision tool, better applied to focusing in on specific structures rather than characterizing large areas. In fact, use of Spike may dovetail nicely with TLS or other laser-based or drone-based surveys, with the user able to supplement a data set with Spike photos of cavity entrances or other inaccessible structures accurately and opportunistically.

The upfront requirements for implementation of the Spike device include purchasing the laser device, which costs < US$600, and downloading the mobile app, which is free. The Spike device is compact, lightweight, compatible with technology most people already have (smartphones and tablets), and has a long battery life, making it easy to employ in the field when needed. The Spike mobile app has a touchscreen interface, creates geo-referenced photo records for each sample (location accuracy 10 m, not rigorously tested here), and allows data uploads and storage in the cloud for easy online access (IkeGPS, 2018). Web access provides records viewed as a map; post hoc measurements can also be taken from each photo record and all data can be shared between multiple collaborators. Although smartphones and tablets without a Spike device can capture geo-referenced photos in the field, they cannot measure dimensions of structures within those photos without an external reference for scale. Thus, Spike serves as a novel tool for remote measurement that extends the capabilities of a typical smartphone for research.

Handheld LIDAR may add the most value in terms of time savings, by providing users safe, accurate, and rapid remote access to cavity entrance dimensions—metrics that were previously inaccessible or labor- and time-intensive to gather directly. Plus, as a noninvasive method of sampling, Spike could be safe for wildlife and other uses beyond the characterization of tree cavity entrances. The accuracy at small spatial scales (3–12 cm in length) suggests that tools like Spike could be applied to larger structures and obtain accurate results, proving useful for vegetation assessments, including the monitoring and measurement of additional habitat features. For instance, we found Spike to be accurate enough for opportunistic measures of tree DBH at distances 10–50 m away for isolated trees ranging from 11 to 113 cm in diameter, as compared against standard DBH tape measures (J. Stitt, unpublished data; $n = 103$, $r = 0.98$). This tool might be of use in situations where a tree cannot be measured directly, such as those actively being used for nesting or those that are difficult to access, but which have a clear line of sight to their base. We would also encourage explorations into the utility of Spike to assist in noninvasive measurements of animal morphology where applicable and useful (e.g., body size of megafauna or specific bird morphometrics).

Finally, as a handheld, portable, user-friendly device, Spike can also be a powerful tool for educational endeavors and science outreach, engaging both adults and children in novel ways of observing and measuring their surroundings with visual and interactive techniques. With collaborative efforts and citizen science approaches developing into valuable tools for natural resources management and conservation (e.g., Dickinson et al., 2012; Sullivan et al., 2014; Ellwood et al., 2017), the use of Spike and other handheld LIDAR devices as instruments of investigation has potential future use to augment surveys, provide additional metrics noninvasively, and improve approaches to habitat quantification. With the rate at which these technologies continue to advance, Spike and future handheld LIDAR devices may herald the advent of powerful and practical tools to remotely investigate our world from the palm of our hand.

Literature Cited

Aitken, K. E. H., & Martin, K. (2007). The importance of excavators in hole-nesting communities: availability and use of natural tree holes in old mixed forests of western Canada. *Journal of Ornithology, 148*(S2), 425–434. https://doi.org/10.1007/s10336-007-0166-9

Anderson, D. R., & Burnham, K. P. (2002). Avoiding pitfalls when using information-theoretic methods. *The Journal of Wildlife Management, 66*(3), 912–918. https://doi.org/10.2307/3803155

Blanc, L. A., & Walters, J. R. (2008). Cavity excavation and enlargement as mechanisms for indirect interactions in an avian community. *Ecology, 89*(2), 506–514. https://doi.org/10.1890/07-0219.1

Bright, B. C., Loudermilk, E. L., Pokswinski, S. M., Hudak, A. T., & O'Brien, J. J. (2016). Introducing close-range photogrammetry for characterizing forest understory plant diversity and surface fuel structure at fine scales. *Canadian Journal of Remote Sensing, 42*(5), 460–472. https://doi.org/10.1080/07038992.2016.1229598

Bull, E. L., & Jackson, J. A. (2011). Pileated woodpecker (*Dryocopus pileatus*). The Birds of North America. http://birdsna.org/Species-Account/bna/species/pilwoo

Bunnell, F. L. (2013). Sustaining cavity-using species: patterns of cavity use and implications to forest management. *International Scholarly Research Notices*. https://doi.org/10.1155/2013/457698

Calders, K., Newnham, G., Burt, A., Murphy, S., Raumonen, P., Herold, M., Culvenor, D., Avitabile, V., Disney, M., Armston, J., & Kaasalainen, M. (2015). Nondestructive

estimates of above-ground biomass using terrestrial laser scanning. *Methods in Ecology and Evolution, 6*(2), 198–208. https://doi.org/10.1111/2041-210x.12301

Davies, A. B., & Asner, G. P. (2014). Advances in animal ecology from 3D-LiDAR ecosystem mapping. *Trends in Ecology & Evolution, 29*(12), 681–691. https://doi.org/10.1016/j.tree.2014.10.005

Dickinson, J. L., Shirk, J., Bonter, D., Bonney, R., Crain, R. L., Martin, J., Phillips, T., & Purcell, K. (2012). The current state of citizen science as a tool for ecological research and public engagement. *Frontiers in Ecology and the Environment, 10*(6), 291–297. https://doi.org/10.1890/110236

Eitel, J. U. H., Höfle, B., Vierling, L. A., Abellán, A., Asner, G. P., Deems, J. S., Glennie, C. L., Joerg, P. C., LeWinter, A. L., Magney, T. S., Mandlburger, G., Morton, D. C., Müller, J., & Vierling, K. T. (2016). Beyond 3-D: The new spectrum of lidar applications for earth and ecological sciences. *Remote Sensing of Environment, 186*, 372–392. https://doi.org/10.1016/j.rse.2016.08.018

Eitel, J. U. H., Vierling, L. A., & Magney, T. S. (2013). A lightweight, low cost autonomously operating terrestrial laser scanner for quantifying and monitoring ecosystem structural dynamics. *Agricultural and Forest Meteorology, 180*, 86–96. https://doi.org/10.1016/j.agrformet.2013.05.012

Ellwood, E. R., Crimmins, T. M., & Miller-Rushing, A. J. (2017). Citizen science and conservation: Recommendations for a rapidly moving field. *Biological Conservation, 208*, 1–4. https://doi.org/10.1016/j.biocon.2016.10.014

Gentry, D. J., & Vierling, K. T. (2008). Reuse of woodpecker cavities in the breeding and non-breeding seasons in old burn habitats in the Black Hills, South Dakota. *The American Midland Naturalist*. https://doi.org/10.1674/0003-0031(2008)160[413:rowcit]2.0.co;2

Hill, R. A., & Hinsley, S. A. (2015). Airborne lidar for woodland habitat quality monitoring: Exploring the significance of lidar data characteristics when modelling organism-habitat relationships. *Remote Sensing, 7*(4), 3446–3466. https://doi.org/10.3390/rs70403446

IkeGPS. (2018). Spike laser measurement device by IkeGPS. http://ikegps.com/spike

Jackson, J. A., & Ouellet, H. R. (2018). Downy woodpecker (*Dryobates pubescens*). The Birds of North America. http://birdsna.org/Species-Account/bna/species/dowwoo

Jackson, J. A., Ouellet, H. R., & Jackson, B. J. (2018). Hairy woodpecker (*Dryobates villosus*). The Birds of North America. http://birdsna.org/Species-Account/bna/species/haiwoo

Jusino, M. A., Lindner, D. L., Cianchetti, J. K., Grisé, A. T., Brazee, N. J., & Walters, J. R. (2014). A minimally invasive method for sampling nest and roost cavities for fungi: A novel approach to identify the fungi associated with cavity-nesting birds. *Acta Ornithologica*. https://doi.org/10.3161/173484714x687127

Kankare, V., Holopainen, M., Vastaranta, M., Puttonen, E., Yu, X., Hyyppä, J., Vaaja, M., Hyyppä, H., & Alho, P. (2013). Individual tree biomass estimation using terrestrial

laser scanning. *ISPRS Journal of Photogrammetry and Remote Sensing*. https://doi.org/10.1016/j.isprsjprs.2012.10.003

Kato, A., Kajiwara, K., Honda, Y., Watanabe, M., Enoki, T., Yamaguchi, Y., & Kobayashi, T. (2014). Efficient field data collection of tropical forest using terrestrial laser scanner. *IEEE Geoscience and Remote Sensing Symposium*, 816–819. https://doi.org/10.1109/igarss.2014.6946549

Lorenz, T. J., Vierling, K. T., Johnson, T. R., & Fischer, P. C. (2015). The role of wood hardness in limiting nest site selection in avian cavity excavators. *Ecological Applications, 25*(4), 1016–1033. https://doi.org/10.1890/14-1042.1

Martin, K., Aitken, K. E. H., & Wiebe, K. L. (2004). Nest sites and nest webs for cavity-nesting communities in interior British Columbia, Canada: Nest characteristics and niche partitioning. *The Condor*. https://doi.org/10.1650/7482

Martinuzzi, S., Vierling, L. A., Gould, W. A., Falkowski, M. J., Evans, J. S., Hudak, A. T., & Vierling, K. T. (2009). Mapping snags and understory shrubs for a LiDAR-based assessment of wildlife habitat suitability. *Remote Sensing of Environment, 113*(12), 2533–2546. https://doi.org/10.1016/j.rse.2009.07.002

O'Neil, T. A., Bettinger, P., Marcot, B. G., Wayne Luscombe, B., Koeln, G. T., Bruner, H. J., Barrett, C., Pollock, J. A., & Bernatas, S. (2005). Application of spatial technologies in wildlife biology. *The Wildlife Society*, 418–447. https://www.fs.usda.gov/treesearch/pubs/24891

Palminteri, S., Powell, G. V. N., Asner, G. P., & Peres, C. A. (2012). LiDAR measurements of canopy structure predict spatial distribution of a tropical mature forest primate. *Remote Sensing of Environment*. https://doi.org/10.1016/j.rse.2012.08.014

Pirotti, F., Grigolato, S., Lingua, E., Sitzia, T., & Tarolli, P. (2012). Laser scanner applications in forest and environmental sciences. *Italian Journal of Remote Sensing, 44*(1), 109–123. http://dx.doi.org/10.5721/ItJRS20124419.

Sullivan, B. L., Aycrigg, J. L., Barry, J. H., Bonney, R., Bruns, N. E., Cooper, C. B., Damoulas, T., Dhondt, A. A., Dietterich, T. G., Farnsworth, A., Farnsworth, A., Fink, D., Fitzpatrick, J. W., Fredericks, T., Gerbracht, J., Gomes, C. P., Hochachka, W. M., Iliff, M. J., Lagoze, C., … Kelling, S. (2014). The eBird enterprise: An integrated approach to development and application of citizen science. *Biological Conservation*. https://doi.org/10.1016/j.biocon.2013.11.003

Vierling, K. T., Lorenz, T. J., Cunningham, P. G., & Potterf, K. (2018). Thermal conditions within tree cavities in ponderosa pine (*Pinus ponderosa*) forests: Potential implications for cavity users. *International Journal of Biometeorology*. https://doi.org/10.1007/s00484-017-1464-4

Vierling, K. T., Vierling, L. A., Gould, W. A., Martinuzzi, S., & Clawges, R. M. (2008). Lidar: Shedding new light on habitat characterization and modeling. *Frontiers in Ecology and the Environment, 6*(2), 90–98. https://doi.org/10.1890/070001

Wiebe, K. L., & Moore, W. S. (2017). Northern flicker (*Colaptes auratus*). The Birds of North America. http://birdsna.org/Species-Account/bna/species/norfli

Tables

Table 2.1 Measurements of cavity entrance dimensions

Means and standard errors (in cm) of Spike measurements of cavity entrance dimensions across all photos of dummy cavity entrances obtained during September–October 2017 at the University of Idaho Experimental Nursery in Moscow (ID, USA), based on 4 woodpecker species.

	Vertical diameter		**Horizontal diameter**		**Cavity entrance area**	
Species[a]	$\overline{x}$	*SE*	$\overline{x}$	*SE*	$\overline{x}$	*SE*
DOWO	3.27	0.07	3.79	0.04	9.95	0.28
HAWO	5.01	0.06	4.89	0.06	19.41	0.41
NOFL	7.50	0.05	6.85	0.07	40.49	0.51
PIWO	11.53	0.12	8.51	0.07	77.17	1.07

[a] DOWO, downy woodpecker; HAWO, hairy woodpecker; NOFL, northern flicker; and PIWO, pileated woodpecker

Table 2.2 Measurement errors for each response variable

Results of Tukey honestly significant difference tests for errors of Spike measurement (difference between Spike value and known value) of dummy cavity entrances, obtained during September–October 2017 at the University of Idaho Experimental Nursery in Moscow (ID, USA), across experimental conditions, based on 3 response variables: **(a)** vertical diameter of cavity entrance, **(b)** horizontal diameter of cavity entrance, and **(c)** cavity entrance area. Please see Figure 2.1 for further clarification of experimental design.

(a) Errors, vertical diameter (cm)				
	Estimate	**Lower CI**	**Upper CI**	***P*** [a]
SIZE[b]				
HAWO–DOWO	0.09	−0.21	0.39	0.87
NOFL–DOWO	0.14	−0.16	0.44	0.63
PIWO–DOWO	0.30	0.00	0.61	0.05
NOFL–HAWO	0.05	−0.25	0.35	0.97
PIWO–HAWO	0.21	−0.09	0.52	0.27
PIWO–NOFL	0.16	−0.14	0.46	0.51
HEIGHT[c]				
Mid–ground	0.15	−0.07	0.38	0.25
Canopy–ground	0.55	0.32	0.77	<0.001***
Canopy–mid	0.39	0.16	0.63	<0.001***
DISTANCE[d]				
20 m–10 m	−0.13	−0.37	0.11	0.39
30 m–10 m	−0.04	−0.27	0.20	0.93
30 m–20 m	0.10	−0.15	0.35	0.62
ANGLE[e]				
25 deg–0 deg	0.09	−0.16	0.34	0.70
45 deg–0 deg	−0.03	−0.27	0.22	0.97
45 deg–25 deg	−0.11	−0.34	0.12	0.49

[a] Adjusted *P*-values: '*' < 0.05, '**' < 0.01, '***' < 0.001.

[b] SIZE refers to the dimensions of the dummy cavity entrance, ranked by size of woodpecker species: DOWO, downy woodpecker; HAWO, hairy woodpecker; NOFL, northern flicker; and PIWO, pileated woodpecker.

[c] HEIGHT refers to height above ground at which we placed dummy cavity entrances on the pole: "Ground" (1 m), "Mid" (10 m), and "Canopy" (15 m).

[d] DISTANCE refers to how far from the pole photos were taken: standing 10 m, 20 m, and 30 m away.

[e] ANGLE refers to the obliqueness (in degrees) of the photographic view angle relative to the cavity entrance: "0 deg" (standing directly in front of the cavity entrance), "25 deg" (standing at a 25° angle clockwise from azimuth), and "45 deg" (standing at a 45° angle clockwise from azimuth).

(b) Errors, horizontal diameter (cm)				
	Estimate	**Lower CI**	**Upper CI**	***P*** [a]
SIZE[b]				
HAWO–DOWO	−0.06	−0.28	0.17	0.92
NOFL–DOWO	−0.09	−0.31	0.13	0.74
PIWO–DOWO	0.09	−0.13	0.32	0.71
NOFL–HAWO	−0.03	−0.25	0.19	0.98
PIWO–HAWO	0.15	−0.07	0.37	0.31
PIWO–NOFL	0.18	−0.04	0.40	0.15
HEIGHT[c]				
Mid–ground	−0.04	−0.22	0.13	0.84
Canopy–ground	−0.05	−0.23	0.12	0.77
Canopy–mid	−0.01	−0.19	0.17	0.99
DISTANCE[d]				
20 m–10 m	−0.12	−0.29	0.05	0.23
30 m–10 m	0.07	−0.10	0.25	0.57
30 m–20 m	0.20	0.02	0.38	0.03*
ANGLE[e]				
25 deg–0 deg	0.17	0.00	0.35	0.05*
45 deg–0 deg	0.46	0.29	0.63	<0.001***
45 deg–25 deg	0.29	0.13	0.45	<0.001***

[a] Adjusted *P*-values: '*' < 0.05, '**' < 0.01, '***' < 0.001.

[b] SIZE refers to the dimensions of the dummy cavity entrance, ranked by size of woodpecker species: DOWO, downy woodpecker; HAWO, hairy woodpecker; NOFL, northern flicker; and PIWO, pileated woodpecker.

[c] HEIGHT refers to height above ground at which we placed dummy cavity entrances on the pole: "Ground" (1 m), "Mid" (10 m), and "Canopy" (15 m).

[d] DISTANCE refers to how far from the pole photos were taken: standing 10 m, 20 m, and 30 m away.

[e] ANGLE refers to the obliqueness (in degrees) of the photographic view angle relative to the cavity entrance: "0 deg" (standing directly in front of the cavity entrance), "25 deg" (standing at a 25° angle clockwise from azimuth), and "45 deg" (standing at a 45° angle clockwise from azimuth).

(c) Errors, cavity entrance area (cm^2)	Estimate	Lower CI	Upper CI	*P* [a]
SIZE[b]				
HAWO–DOWO	1.08	−1.29	3.44	0.64
NOFL–DOWO	3.01	0.66	5.36	0.006**
PIWO–DOWO	7.52	5.16	9.87	<0.001***
NOFL–HAWO	1.94	−0.42	4.29	0.15
PIWO–HAWO	6.44	4.09	8.79	<0.001***
PIWO–NOFL	4.51	2.16	6.85	<0.001***
HEIGHT[c]				
Mid–ground	−0.02	−2.09	2.05	1.00
Canopy–ground	1.88	−0.17	3.92	0.08
Canopy–mid	1.90	−0.22	4.02	0.09
DISTANCE[d]				
20 m–10 m	−1.69	−3.74	0.36	0.13
30 m–10 m	0.89	−1.15	2.93	0.56
30 m–20 m	2.58	0.46	4.70	0.01*
ANGLE[e]				
25 deg–0 deg	1.46	−0.68	3.60	0.24
45 deg–0 deg	2.67	0.53	4.80	0.01**
45 deg–25 deg	1.21	−0.77	3.18	0.32

[a] Adjusted *P*-values: '*' < 0.05, '**' < 0.01, '***' < 0.001.

[b] SIZE refers to the dimensions of the dummy cavity entrance, ranked by size of woodpecker species: DOWO, downy woodpecker; HAWO, hairy woodpecker; NOFL, northern flicker; and PIWO, pileated woodpecker.

[c] HEIGHT refers to height above ground at which we placed dummy cavity entrances on the pole: "Ground" (1 m), "Mid" (10 m), and "Canopy" (15 m).

[d] DISTANCE refers to how far from the pole photos were taken: standing 10 m, 20 m, and 30 m away.

[e] ANGLE refers to the obliqueness (in degrees) of the photographic view angle relative to the cavity entrance: "0 deg" (standing directly in front of the cavity entrance), "25 deg" (standing at a 25° angle clockwise from azimuth), and "45 deg" (standing at a 45° angle clockwise from azimuth).

Table 2.3 Support for generalized linear model selection

Support for generalized linear model selection based on Akaike's Information Criterion corrected for small sample sizes (AIC_c), explaining drivers of error in Spike measurements of dummy cavity entrances across 3 response variables: vertical diameter of cavity entrance, horizontal diameter of cavity entrance, and cavity entrance area. Measurements collected during September–October 2017 at the University of Idaho Experimental Nursery in Moscow, Idaho, USA. Please see Figure 2.1 for further clarification of experimental design.

Model[a]	***K***	**AIC_c**	**ΔAIC_i**	**w_i**
Vertical diameter				
Height × Distance	5	587.81	0.00	0.77
Horizontal diameter				
Global	9	417.97	0.00	0.69
Cavity entrance area				
Angle	3	1,903.86	0.00	0.35
Height + Distance + Angle	5	1,904.52	0.66	0.25
Height × Angle	5	1,905.09	1.23	0.19

[a] "Height" refers to the height above ground at which we placed dummy cavity entrances on the pole; "Distance" refers to how far from the base of the pole photos were taken; "Angle" refers to the obliqueness (in degrees) of the photographic view angle, relative to the cavity entrance. Global models include all interactions across Height, Distance, and Angle.

Table 2.4 Parameter estimates and confidence intervals for drivers of error in each top-ranked model

Parameter estimates and confidence intervals for drivers of error in each top-ranked model of Spike measurements, collected during September–October 2017 at the University of Idaho Experimental Nursery in Moscow (ID, USA), across 3 response variables: vertical diameter of cavity entrance, horizontal diameter of cavity entrance, and cavity entrance area. Please see Figure 2.1 for further clarification of experimental design.

Model[a]	**Estimate**	**Lower CI**	**Upper CI**
Vertical diameter			
(Intercept)	−0.297	−0.636	0.043
Height	0.125[b]	0.092	0.157
Distance	0.037[b]	0.021	0.053
Height × Distance	−0.004[b]	−0.006	−0.003
Horizontal diameter			
(Intercept)	−0.072	−0.480	0.336
Height	0.029	−0.011	0.069
Distance	0.021[b]	0.002	0.040
Angle	0.035[b]	0.021	0.048
Height × Distance	−0.001	−0.003	0.001
Height × Angle	−0.002[b]	−0.003	−0.001
Distance × Angle	−0.001[b]	−0.002	−0.0001
Height × Distance × Angle	<0.001[b]	<0.001	<0.001
Cavity entrance area			
(Intercept)	4.526[b]	3.302	5.750
Angle	0.059[b]	0.020	0.099

[a] "Height" refers to the height above ground at which we placed dummy cavity entrances on the pole; "Distance" refers to how far from the base of the pole photos were taken; "Angle" refers to the obliqueness (in degrees) of the photographic view angle, relative to the cavity entrance.

[b] We considered estimates significant if 95% CIs did not include 0.

Figures

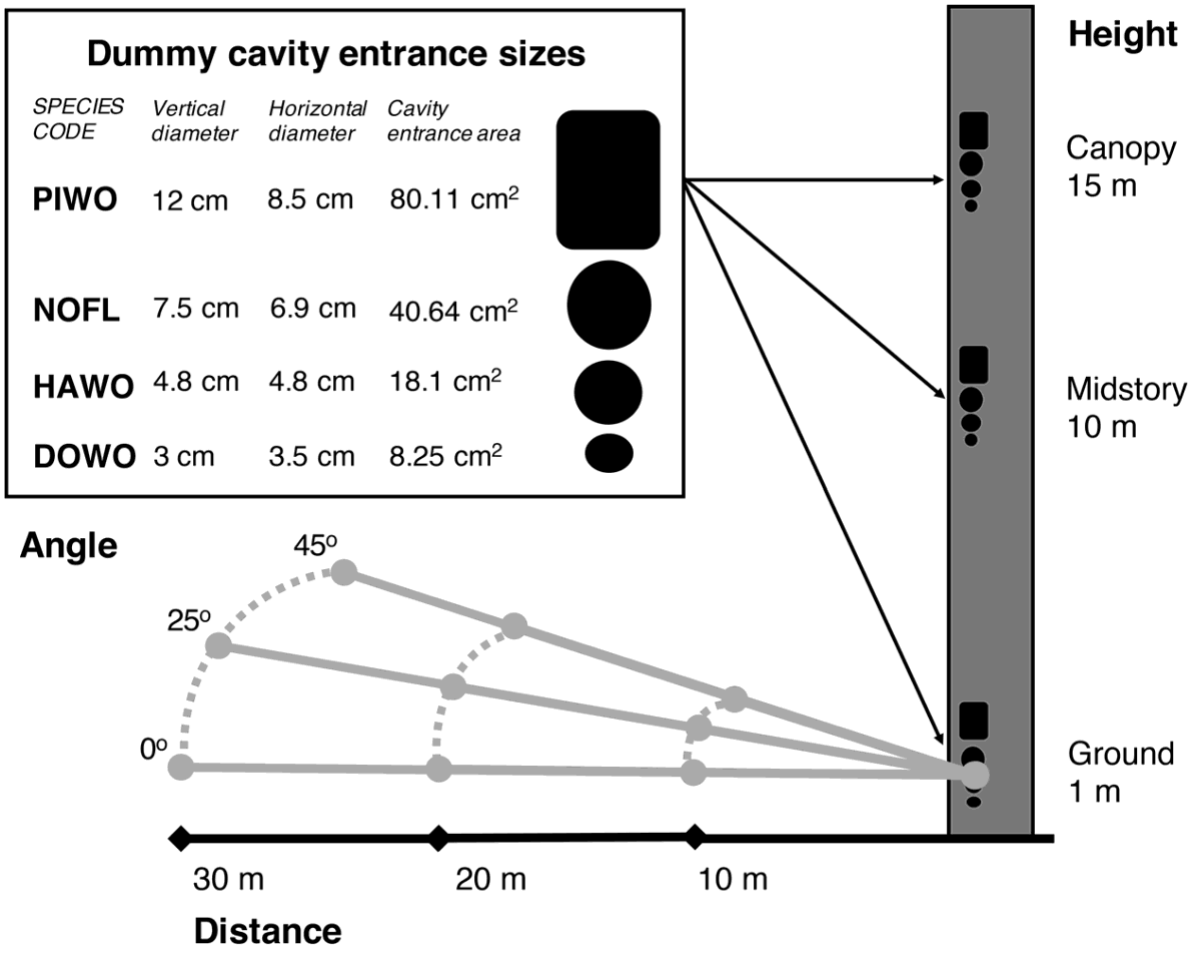

Figure 2.1 Experimental setup for measuring cavity entrance dimensions

Experimental setup for testing the Spike device to measure cavity entrance dimensions at the University of Idaho Experimental Nursery in Moscow (ID, USA) during September–October 2017. For the "Dummy cavity entrance sizes" inset: SPECIES CODE refers to the 4 woodpecker species: pileated woodpecker (PIWO), northern flicker (NOFL), hairy woodpecker (HAWO), and downy woodpecker (DOWO). Dummy cavity entrance sizes were created based on averages for 2 dimensions/species: vertical diameter and horizontal diameter of cavity entrance (cm). Three sets of dummy cavity entrances were taped to a logger climbing pole. For each set, "Height" was centered between the HAWO and NOFL cavities. "Distance" refers to how far from the base of the pole photos were taken: standing 10 m, 20 m, and 30 m away. "Angle" refers to the obliqueness (in degrees) of the photographic view angle relative to the cavity: 0º angle (standing directly in front of the cavity entrances), standing at a 25º angle clockwise from azimuth, and standing at a 45º angle clockwise from azimuth. Note: figure not to scale.

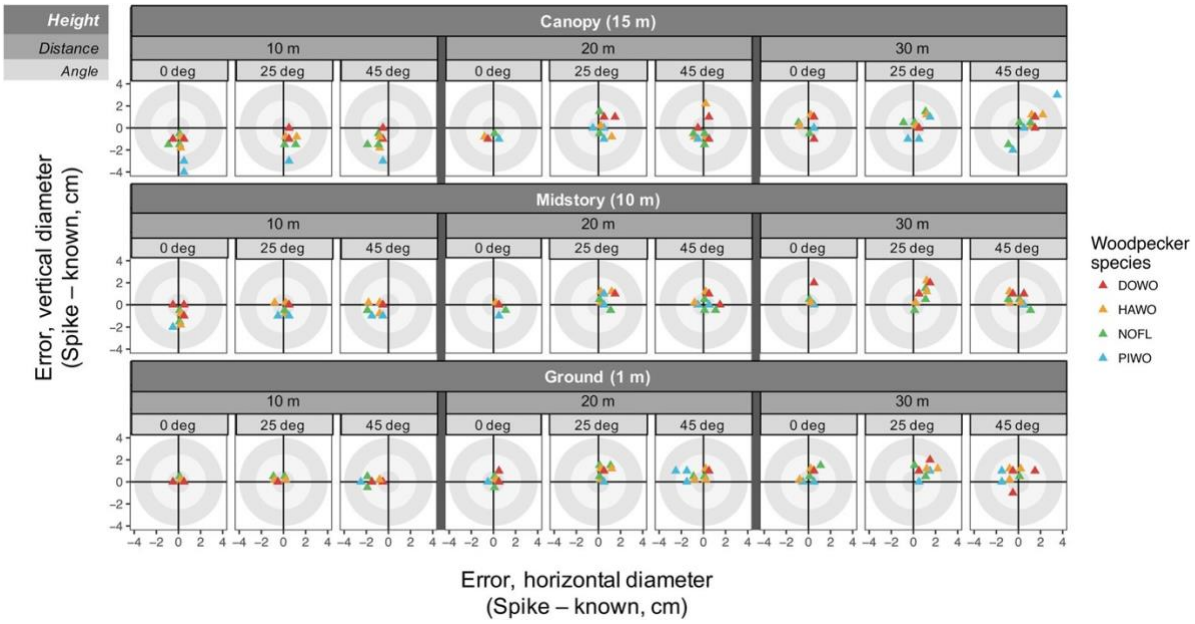

Figure 2.2 Drivers of error for measurements of cavity entrance dimension

A series of scatterplots showing drivers of error for Spike measurements of horizontal diameter (x-axis) and vertical diameter (y-axis) of cavity entrances across experimental conditions at the University of Idaho Experimental Nursery in Moscow (ID, USA) during September–October 2017. Error refers to the difference, in centimeters, for the Spike value minus the known value of a given measurement. The black cross lines indicate an error of 0. These 27 scatterplots represent the full spectrum of combinations across experimental conditions: interactions between cavity height above ground ("Height"), distance from base ("Distance"), and obliqueness of viewing angle ("Angle") as drivers of error in Spike photos across 4 woodpecker cavity sizes. Please see Figure 2.1 for full experimental design.

Chapter 3: Characterizing individual tree-level snags using airborne lidar-derived forest canopy gaps within closed-canopy conifer forests

Stitt, J. M., Hudak, A. T., Silva, C. A., Vierling, L. A., & Vierling, K. T. (2021). Characterizing individual tree-level snags using airborne lidar-derived forest canopy gaps within closed-canopy conifer forests. *Methods in Ecology and Evolution, 13*, 473–484. https://doi.org/10.1111/2041-210X.13752

Abstract

Airborne lidar is often used to calculate forest metrics about trees but it may also provide a wealth of information about the space between trees. Forest canopy gaps are defined by the absence of vegetative structure and serve important roles for wildlife, such as facilitating animal movement. Forest canopy gaps also occur around snags, keystone structures that provide important substrates to wildlife species for breeding, roosting, and foraging. We wanted to test a method for quantifying canopy gaps around individual snags and live trees, with the working hypothesis that snags would have more gaps surrounding them overall than live trees. We evaluated canopy gaps around individual snags (n = 270) and live trees (n = 2186) and evaluated correlations between canopy structure and snag occurrence in dense conifer stands of the Idaho Panhandle National Forest, USA. We paired airborne lidar with ground reference data collected at fixed-radius plots (n = 53) to evaluate local gap structure. The R package ForestGapR was used to quantify canopy gaps throughout the canopy to determine where the differences were greatest. A canopy space profile was created for each tree by mapping gaps (a) vertically every 2 m in height (2–50 m above ground), and (b) horizontally across small (16 m^2), medium (36 m^2), and large (64 m^2) footprint sizes. Our results suggest this method is robust for quantifying canopy gaps around individual trees. The canopy space profiles were distinctly different for snags and live trees, with more canopy gaps within the area surrounding snags relative to live trees. The greatest differences occurred at mid-canopy heights (~20 m above ground) and at the smallest footprint size (16 m^2). These results show potential to improve understanding of gap dynamics in closed-canopy conifer forests, and we suggest snag modeling could be improved by incorporating lidar-derived canopy gap analyses alongside existing methodologies.

Introduction

Standing dead trees (hereafter, snags) are keystone structures that play a disproportionately large role in wildlife community composition and dynamics across forest systems (Tews et al., 2004). Structurally, snags provide unique ecological substrates for wildlife in breeding, roosting and foraging (Bunnell et al., 1999; Cockle et al., 2011; Drever et al., 2008; Gentry & Vierling, 2008; Martin & Eadie, 1999; Mikusiński et al., 2001), with species reliant on the standing deadwood or microhabitats contained within (including nest cavities, bark fissures and other structures; Asbeck et al., 2020; Larrieu et al., 2018; Martin et al., 2004). Snags serve as useful indicators of biodiversity (Basile et al., 2020; Michel & Winter, 2009; Paillet et al., 2017), with snag densities and distributions supporting an array of species across many taxonomic groups, including birds, mammals, amphibians, reptiles (Bunnell et al., 1999; Drever et al., 2008; Drever & Martin, 2010; Martin et al., 2004; Titus, 1983), invertebrates (Bunnell et al., 1999; Hanula et al., 2006; Janssen et al., 2011), and fungi (Bunnell et al., 1999; Jackson & Jackson, 2004). Additionally, snags differ from live trees in their roles regarding carbon storage and sequestration (Curtis, 2008; Powers et al., 2013; Russell et al., 2015), nutrient cycling (Lovett et al., 2010), wildfire fuel loading (Powers et al., 2013; Ritchie et al., 2013), and structural heterogeneity of forest stands (Hansen et al., 1991; Martinuzzi et al., 2009). As snags harbor a wealth of information about forest function, accurately characterizing snag sizes and distributions across a landscape is therefore of high interest for studies and management activities that cross multiple disciplines.

Lidar (light detection and ranging) has improved scientists' ability to describe 3D forest characteristics remotely and may enhance the quantification of snag sizes and distributions for many applications. Airborne lidar (also airborne laser scanning or ALS) is a tool well suited for mapping forest structure, as it provides 3D scans of the canopy structure from above, which can be analyzed at varying resolutions—from the landscape scale (~10^2–10^5 km^2) to individual trees (e.g., Eitel et al., 2016; Falkowski et al., 2009; Goetz & Dubayah, 2011; Guo et al., 2017; Vierling et al., 2008). Most previous lidar work on remote detection of snags has been carried out at two levels: the survey plot level (~0.04–1 ha) and the individual tree level (~1–10 m^2). At the plot level, progress has been made in predicting probable snag densities and distributions using airborne lidar structural metrics (Bater et al., 2009; Martinuzzi et al., 2009) and intensity data (Wing et al., 2015). At the individual tree

level, a focus on segmentation of individual trees (isolating one crown from surrounding crowns) has provided great insights into volume and biomass calculations (Kankare et al., 2013; Klockow et al., 2020; Krzystek et al., 2020; Popescu et al., 2003; Putman et al., 2018; Yao et al., 2012). Both scales of analysis have been applied to wildlife management in the form of habitat mapping for individual species (e.g., Casas et al., 2016; Vogeler and Cohen, 2016).

While focusing on individual tree crown-level metrics is powerful, forest canopy structure consists of not only crowns but also the space between crowns, often referred to as canopy gaps (Shugart, 1984; Urban et al., 1987). Canopy gap characteristics are important features of a forest environment, and recent methodologies have been developed to better quantify gap dynamics through space and time using lidar-based approaches (e.g., Silva et al., 2019). Structurally, snags have a three-dimensional shape that differs from live trees, lacking the green vegetation characteristic of crowns and retaining only the sparser yet coarser woody components of branches and trunks. Within a lidar point cloud, an absence of points need not equal an absence of information, and canopy gap analysis provides a promising avenue for further refinement of snag detection methods and subsequent wildlife habitat mapping based on information about the spaces between trees. For instance, birds fly through and therefore utilize the empty space between tree crowns, so it is more holistic and perhaps accurate to think of both the space occupied by tree crowns and the unoccupied space when characterizing suitable or preferred wildlife habitat.

To evaluate whether airborne lidar data can capture differences in the proportion of empty gap space surrounding snags and live trees (known as gap fraction), we analyzed two features of the vertical and horizontal gap space around individual snags and live trees: height above-ground (representing a vertical perspective) and size of gap around a given tree (representing the horizontal space). Our main objective is to quantify how canopy gap profiles differ between snags and live trees, such that canopy gap profiles could potentially be used as an indicator of snag presence. We hypothesize that snags should have distinct canopy gap space profiles due to the loss of foliage and branches, and we would expect snags to have greater total gap area than live trees. We compare the vertical and horizontal gap characteristics around snags and live trees within closed-canopy conifer stands. From a vertical perspective, we would expect these characteristics to differ most in the mid-canopy;

in the lower canopy, we would anticipate fewer gaps due to forest structures such as saplings, shrubs and/or stumps. In the higher canopy, we would anticipate fewer gap differences between live trees and snags due to the conical shape of conifer tree crowns, as both decrease in woody and needle biomass approaching the top of the tree. From a horizontal perspective, we would expect that there is an optimal footprint size that captures the gaps that are associated with an individual tree. No other studies to our knowledge have used this approach at the individual-tree level or applied it to snags. Therefore, this method may hold promise for describing canopy gap structure that might correlate with snag presence.

Methods and Materials

Study area

The study was conducted in closed canopy forest stands within the Idaho Panhandle National Forest (IPNF), Idaho, USA. The study area consisted of two sites within IPNF: one site in the Coeur d'Alene River Ranger District (herein CdA), and one site in the Saint Joe Ranger District (herein StJ; Figure 3.1). Both sites are composed of mature mixed-conifer forest stands managed for multiple uses, including timber production, recreation, and wildlife habitat (IDFG, 2016). At CdA, the most abundant live tree species were grand fir (*Abies grandis*), western hemlock (*Tsuga heterophylla*), and Douglas fir (*Pseudotsuga menziesii*). At StJ, the most abundant live species were grand fir, western red cedar (*Thuja plicata*), and western larch (*Larix occidentalis*). Across both sites, the most abundant species of snags found were grand fir and western larch, followed by Douglas fir at CdA and western redcedar at StJ.

Field measurements

To map snags within closed-canopy forest, ground reference surveys were conducted within 25-m fixed-radius plots at each site. Survey plot locations were selected through a stratified random sampling design based on canopy cover and height metrics from lidar and constrained using criteria to enable subsequent point count surveys of forest birds, based on existing protocols (e.g., Dudley and Saab, 2003; Vogeler et al., 2013) including a 300-m minimum distance from other plot centers and a road buffer (minimum of 60 m and maximum of 250 m away from roads). Plot centers were recorded using a global navigation satellite system (GNSS) receiver (Trimble GeoXH; accuracy < 1 m) and differentially

corrected in post-processing. We surveyed each plot for snags within a 25-m radius (0.2 ha plots), recording only snags taller than 1.37 m (to measure diameter at breast height, DBH) and with a DBH > 15 cm, based on minimum diameter for nesting by regional woodpecker species (Schroeder, 1983). Information on snag condition was recorded including DBH, tree species (when possible), height, and spatial coordinates. Coordinates were determined using the same handheld Trimble GNSS receiver as used for plot centers, positioned on the north side of each bole. Coordinates for each snag were then centered by subtracting half the measured DBH from the northing value to correct for placement bias.

Lidar data acquisition and pre-processing

Discrete-return ALS data were acquired across both sites as part of an ongoing effort by the U.S. Forest Service Rocky Mountain Research Station (USFS RMRS) to develop advanced protocols for forest mapping and monitoring. Details on the lidar acquisition parameters can be found in Table 3.1. The georeferenced lidar data were processed at the plot level using the R environment (R Core Team, 2020, version 4.0.3). Point clouds were preprocessed using the lidR package (Roussel et al., 2020) at a 50-m radius around plot centers (0.8 ha plots) to generate buffered, height-normalized, filtered, and pit-free canopy height models (CHMs; following methods similar to Silva et al. [2016]) with 0.5-m spatial resolution, as depicted in Figure 3.2a. CHMs were then clipped to the 0.2-ha plot level for canopy gap analyses.

Individual tree and forest canopy gap detection

The 0.8-ha pit-free, filtered, height-normalized CHMs were also the basis for individual tree detection (ITD) methods used to generate a list of live tree locations to compare against ground reference snag locations per 0.2-ha plot, as live trees were not surveyed at the 0.2-ha scale. However, a subset of plots from each site was sampled by USFS RMRS in 2017 simultaneously, providing a count of live trees within 11.3-m fixed-radius subplots (0.04 ha; also centered on plot center). As GNSS coordinates were not collected for live trees, these counts of live trees per subplot were used to calibrate ITD methods to improve the accuracy at the 0.2-ha scale. To account for possible error originating from lidar unable to fully penetrate dense forest stands, the count data were filtered by height (or DBH where height was not recorded) to create three versions per subplot: all live trees, only live trees > 20 m tall or with DBH ≥ 20 cm and only live trees > 30 m tall or with DBH ≥ 20 cm.

Four iterations of ITD were run using the rLiDAR package (Silva et al., 2019), via segmentation based on local maxima within a fixed window size. The minimum height threshold was held constant (2 m), but fixed window size (surrounding pixel extent used to estimate local maxima) was altered by iteration: 3 × 3, 5 × 5, 7 × 7 and 9 × 9 pixels. ITD was performed across the full 0.8-ha CHM raster associated with survey plots and then clipped to the 0.04-ha subplot extent. Each iteration of ITD estimates was compared against the three versions of filtered counts, and the difference in live tree count per subplot (filtered – ITD) was used to evaluate the relative error of ITD estimations (Table 3.3A). Average error per subplot by site was used as the accuracy metric to determine the best configuration to expand to the 0.2-ha scale (Table 3.3B). Please see Figure 3.2b for an overview of the ITD process.

To evaluate canopy space profiles around live trees and snags, the coordinates for the center of each ITD-generated tree and each reference snag were used in conjunction with the 0.8-ha CHM rasters for each plot and analyzed with the ForestGapR package (Silva et al., 2019). The size threshold for canopy gap detection was set to all gaps ≥1 m^2 total area at the given canopy height, and three sizes of square clips were made from CHM rasters around each tree center: 4 m × 4 m (16 m^2), 6 m × 6 m (36 m^2) and 8 m × 8 m (64 m^2; hereafter referred to as footprint sizes: small, medium, and large, respectively). Square clips were used (vs. circular clips) to preserve maximum data from the 0.5-m resolution raster, and the sizes were chosen to encompass the range of average crown diameters for these sites. Canopy gap area per square was calculated from the sum of all gaps for each footprint size. These repeated measures of canopy gap extent at different footprint sizes were used to study how canopy gap area changes across spatial scales.

For each tree, canopy gap area was also calculated over multiple canopy heights, creating a stack of 2D square clips, with a minimum height of 2 m above-ground (to omit noise below breast height) and a maximum height of 50 m above-ground (determined from tallest trees in census), and measured every 2 m to ensure full coverage of the vertical canopy profile. This stacked approach was used to study how canopy gap area changes through vertical space. Pairing the three footprint sizes with the stacked heights enabled the investigation of both vertical and horizontal dimensions of canopy gaps around individual snags and live trees (Figure 3.3). This approach provided 75 gap area measurements around

each tree (across the small, medium, and large footprint sizes over 25 heights, from 2 to 50 m above-ground). Please see Figure 3.2c for an overview of canopy gap profile generation.

Individual snag and canopy gap analysis

For each 2D square, the canopy gap area was divided by footprint area to calculate canopy gap fraction to standardize values across footprint sizes. The response variable for statistical tests was canopy gap fraction per 2D square. Mean (± SE) gap fractions were calculated for live trees versus snags across three categorical predictor variables: site (CdA or StJ), footprint size (small, medium, large), and canopy height (2 m–50 m above-ground). Differences in mean gap fraction between tree types (snag – live) were also calculated across the same three predictor variables. Footprint size and height above-ground were treated as repeated measures, with unique trees as the unit of observation. Data did not meet assumptions of normality, so nonparametric tests were used to compare canopy gap fractions between groups. We used Mann–Whitney *U* tests to evaluate differences between group means by tree type across all combinations of predictor variables, at a significance level of 5%. All statistical analyses were conducted using the R environment (R Core Team, 2020, version 4.0.3).

Results

At the 0.2-ha survey scale, there were 270 snags total across 53 ground reference plots, with an average density of five snags per plot (Table 3.2). A subset of 32 of the 53 ground reference plots contained 0.04-ha subplots with census data, with a total of 538 live trees used to calibrate ITD methods (Table 3.3). Results of the ITD accuracy assessment found that the 7 × 7 fixed window size was the most accurate for both sites and performed best when used with census data filtered to only include trees >30 m tall, with a total average overestimation of 0.2 trees per plot (Table 3.3). The 7 × 7 fixed window size was applied to plots at both sites, and subsequent ITD estimation of live trees at the 0.2-ha survey scale generated a total of 2,186 live tree locations across 53 plots, with an average density of 41 trees per plot (Table 3.2).

A total of 184,200 square-shaped, vertically distributed slices of canopy were analyzed from 2,456 individual trees. Please see Figure 3.4 for a visualization of canopy gap

profiles around a live tree and snag. Snags were surrounded by a greater fraction of canopy gap than live trees (13% greater overall; $p < 0.001$). At the predictor variable level, live trees and snags differed in the canopy gap fractions surrounding them across heights, sites, and footprint sizes, with distinct patterns that differed ($p < 0.0001$) between snags and live trees for each variable (Figure 3.5).

The fraction of gaps around both snags and live trees increased with height (Figure 3.5). At 2-m above-ground, snags showed mean canopy gap fractions ranging from 0.05 to 0.21, compared to live trees with mean canopy gap fractions ranging from 0 to 0.03. Mean canopy gap fraction approached 1 (≥ 0.98) at 40 m above-ground for all groups. The shape of the line for mean canopy gap fractions across heights (i.e., slope) was similar across tree types. Both snags and live trees followed a sigmoidal curve in gap fraction as height increased (i.e., slope started steep lower in the canopy, flattened in the mid-canopy, then rose steeply again higher in the canopy), though this curve was more pronounced for live trees relative to snags at both sites.

Mean canopy gap fractions showed distinct trends by site as well, with higher canopy gap fractions at the CdA site relative to StJ for both snags (13% higher at CdA) and live trees (2% higher at CdA; Figure 3.5). Mean canopy gap fractions differed by footprint size for live trees, increasing as footprint size increased (5% increase from small to medium, 4% increase from medium to large; Figure 3.5). However, this pattern was not seen with snags; mean canopy gap fractions around snags remained consistent across all three footprint sizes (0.1% increase from small to medium, 0.04% decrease from medium to large footprint size).

By focusing on mean differences in canopy gap fractions between snags and live trees at each height (mean snag – mean live tree, from 2 m to 50 m above-ground), further distinctions within the canopy space can be discerned (Figure 3.6). The greatest differences in canopy gap fraction occurred at heights 10 m–30 m above-ground, whereby snags had ~22% more gap area compared to live trees (Figure 3.6). Differences between snags and live trees were significant ($p < 0.001$) for small and medium footprint sizes at all heights below 28 m (Figure 3.6).

Discussion

Exploring how empty space is structured around individual trees opens additional avenues of study when collecting lidar-based forest metrics. Our primary objective was to explore whether gap characteristics around individual trees could be quantified and compared between snags and live trees. We hypothesized that the greatest differences in gap characteristics would occur within the mid-canopy strata, and that there would be an optimal footprint size differentiating snags from live trees. Within our study sites, our hypotheses were supported and we found distinct canopy space profiles between snags and live trees, with the largest distinctions found at heights 10 m–30 m above-ground level, greatest for the smallest footprint size (16 m^2).

The largest unexpected result found in this study occurred among snags between sites; snags at StJ had consistently lower gap fractions than snags at CdA. Many factors may account for this difference. For instance, differences in gaps around snags across the two sites could simply reflect an effect of tree density, as StJ had greater average stem density in plots than CdA (Table 3.2) leading to less open area. Stand-level differences in gaps could also be driven by broader sitewide factors such as disturbance history, causes of tree mortality, successional stage and stand age, and/or tree species composition (Lefsky et al., 1999). How these stand-level characteristics affect gaps at the individual tree level requires expanded analyses beyond the scope of this study, however.

This study establishes the importance, feasibility, and utility of investigating associations between canopy gap structure, live trees, and snags at the individual tree level using airborne lidar. The results of this study contribute to the strong foundation of canopy gap research that integrates remote sensing with studies of forest structure and successional processes (e.g., Lefsky et al., 1999). Assessment of the ecological value of canopy gaps has been well studied (Canham, 1988; Spies et al., 1990; Whitmore, 1989), and more recent investigations apply remote sensing tools to monitor biodiversity linked to canopy gaps (Bagaram et al., 2018), study the gap sizes and distribution related to forest stand characteristics and processes (e.g. Asner et al., 2013), and identify and quantify gaps using remote sensing (e.g. Bagaram et al., 2018; Bonnet et al., 2015; Silva et al., 2019; White et al., 2018).

Focusing on canopy gaps around individual trees may not be feasible when dealing with dense forests in an applied context, so the next step will be to evaluate the relationship between canopy gaps and snags at the plot level. This brings in the added challenge of distinguishing gaps around snags from 'true' canopy gaps, where there are no standing trees or snags. We suggest that this can be achieved by focusing on one or two heights above-ground that strongly differentiate snags from live trees and constraining canopy gap area (as true gaps may have larger total areas): for example, evaluating gaps at heights 10 m and 20 m above-ground, constrained to 25%–75% gap fraction of the small footprint size (equal to a gap area of 4 m^2–12 m^2 only). We note that this suggestion is based on one forest type, though this methodology could provide additional benefit from comparisons of canopy gap profiles across multiple forest types. Furthermore, the ForestGapR package (Silva et al., 2019) contains additional functions not applied here, including a function for change detection that could provide greater information and distinction between snags and true gaps by evaluating change in gap extent across selected heights or height percentiles within the canopy. Future studies could employ a standardized method to evaluate gap fractions across multiple forest types: calculating gap fraction at 10 m height in the canopy on a gridded map (2 m × 2 m pixels), then flagging pixels with higher-than-average gap fraction for the given forest type. If the gap of a given pixel does not extend fully to the ground (a gap fraction of 1.0 at < 2 m above-ground, indicating a true gap), it may suggest snag presence.

Fusing previous lidar-based snag modelling approaches with canopy gap analyses such as the ones we have described might provide a promising next step in advancing our understanding of snag distributions in forested landscapes. Prior methods have modelled snags using stand-level lidar-derived metrics focused on structure-based values, via ordinal regression (Bater et al., 2009) or Random Forest classification (Martinuzzi et al., 2009), and intensity-based values via neighborhood attribute filtering (Wing et al., 2015). Another approach may be to first identify gaps and use them to filter lidar point clouds before beginning more targeted snag modelling, implementing any of the prior methods discussed above. This would serve to pare down the overall file size needed for further processing, improve the speed and/or expand the spatial extent of analyses to potentially improve overall accuracy of snag mapping. Distinctions in canopy space profiles between live trees and snags

were robust enough at the single tree level that we suggest incorporating canopy gap evaluation into snag modelling methods in some form.

These methods and the information they provide about the space around trees can help better characterize canopy gaps in dense forests where tree segmentation methods may be less robust due to fewer returns penetrating closed canopy. One of the problems previously reported in mapping snags using airborne lidar was the limited number of returns (e.g., Martinuzzi et al., 2009), likely due to the reduced physical structure of a snag relative to a live tree canopy. Our study found snags to have overall point densities around 25% lower than live trees (Table 3.4), and several snags had fewer than 100 returns in total. Reframing the problem of fewer returns in the context of canopy gap analysis may help tease apart true gaps from gaps containing snags.

Conclusions

Canopy gaps and snags are both important elements of forest structure and canopy architecture, and both have ties to successional and disturbance regimes. Use of airborne lidar data can provide a more nuanced understanding of their inter-relatedness and patterns of co-occurrence, which will be of added value to researchers and managers across a range of disciplines. The power of canopy gap analyses coupled with snag detection will only continue to increase as higher resolution airborne lidar surveys are integrated with mobile, terrestrial, and UAV-based lidar data collections, and as point cloud analyses become more robust. We urge the consideration of both the presence and absence of data found within lidar point clouds to gain greater insight into spatial and temporal patterns found throughout forest canopies worldwide.

Literature Cited

Asbeck, T., Basile, M., Stitt, J., Bauhus, J., Storch, I., & Vierling, K. T. (2020). Tree-related microhabitats are similar in mountain forests of Europe and North America and their occurrence may be explained by tree functional groups. *Trees, 34*(6), 1453–1466. https://doi.org/10.1007/s00468-020-02017-3

Asner, G. P., Kellner, J. R., Kennedy-Bowdoin, T., Knapp, D. E., Anderson, C., & Martin, R. E. (2013). Forest canopy gap distributions in the southern Peruvian Amazon. *PloS one, 8*(4), e60875. https://doi.org/10.1371/journal.,pone.0060875

Bagaram, M. B., Giuliarelli, D., Chirici, G., Giannetti, F., & Barbati, A. (2018). UAV remote sensing for biodiversity monitoring: are forest canopy gaps good covariates? *Remote Sensing, 10*(9), 1397. https://doi.org/10.3390/rs10091397

Basile, M., Asbeck, T., Jonker, M., Knuff, A. K., Bauhus, J., Braunisch, V., ... & Storch, I. (2020). What do tree-related microhabitats tell us about the abundance of forest-dwelling bats, birds, and insects? *Journal of environmental management, 264*, 110401. https://doi.org/10.1016/j.jenvman.2020.110401

Bater, C. W., Coops, N. C., Gergel, S. E., LeMay, V., & Collins, D. (2009). Estimation of standing dead tree class distributions in northwest coastal forests using lidar remote sensing. *Canadian Journal of Forest Research, 39*(6), 1080–1091. https://doi.org/10.1139/X09-030

Bonnet, S., Gaulton, R., Lehaire, F., & Lejeune, P. (2015). Canopy gap mapping from airborne laser scanning: An assessment of the positional and geometrical accuracy. *Remote Sensing, 7*(9), 11267-11294. https://doi.org/10.3390/rs70911267

Bunnell, F. L., Kremsater, L. L., & Wind, E. (1999). Managing to sustain vertebrate richness in forests of the Pacific Northwest: relationships within stands. *Environmental Reviews, 7*(3), 97–146. https://doi.org/10.1139/a99-010

Canham, C. D. (1988). Growth and canopy architecture of shade-tolerant trees: response to canopy gaps. *Ecology, 69*(3), 786–795. https://doi.org/10.2307/1941027

Casas, Á., García, M., Siegel, R. B., Koltunov, A., Ramírez, C., & Ustin, S. (2016). Burned forest characterization at single-tree level with airborne laser scanning for assessing wildlife habitat. *Remote Sensing of Environment, 175*, 231–241. https://doi.org/10.1016/j.rse.2015.12.044

Cockle, K. L., Martin, K., & Wesołowski, T. (2011). Woodpeckers, decay, and the future of cavity-nesting vertebrate communities worldwide. *Frontiers in Ecology and the Environment, 9*(7), 377–382. https://doi.org/10.1890/110013

Curtis, P. S. (2008). Estimating aboveground carbon in live and standing dead trees. In Field Measurements for Forest Carbon Monitoring (pp. 39–44). Springer, Dordrecht.

Drever, M. C., & Martin, K. (2010). Response of woodpeckers to changes in forest health and harvest: Implications for conservation of avian biodiversity. *Forest ecology and management, 259*(5), 958–966. https://doi.org/10.1016/j.foreco.2009.11.038

Drever, M. C., Aitken, K. E., Norris, A. R., & Martin, K. (2008). Woodpeckers as reliable indicators of bird richness, forest health and harvest. *Biological conservation, 141*(3), 624–634. https://doi.org/10.1016/j.biocon.2007.12.004

Dudley, J. G., and Saab, V. (2003). A field protocol to monitor cavity-nesting birds. United States Department of Agriculture, Forest Service, Rocky Mountain Research Station.

Eitel, J. U., Höfle, B., Vierling, L. A., Abellán, A., Asner, G. P., Deems, J. S., ... & Vierling, K. T. (2016). Beyond 3-D: The new spectrum of lidar applications for earth and ecological sciences. *Remote Sensing of Environment, 186*, 372–392. https://doi.org/10.1016/j.rse.2016.08.018

Falkowski, M. J., Evans, J. S., Martinuzzi, S., Gessler, P. E., & Hudak, A. T. (2009). Characterizing forest succession with lidar data: An evaluation for the Inland Northwest, USA. *Remote Sensing of Environment, 113*(5), 946–956. https://doi.org/10.1016/j.rse.2009.01.003

Fekety, P. A., Falkowski, M. J., Hudak, A. T., Jain, T. B., & Evans, J. S. (2018). Transferability of lidar-derived basal area and stem density models within a northern Idaho ecoregion. *Canadian Journal of Remote Sensing, 44*(2), 131–143. https://doi.org/10.1080/07038992.2018.1461557

Fekety, P. A., Hudak, A. T., & Bright, B. C. (2020). Field observations for "A carbon monitoring system for mapping regional, annual aboveground biomass across the northwestern USA". *Fort Collins, CO: Forest Service Research Data Archive.* https://doi.org/10.2737/RDS-2020-0026

Gentry, D. J., & Vierling, K. T. (2008). Reuse of woodpecker cavities in the breeding and non-breeding seasons in old burn habitats in the Black Hills, South Dakota. *The American Midland Naturalist, 160*(2), 413–429. https://doi.org/10.1674/0003-0031(2008)160[413:ROWCIT]2.0.CO;2

Goetz, S., & Dubayah, R. (2011). Advances in remote sensing technology and implications for measuring and monitoring forest carbon stocks and change. *Carbon Management, 2*(3), 231–244. https://doi.org/10.4155/cmt.11.18

Guo, X., Coops, N. C., Tompalski, P., Nielsen, S. E., Bater, C. W., & Stadt, J. J. (2017). Regional mapping of vegetation structure for biodiversity monitoring using airborne lidar data. *Ecological informatics, 38*, 50–61. https://doi.org/10.1016/j.ecoinf.2017.01.005

Hansen, A. J., Spies, T. A., Swanson, F. J., & Ohmann, J. L. (1991). Conserving biodiversity in managed forests. *BioScience, 41*(6), 382–392. https://doi.org/10.2307/1311745

Hanula, J. L., Horn, S., & Wade, D. D. (2006). The role of dead wood in maintaining arthropod diversity. In *Insect biodiversity and dead wood: Proceedings of a symposium for the 22nd International Congress of Entomology (93)*, 57–74. US Department of Agriculture, Forest Service, Southern Research Station.

Idaho Department of Fish and Game (IDFG). (2016). Idaho species of greatest conservation need. Idaho Department of Fish and Game, Boise, Idaho. https://idfg.idaho.gov/species/taxa/list/sgcn

Jackson, J. A., & Jackson, B. J. (2004). Ecological relationships between fungi and woodpecker cavity sites. *The Condor, 106*(1), 37–49. https://doi.org/10.1093/condor/106.1.37

Janssen, P., Hébert, C., & Fortin, D. (2011). Biodiversity conservation in old-growth boreal forest: black spruce and balsam fir snags harbour distinct assemblages of saproxylic beetles. *Biodiversity and Conservation, 20*(13), 2917–2932. https://doi.org/10.1007/s10531-011-0127-8

Kankare, V., Holopainen, M., Vastaranta, M., Puttonen, E., Yu, X., Hyyppä, J., ... & Alho, P. (2013). Individual tree biomass estimation using terrestrial laser scanning. *ISPRS Journal of Photogrammetry and Remote Sensing, 75*, 64–75. https://doi.org/10.1016/j.isprsjprs.2012.10.003

Klockow, P. A., Putman, E. B., Vogel, J. G., Moore, G. W., Edgar, C. B., & Popescu, S. C. (2020). Allometry and structural volume change of standing dead southern pine trees using non-destructive terrestrial LiDAR. *Remote Sensing of Environment*, 241, 111729. https://doi.org/10.1016/j.rse.2020.111729

Heidrich, L., Bae, S., Levick, S., Seibold, S., Weisser, W., Krzystek, P., ... & Müller, J. (2020). Heterogeneity–diversity relationships differ between and within trophic levels in temperate forests. *Nature ecology & evolution, 4*(9), 1204–1212. https://doi.org/10.1038/s41559-020-1245-z

Larrieu, L., Paillet, Y., Winter, S., Bütler, R., Kraus, D., Krumm, F., Lachat, T., Michel, A. K., Regnery, B., & Vandekerkhove, K. (2018). Tree related microhabitats in temperate and Mediterranean European forests: A hierarchical typology for inventory standardization. *Ecological Indicators, 84*, 194–207. https://doi.org/10.1016/j.ecolind.2017.08.051

Lefsky, M. A., Cohen, W. B., Acker, S. A., Parker, G. G., Spies, T. A., & Harding, D. (1999). Lidar remote sensing of the canopy structure and biophysical properties of Douglas-fir western hemlock forests. *Remote sensing of environment, 70*(3), 339–361. https://doi.org/10.1016/S0034-4257(99)00052-8

Lovett, G. M., Arthur, M. A., Weathers, K. C., & Griffin, J. M. (2010). Long-term changes in forest carbon and nitrogen cycling caused by an introduced pest/pathogen complex. *Ecosystems, 13*(8), 1188–1200.

Martin, K., & Eadie, J. M. (1999). Nest webs: A community-wide approach to the management and conservation of cavity-nesting forest birds. F*orest Ecology and Management, 115*(2), 243–257. https://doi.org/10.1016/S0378-1127(98)00403-4

Martin, K., Aitken, K. E., & Wiebe, K. L. (2004). Nest sites and nest webs for cavity-nesting communities in interior British Columbia, Canada: nest characteristics and niche partitioning. *The condor, 106*(1), 5–19. https://doi.org/10.1093/condor/106.1.5

Martinuzzi, S., Vierling, L. A., Gould, W. A., Falkowski, M. J., Evans, J. S., Hudak, A. T., & Vierling, K. T. (2009). Mapping snags and understory shrubs for a LiDAR-based assessment of wildlife habitat suitability. *Remote Sensing of Environment, 113*(12), 2533–2546. https://doi.org/10.1016/j.rse.2009.07.002

Michel, A. K., & Winter, S. (2009). Tree microhabitat structures as indicators of biodiversity in Douglas-fir forests of different stand ages and management histories in the Pacific Northwest, USA. *Forest Ecology and Management, 257*(6), 1453–1464.

Mikusiński, G., Gromadzki, M., & Chylarecki, P. (2001). Woodpeckers as indicators of forest bird diversity. *Conservation biology*, *15*(1), 208–217. https://doi.org/10.1111/j.1523-1739.2001.99236.x

Paillet, Y., Archaux, F., Boulanger, V., Debaive, N., Fuhr, M., Gilg, O., Gosselin, F., & Guilbert, E. (2017). Snags and large trees drive higher tree microhabitat densities in strict forest reserves. *Forest Ecology and Management, 389*, 176–186. https://doi.org/10.1016/j.foreco.2016.12.014

Popescu, S. C., Wynne, R. H., & Nelson, R. F. (2003). Measuring individual tree crown diameter with lidar and assessing its influence on estimating forest volume and biomass. *Canadian journal of remote sensing*, *29*(5), 564–577. https://doi.org/10.5589/m03-027

Powers, E. M., Marshall, J. D., Zhang, J., & Wei, L. (2013). Post-fire management regimes affect carbon sequestration and storage in a Sierra Nevada mixed conifer forest. *Forest Ecology and Management*, *291*, 268–277. https://doi.org/10.1016/j.foreco.2012.07.038

Putman, E. B., & Popescu, S. C. (2018). Automated estimation of standing dead tree volume using voxelized terrestrial Lidar data. *IEEE Transactions on Geoscience and Remote Sensing, 56*(11), 6484–6503. https://doi.org/10.1109/TGRS.2018.2839088

R Core Team (2020). R: A language and environment for statistical computing. R Foundation for Statistical Computing, Vienna, Austria. https://www.R-project.org/. Accessed 12 March 2021

Ritchie, M. W., Knapp, E. E., & Skinner, C. N. (2013). Snag longevity and surface fuel accumulation following post-fire logging in a ponderosa pine dominated forest. *Forest Ecology and Management, 287*, 113–122. https://doi.org/10.1016/j.foreco.2012.09.001

Roussel, J. R., Auty, D., Coops, N. C., Tompalski, P., Goodbody, T. R., Meador, A. S., ... & Achim, A. (2020). lidR: An R package for analysis of Airborne Laser Scanning (ALS) data. *Remote Sensing of Environment, 251*, 112061. https://doi.org/10.1016/j.rse.2020.112061

Russell, M. B., Fraver, S., Aakala, T., Gove, J. H., Woodall, C. W., D'Amato, A. W., & Ducey, M. J. (2015). Quantifying carbon stores and decomposition in dead wood: A review. *Forest Ecology and Management*, *350*, 107–128. https://doi.org/10.1016/j.foreco.2015.04.033

Schroeder, R. L. (1983). Habitat suitability index models: downy woodpecker (Vol. 82). Western Energy and Land Use Team, Division of Biological Services, Research and Development, Fish and Wildlife Service, US Department of the Interior.

Shugart, H. H. (1984). A theory of forest dynamics. The ecological implications of forest succession models. Springer-Verlag.

Silva, C. A., Hudak, A. T., Vierling, L. A., Loudermilk, E. L., O'Brien, J. J., Hiers, J. K., ... & Khosravipour, A. (2016). Imputation of individual longleaf pine (*Pinus palustris Mill.*) tree attributes from field and LiDAR data. *Canadian journal of remote sensing, 42*(5), 554–573. https://doi.org/10.1080/07038992.2016.1196582

Silva, C. A., Valbuena, R., Pinagé, E. R., Mohan, M., de Almeida, D. R., North Broadbent, E., ... & Klauberg, C. (2019). ForestGapR: An r Package for forest gap analysis from canopy height models. *Methods in Ecology and Evolution, 10*(8), 1347–1356. https://doi.org/10.1111/2041-210X.13211

Spies, T. A., Franklin, J. F., & Klopsch, M. (1990). Canopy gaps in Douglas-fir forests of the Cascade Mountains. *Canadian Journal of Forest Research, 20*(5), 649–658. https://doi.org/10.1139/x90-087

Stitt, J. M., Silva, C. A., Hudak, A. T., Vierling, L. A., & Vierling, K. T. (2021). Data for: Characterizing individual tree-level snags using airborne lidar-derived forest canopy gaps within closed-canopy conifer forests. *Dryad Digital Repository,* https://doi.org/10.5061/dryad.tx95x69xx

Tews, J., Brose, U., Grimm, V., Tielbörger, K., Wichmann, M. C., Schwager, M., & Jeltsch, F. (2004). Animal species diversity driven by habitat heterogeneity/diversity: the importance of keystone structures. *Journal of biogeography, 31*(1), 79–92. https://doi.org/10.1046/j.0305-0270.2003.00994.x

Titus, R. (1983). Management of snags and den trees in Missouri–a process. Davis, JW; Goodwin, GA; Ockenfels, FA (tech. coords.). Gen. Tech. Rep. RM–99, Ft. Colins, CO: US Department of Agriculture. Forest Service, Rocky Mountain Forest and Range Experiment Station, 51–59.

Urban, D. L., O'Neill, R. V., & Shugart Jr, H. H. (1987). A hierarchical perspective can help scientists understand spatial patterns. *BioScience, 37*(2), 119–127.

Vierling, K. T., Vierling, L. A., Gould, W. A., Martinuzzi, S., & Clawges, R. M. (2008). Lidar: shedding new light on habitat characterization and modeling. *Frontiers in Ecology and the Environment, 6(2),* 90-98. https://doi.org/10.1890/070001

Vogeler, J. C., Hudak, A. T., Vierling, L. A., & Vierling, K. T. (2013). Lidar-derived canopy architecture predicts brown creeper occupancy of two western coniferous forests. *The Condor, 115*(3), 614–622. https://doi.org/10.1525/cond.2013.110082

Vogeler, J. C., & Cohen, W. B. (2016). A review of the role of active remote sensing and data fusion for characterizing forest in wildlife habitat models. *Revista de Teledetección.(45),* 1–14. https://doi.org/10.4995/raet.2016.3981

White, J. C., Tompalski, P., Coops, N. C., & Wulder, M. A. (2018). Comparison of airborne laser scanning and digital stereo imagery for characterizing forest canopy gaps in coastal temperate rainforests. *Remote Sensing of Environment, 208,* 1–14. https://doi.org/10.1016/j.rse.2018.02.002

Whitmore, T. (1989). Canopy gaps and the two major groups of forest trees. *Ecology, 70*(3), 536–538. https://doi.org/10.2307/1940195

Wing, B. M., Ritchie, M. W., Boston, K., Cohen, W. B., & Olsen, M. J. (2015). Individual snag detection using neighborhood attribute filtered airborne lidar data. *Remote Sensing of Environment, 163,* 165–179. https://doi.org/10.1016/j.rse.2015.03.013

Yao, W., Krzystek, P., & Heurich, M. (2012). Identifying standing dead trees in forest areas based on 3D single tree detection from full waveform lidar data. *ISPRS Annals of the Photogrammetry, Remote Sensing and Spatial Information Sciences, 1*(7). https://doi.org/10.5194/isprsannals-I-7-359-201

Tables

Table 3.1 Airborne lidar acquisition parameters

The discrete-return airborne lidar (also airborne laser scanning, ALS) data from the two study sites for this paper (based on two IPNF Ranger Districts: Coeur d'Alene River, CdA; Saint Joe, StJ) were part of a larger acquisition carried out by USFS RMRS in 2016 (see Fekety et al., 2018 for more details). The lidar extent of CdA spanned 78,706 ha to the east of Coeur d'Alene, ID, USA (centered at 47°44'40.0"N, 116°36'38.8"W). The lidar extent of StJ spanned 7,598 ha to the east of Avery, ID, USA (centered at 47°08'28.5"N, 116°05'38.9"W).

Parameter	**Specification**
Date collected	12 October 2016
Vendor	Atlantic Group, LLC
Sensor	Leica ALS70-HP
Flight altitude	1965 m above ground level
Flight speed	110 kts
Pulse frequency	278 kHz
Scan frequency	41 Hz
Scan angle	± 30º
Swath width	1098 m
Swath overlap	50%
Laser wavelength	1064 nm
Laser beam divergence	0.22 mrad
Vertical accuracy	5.9 cm
Footprint diameter	43 cm
Nominal pulse density	4.2 pulses/m^2

Table 3.2 Summary statistics for all plots and trees in the study

All reference snags and ITD-generated live trees included in analyses were within 0.2-ha survey plots, located at one of two sites within the Idaho Panhandle National Forests: Coeur d'Alene River (CdA) or Saint Joe (StJ) Ranger Districts. Averages are shown with standard error in parentheses.

Attribute	CdA	StJ
Plots, total	32	21
Elevation (m)	675 – 1545	1041 – 1668
Snags, total	180	90
Average snags / plot	6 (± 1)	4 (± 1)
Range of snags / plot	0 – 23	0 – 12
Live trees, total	1187	999
Average live trees / plot	37 (± 2)	48 (± 4)
Range of live trees / plot	12 – 66	22 – 85

Table 3.3 Accuracy of live tree estimation across multiple configurations of tree census data and ITD parameters

To calibrate the individual tree detection (ITD) methods used for this study, we compared individual tree counts from field-derived census data and lidar-derived ITD data across the same spatial extents. Field-derived census data consisted of ground survey counts of all live trees within fixed-radius circular subplots (0.04 ha) across both study sites, but did not include GNSS-based coordinates of each tree. Lidar-derived ITD data were used to estimate live tree central coordinates within subplots, based on canopy height models (CHM; 0.5 m grid cell) built from airborne lidar data as the basis for ITD-generated estimates of tree locations within each subplot (via segmentation using local maxima within fixed window sizes). Aggregated by study site, Table 3.3A shows **(a)** the summary statistics for the field-derived census counts (mean number of trees per subplot ± SE) across three variations used to filter tree counts based on height threshold; and **(b)** the summary statistics for the lidar-derived ITD counts (mean number of trees per subplot ± SE) repeated across four different fixed window sizes (in pixels) for each subplot. Table 3.3B shows the error rates in live tree estimation (mean error per subplot ± SE) calculated as the differences between field-derived census counts and lidar-derived ITD counts across three height filters and four fixed window sizes (ITD count – census count). Negative numbers represent an underestimation, and positive numbers represent an overestimation of trees per subplot. The configuration with the smallest difference in tree count was used for further analyses; for both sites, this configuration was the same: a 7 × 7 (pixel) fixed window size for ITD paired with census data filtered to include only trees >30 m tall (bolded in table).

3.3A	**(a) Census count, by height filter**			**(b) ITD count, by fixed window size**			
Study site (# of subplots)	**All live trees**	**Trees >20m tall**	**Trees >30m tall**	**3x3**	**5x5**	**7x7**	**9x9**
CdA (23)	16 ± 1.6	9 ± 1.2	7 ± 1.1	18 ± 0.9	10 ± 0.7	8 ± 0.6	6 ± 0.5
StJ (9)	20 ± 2.4	12 ± 2.4	9 ± 2.2	14 ± 1.0	11 ± 0.9	9 ± 0.9	7 ± 1.0

3.3B		**Error in live tree estimation (ITD – census count)**		
Study site	**Fixed window size**	**All live trees**	**Trees >20m tall**	**Trees >30m tall**
CdA	3x3	1.8 ± 1.4	8.3 ± 1.2	10.3 ± 1.1
	5x5	-5.6 ± 1.2	0.9 ± 0.9	2.9 ± 0.7
	7x7	-8.0 ± 1.2	-1.5 ± 0.9	**0.5 ± 0.7**
	9x9	-9.4 ± 1.1	-3.0 ± 0.8	-1.0 ± 0.7
StJ	3x3	-5.3 ± 1.8	2.4 ± 1.7	4.9 ± 1.7
	5x5	-8.4 ± 1.8	-0.7 ± 1.7	1.8 ± 1.6
	7x7	-10.7 ± 1.7	-2.9 ± 1.5	**-0.4 ± 1.4**
	9x9	-12.2 ± 1.6	-4.4 ± 1.4	-2.0 ± 1.3

Table 3.4 Average lidar point densities around individual trees across three footprint sizes

After ITD methods were calibrated at the 0.04 ha subplot level, probable live tree locations were generated for each 0.2 ha survey plot, and the central coordinates of those ITD-generated trees were used as the basis for clipping the lidar point clouds around live trees for each footprint size. Field-derived reference snag central coordinates were used as the basis for clipping the lidar point clouds around snags for each footprint size. The number of total returns for each individual tree clip was calculated and divided by the footprint size, for a measure of point density per square meter (mean number of returns ± SE). Overall, live trees had higher point densities than snags across all footprint sizes for both sites. Among study sites, point densities were lower around snags at CdA than at StJ.

Study site	Footprint size (m^2)	Live tree point density/m^2	Snag point density/m^2
CdA	16	18.5 ± 0.3	10.9 ± 0.5
	36	17.5 ± 0.2	11.1 ± 0.5
	64	16.4 ± 0.2	11.2 ± 0.5
StJ	16	17.1 ± 0.3	14.3 ± 0.7
	36	15.9 ± 0.2	13.9 ± 0.5
	64	14.8 ± 0.2	13.6 ± 0.4

Figures

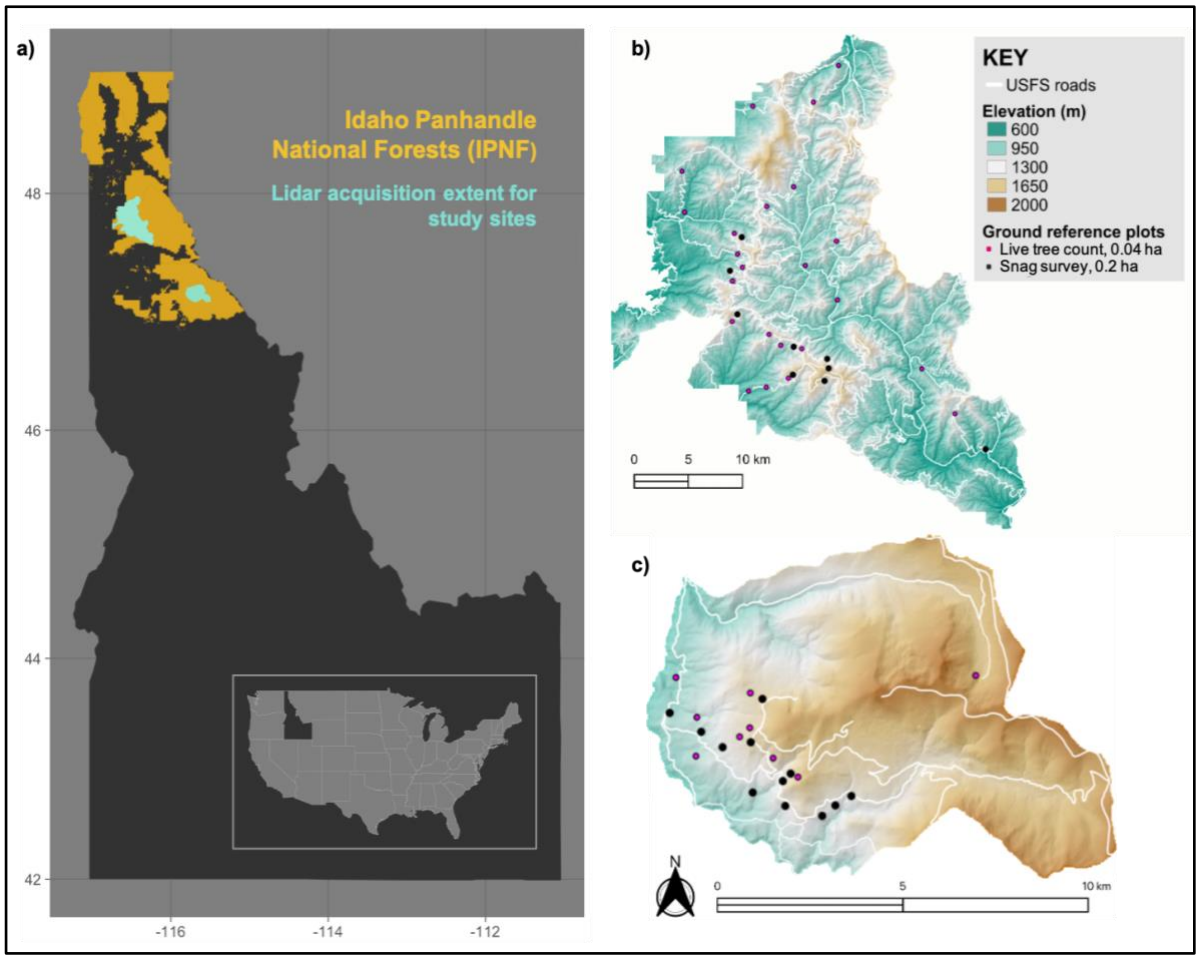

Figure 3.1 Map of the study sites

(a) Study area within Idaho Panhandle National Forests (IPNF) in northern Idaho, United States. There were two lidar acquisitions in the IPNF where all ground reference survey data were collected: within the **(b)** Coeur d'Alene River (CdA) and **(c)** Saint Joe (StJ) Ranger Districts. Please note the different scales for each site. Across the two sites there were a total of 53 25-m radius ground reference plots with snag surveys (0.2 ha; black circles), and 32 of those contained 11.3-m radius subplots (0.04 ha; pink dots) with live tree counts.

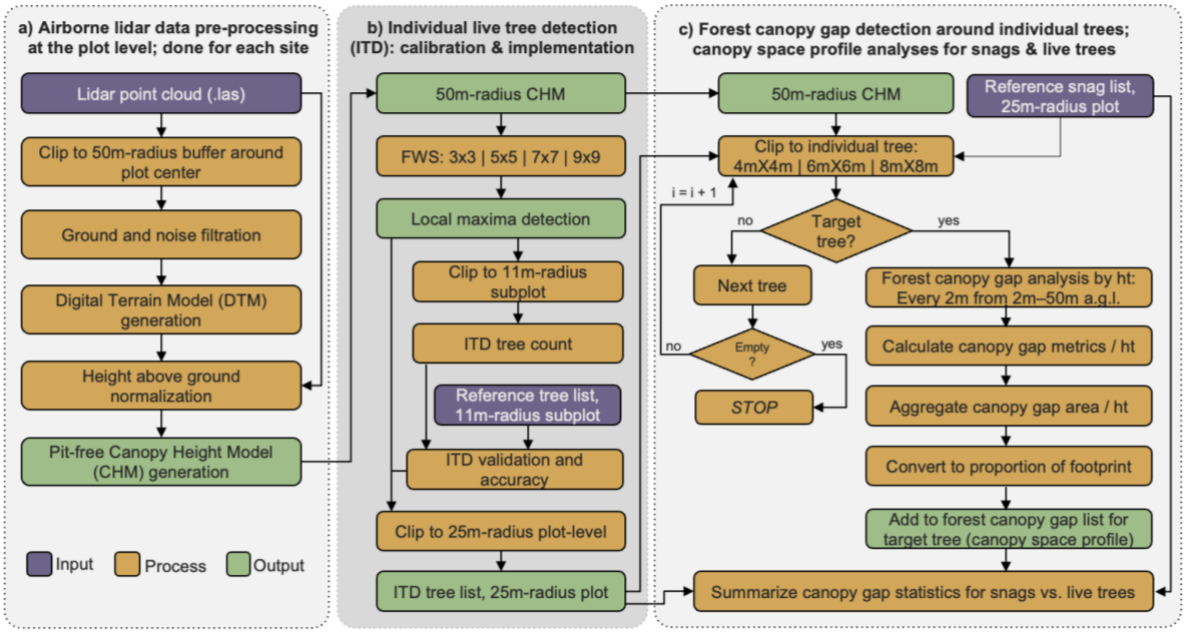

Figure 3.2 Workflow of the airborne lidar data processing for canopy gap profile generation using the ForestGapR package

Overview of the inputs, processes, and outputs to go from the point cloud to the canopy gap profile around individual trees. **(a)** Sitewide lidar data were pared down to the ground reference plot level and processed to generate a canopy height model (CHM) for each plot. **(b)** Live trees sampled within a subset of plots were used to calibrate individual tree detection (ITD) algorithms used to generate a list of live tree locations for each plot to compare against a list of reference snag locations obtained from field surveys. FWS stands for fixed window size, which was the focus of the ITD calibration. **(c)** Forest canopy gap detection was carried out around individual trees using ForestGapR, and canopy gap profile statistics were generated and summarized across all snags and all live trees to determine whether profiles differed significantly between the two groups.

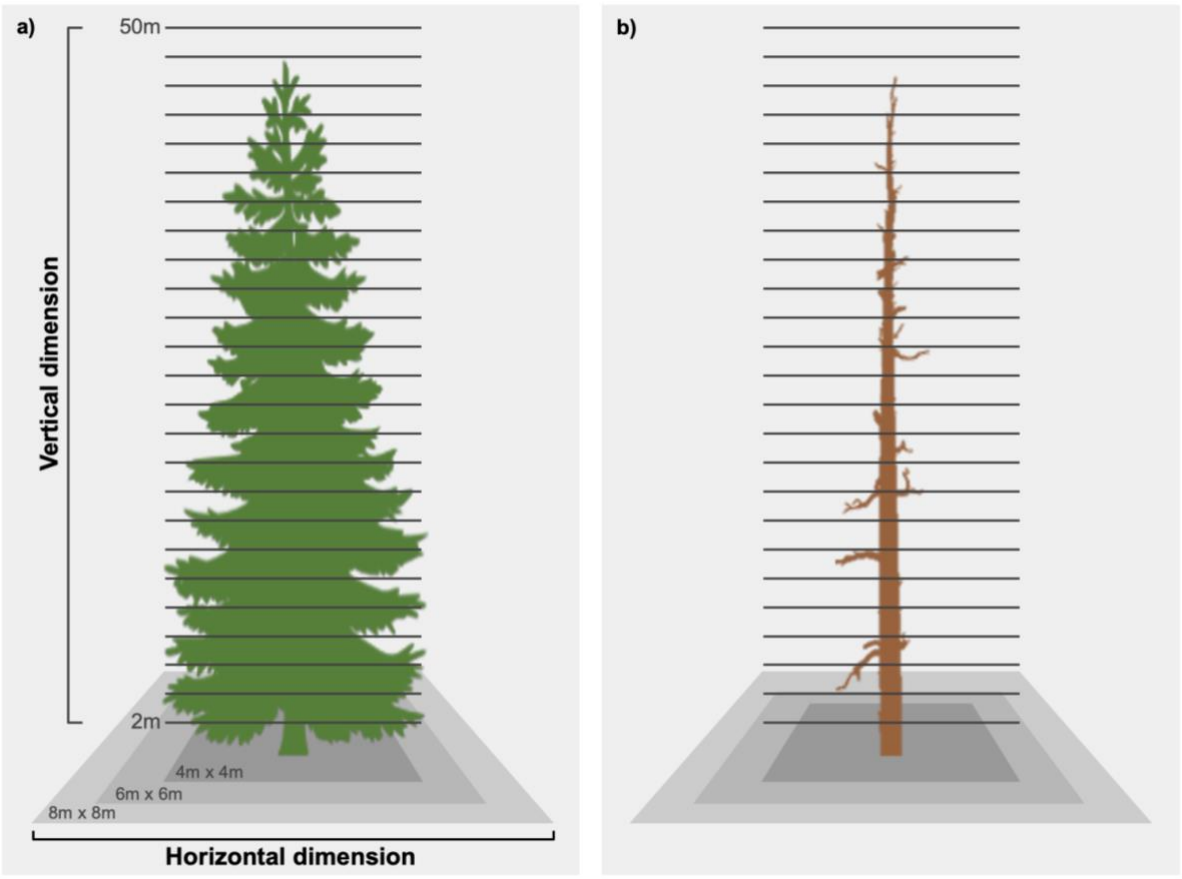

Figure 3.3 Canopy gap profiles

Illustration of the vertical and horizontal dimensions of forest canopy gap detection for **(a)** live trees and **(b)** snags. The vertical dimension encompasses gap analyses run every 2 m above-ground from 2 m to 50 m into the forest canopy. The horizontal dimension incorporates three footprint sizes centered on each tree, including a small size (4 m × 4 m), medium size (6 m × 6 m), and large size (8 m × 8 m). Compiling canopy gap fractions across 25 heights over three footprint sizes (75 data points per tree) created a canopy gap profile for each tree that was used to analyze differences in gap dynamics between snags and live trees.

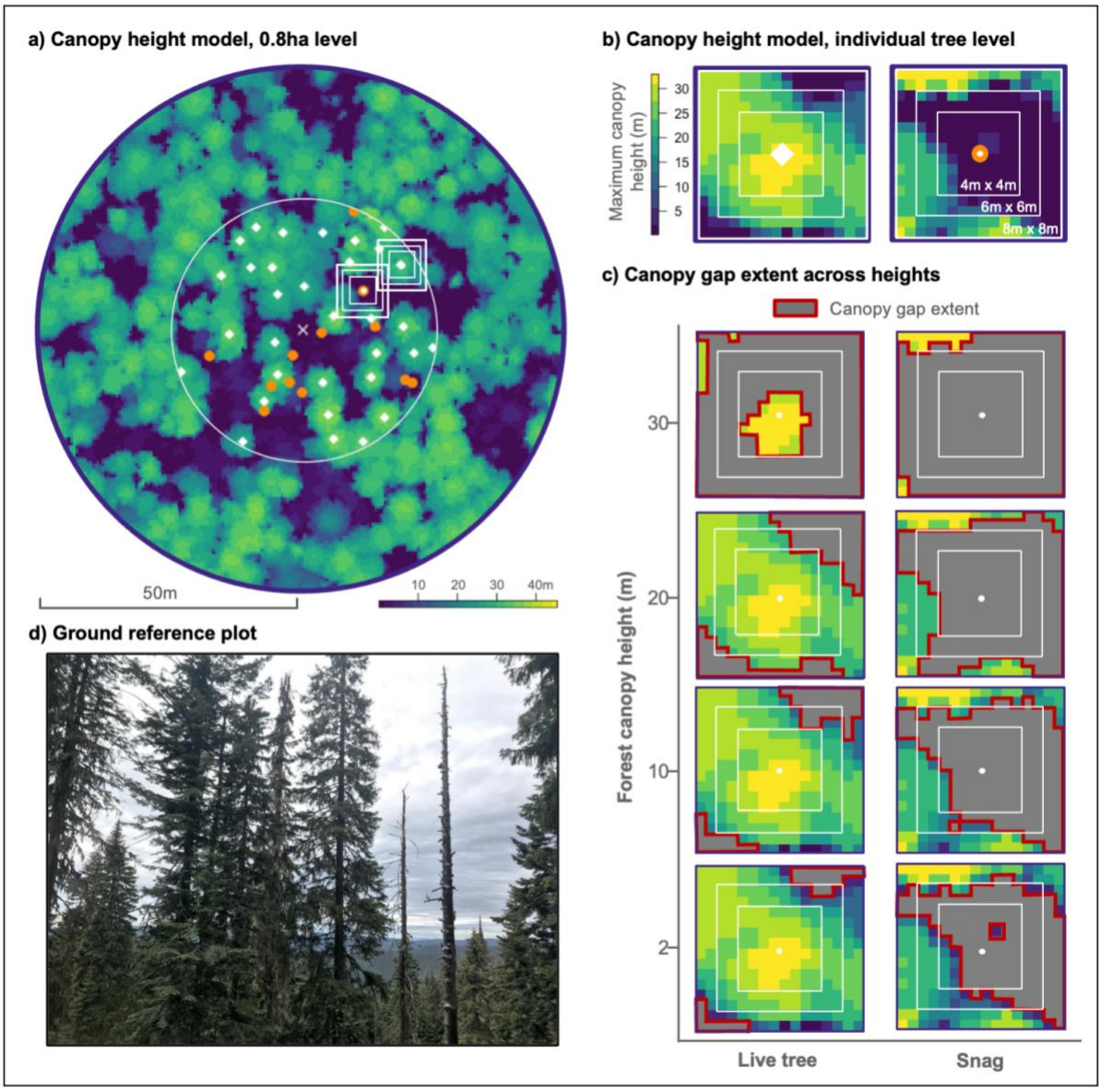

Figure 3.4 Visualization of individual tree-level forest canopy gap detection

Seen from above, **(a)** airborne lidar-derived canopy height models (CHM; 0.5-m grid cell) were generated at a 50-m radius level and clipped around each individual tree within 25-m radius ground reference plots, based on ITD-generated live tree (white diamond) and reference snag (orange circle) locations. **(b)** Representative CHMs for a live tree (left) and snag (right) clipped around tree center (white dot) at three sizes (white squares): small. (4 m × 4 m), medium (6 m × 6 m), and large (8 m × 8 m). **(c)** Forest canopy gaps (gray with red outline) were detected at 25 heights in the forest canopy; here we show four heights: 2 m, 10 m, 20 m, and 30 m above-ground for a live tree (left column) and snag (right column). **(d)** An image taken from a representative ground reference plot, depicting both live trees and snags.

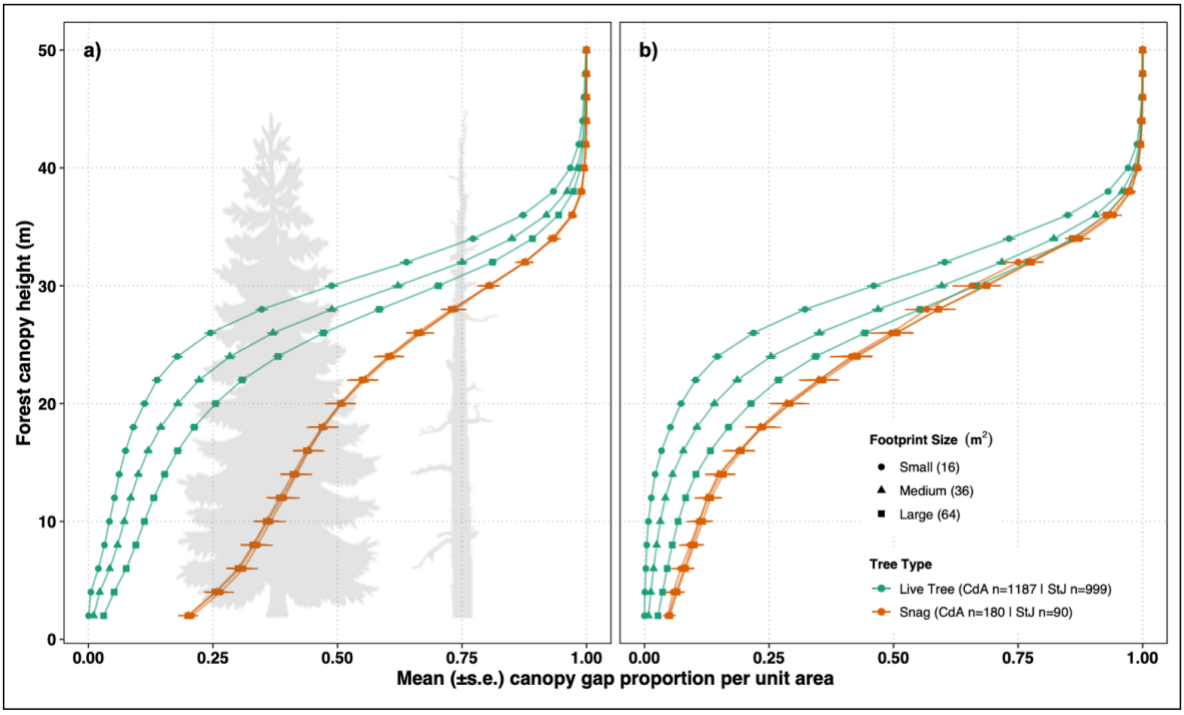

Figure 3.5 Canopy gap fraction around trees by tree type across all forest canopy heights

Mean and standard error are shown for snags (orange) and live trees (green) at each forest canopy height and footprint size, with plots separated by study site: **(a)** Coeur d'Alene River (CdA) and **(b)** Saint Joe (StJ) Ranger Districts.

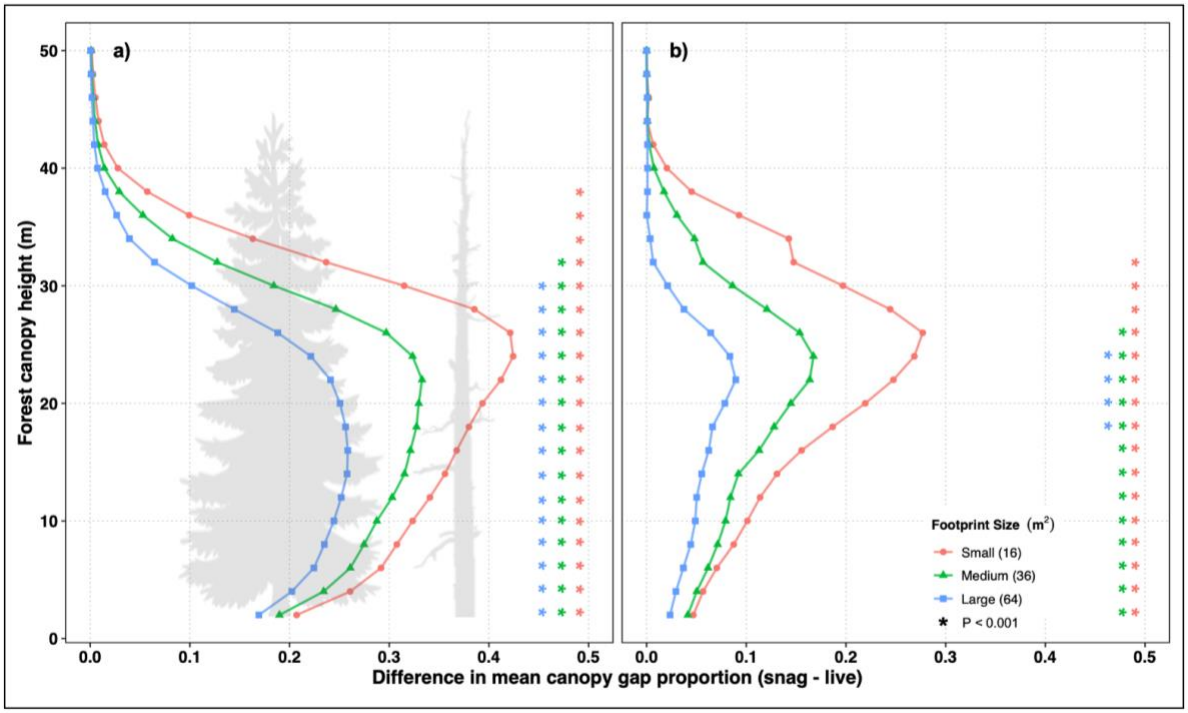

Figure 3.6 Difference in average gap fraction (snag – live) across all forest canopy heights, by site and footprint size

For each height from 2 m to 50 m, the average live tree gap fraction was subtracted from the average snag gap fraction across each footprint size (small [red], medium [green], and large [blue]) at each study site: **(a)** Coeur d'Alene River (CdA) and **(b)** Saint Joe (StJ) Ranger Districts. Differences between tree types that were significant ($p < 0.001$) are marked with color-coded asterisks at each height by footprint size, shown on the right of each graph.

Chapter 4: Evaluating the use of lidar to discern snag characteristics important for wildlife

Stitt, J.M., Hudak, A.T., Silva, C.A., Vierling, L.A., & Vierling, K.T. (2022) Evaluating the use of lidar to discern snag characteristics important for wildlife. *Remote Sensing*, *14*(3), 720. https://doi.org/10.3390/rs14030720

Abstract

Standing dead trees (known as snags) are historically difficult to map and model using airborne laser scanning (ALS), or lidar. Specific snag characteristics are important for wildlife; for instance, a larger snag with a broken top can serve as a nesting platform for raptors. The objective of this study was to evaluate whether characteristics such as top intactness could be inferred from discrete-return ALS data. We collected structural information for 198 snags in closed-canopy conifer forest plots in Idaho. We selected 13 lidar metrics within 5-m diameter point clouds to serve as predictor variables in random forest (RF) models to classify snags into four groups by size (small [<40 cm diameter] or large [≥40 cm diameter]) and intactness (intact or broken top) across multiple iterations. We conducted these models first with all snags combined, and then ran the same models with only small or large snags. Overall accuracies were highest in RF models with large snags only (77%), but kappa statistics for all models were low (0.29–0.49). ALS data alone were not sufficient to identify top intactness for large snags; future studies combining ALS data with other remotely sensed data to improve classification of snag characteristics important for wildlife is encouraged.

Introduction

As keystone structures (Tews et al., 2004), standing dead trees (hereafter, snags) serve essential roles for wildlife species, due in part to how structurally distinct snags are compared to live trees. Snag and live tree characteristics differ across multiple dimensions, including the degree of open space occupied, the unique physical structures provided, and the composition and decay status of wood. These combined characteristics contribute to a wide range of forest microhabitats relevant to wildlife, with many microhabitats associated primarily with snags (Michel and Winter, 2009; Larrieu et al., 2018).

In terms of open space, snag presence and breakdown can be central to the generation of gaps within the canopy used by volant organisms as travel corridors (Jung et al., 2012; Davies et al., 2014). Stitt et al. (2021) evaluated forest canopy gaps around individual trees to establish that snags were associated with significantly larger gap fractions in the immediate vicinity than live conifer trees, especially at midcanopy heights (5 to 20 m above ground). Snags also had higher variability in gap distributions across all canopy heights (Stitt et al., 2021). This greater variability in openness around snags contributes to greater forest structural complexity and may be correlated with greater foliar height diversity and species richness (MacArthur and MacArthur, 1961).

In terms of physical structures, snags add unique microhabitat characteristics to forested landscapes that are not common in live trees. Snags may retain exposed branches on which to perch, which is important for aerial avian flycatchers and birds of prey (Miller and Miller, 1980; Sadoti et al., 2014; Fielder and Starkey, 1986; North et al., 1999). Snags may have a broken top that can serve as a nesting platform for management-sensitive species such as northern goshawks (*Accipiter gentilis*; Squires and Reynolds, 1997) and great gray owls (*Strix nebulosa*; Wu et al., 2015). Snag diameter at breast height (DBH) has been found to be a strong predictor of use by wildlife species (Michel and Winter, 2009; Martinuzzi et al., 2009a; Basile et al., 2020). Branches on snags can be colonized by moss and lichens, creating further subsystems within the canopy (Staniaszek-Kik et al., 2019; Asbeck et al., 2020). This greater variability in structural elements associated with snags likely also contributes to greater forest structural complexity in the forms of increased microhabitat diversity and niche availability, leading to greater species richness (MacArthur and MacArthur, 1961).

In terms of wood composition, dead wood is more suitable than live wood for cavity excavation and nesting opportunities for many species, due to greater decay (resulting from the cessation of tree defenses; Rayner and Boddy, 1988). Decaying wood is utilized by insects for foraging and laying eggs, and the insects in turn are foraged by woodpeckers (among other insectivores). As wood decays, it softens, enabling woodpeckers to excavate cavities (Rayner and Boddy, 1988: Lorenz et al., 2015; Jusino et al., 2015), and as tree limbs decay, they fall, which may also create sites for natural cavity formation (Miller and Miller, 1980; Rayner and Boddy, 1988; Conner et al., 1976). Tree microhabitats derived from dead

wood, along with other microhabitats created as a tree breaks down (e.g., bark pockets and fissures; Michel and Winter, 2009; Asbeck et al., 2020), provide important wildlife habitat that make snags a valuable feature for species mapping and management efforts (Michel and Winter, 2009; Martinuzzi et al., 2009a; Martinuzzi et al., 2009b).

Remote detection of snags is difficult because there is often less information to work with relative to live trees, and because the snag decay process is highly variable. Previous attempts using airborne laser scanning (ALS), or lidar, to identify snags focused on tree crowns as the basis for individual tree segmentation (Reitberger et al., 2008; Yao et al., 2012; Vauhkonen et al., 2011), intensity metrics (Kim et al., 2009; Bright et al., 2013; Wing et al., 2015; Casas et al., 2016), and topographic features (Zellweger et al., 2013). However, approaches focused upon tree crowns can be challenging with snags because dead trees lack the foliar surface area of live tree canopies, and therefore reflect far fewer laser pulses to evaluate and locate snags (Wing et al., 2015). Focusing on the absence of lidar data (in the form of a canopy gap fraction) can provide additional valuable information for characterizing snags from ALS data (Stitt et al., 2021). Determining what further information can be gleaned from the sparse lidar data associated with snags is an area worth investigating.

Few ALS-based studies have focused solely on snags or attempted to differentiate among them, with previous works having focused on snag DBH and volume estimates (Casas et al., 2016; Stitt et al., 2019; Pesonen et al., 2008). Some studies have explored spectral signatures in the form of return intensity metrics (Wing et al., 2015; Casas et al., 2016; Krzystek et al., 2020), but comparisons across sites can be problematic unless the uncalibrated intensity values are normalized. To our knowledge, no other studies have attempted to determine whether ALS data can provide enough information to discern among specific snag characteristics important for wildlife, such as broken versus intact tops.

The focus of this study was to determine whether structural characteristics of snags can be differentiated using ALS data. If differences in structural signatures can be detected via remote sensing, they could be applied to improve mapping efforts and suitability assessments for many wildlife species that depend upon microhabitats related to standing dead trees. In combining field plot survey data with airborne lidar scans, the current study

aimed to determine whether the microhabitats of top intactness (intact vs. broken top) and snag size (small: less than 40 cm in diameter vs. large: greater than or equal to 40 cm in diameter) can be described using ALS data. We compared these field-derived structural characteristics against a suite of airborne-lidar-derived metrics.

Our primary hypothesis was that snags of different structural classes (based on diameter and intactness) would produce significantly different airborne lidar structural metrics. We hypothesized that intact snags may have stronger positive correlations with variables such as point density, percent of first returns, and evenness metrics; intact snags have often experienced more recent mortality, and thus are associated with greater residual branching and crown structures that could present more surface area off which to reflect. We also hypothesized that broken top snags may have stronger positive correlations with variables such as percent of third returns, gap fraction, and roughness metrics; broken top snags are associated with less recent mortality events, and thus with more decay and breakdown of structural features that could more resemble open space. We hypothesized that our ability to detect distinct signatures among snag intactness would be influenced by snag diameter and predicted that snags with larger diameters would have stronger correlations with metrics overall, due to a larger surface area and a lesser proportion of surrounding "noise" within the set footprint (2.5 m radius circle around snag center), relative to smaller snags.

Methods and Materials

Study area

The study was conducted in closed-canopy forest stands within the Idaho Panhandle National Forest (IPNF), Idaho, USA. The study area consisted of two sites within IPNF: one site in the Coeur d'Alene River Ranger District (herein CdA), and one site in the Saint Joe Ranger District (herein StJ; Figure 4.1). Both sites were composed of mature mixed-conifer forest stands managed for multiple uses, including timber production, recreation, and wildlife habitat (Bater et al., 2009). Across both sites, the most abundant species of snags found were

grand fir (*Abies grandis*) and western larch (*Larix occidentalis*), followed by Douglas fir (*Pseudotsuga menziesii*) at CdA and western redcedar (*Thuja plicata*) at StJ.

Field data collection

All snags evaluated for this study were located within 25-m fixed-radius survey plots. Survey plot locations were selected through a stratified random sampling design based on canopy cover and height metrics from lidar (IDFG, 2021) and constrained using criteria to enable subsequent point count surveys of forest birds, based on existing protocols (e.g., Fekety et al., 2018; Dudley and Saab, 2003) including a 300-m minimum distance from other plot centers and a road buffer (minimum of 60 m and maximum of 250 m away from roads). Plot centers were recorded using a global navigation satellite system (GNSS) receiver (Trimble GeoXH; Sunnyvale, CA, USA) and differentially corrected in postprocessing (Fekety et al., 2018).

Snags identified within a 25-m radius survey plot were measured, provided they satisfied the criteria, including: (1) a minimum height equal to breast height (used to measure diameter at breast height, DBH; 1.37m above ground), (2) a minimum DBH of 0.15 m, (3) less than a 45° lean in any direction, and (4) possessed no visible live parts of the tree (primarily the presence of green needles; red/brown needles were accepted and noted). The minimum DBH was selected based on criteria for woodpecker use (see Martinuzzi et al., 2009a). Snag locations were recorded using the same GNSS receiver as used for plot center, which was positioned on the north side of the bole.

Airborne lidar data acquisition and processing

Discrete-return ALS data were acquired across both sites as part of an ongoing effort by the U.S. Forest Service Rocky Mountain Research Station (USFS RMRS; Moscow, ID, USA) to develop advanced protocols for forest mapping and monitoring. The lidar extent of CdA spanned 78,706 ha to the east of Coeur d'Alene, ID, USA (centered at 47°44′40.0″N, 116°36′38.8″W). The lidar extent of StJ spanned 7598 ha to the east of Avery, ID, USA (centered at 47°08′28.5″N, 116°05′38.9″W). Details on the lidar acquisition parameters can be found in Table 4.1. The georeferenced lidar data were processed at the plot level using the R environment (R Core Team 2020, version 4.0.3). Point clouds were preprocessed using the

lidR package (Roussel et al., 2020) at a 50-m radius around plot centers (0.8 ha plots) to generate buffered, height-normalized point clouds. All ground, near-ground, and understory returns below 1.37 m were excluded to retain only canopy returns. Outliers below 50 m height above ground were not removed, as they may represent snag hits.

Snag center coordinates were calculated by subtracting half the measured DBH from the northing value collected in the field, to correct for the GNSS receiver being positioned on the north side of the bole. Snag center coordinates were used as locations to clip the height-normalized ALS point clouds from within each survey plot. Individual snag point clouds were clipped to a 2.5-m circular radius buffer around each snag center, in order to encompass the full tree footprint, offset any error in GPS location, and preserve enough returns to compute all metrics.

Predictor variable selection

Lidar-derived metrics were calculated for each 2.5-m radius snag point cloud, with a minimum height set to 1.37 m above ground. A subset of the full suite of standard height and return-based metrics (as provided in the lidR package; see Roussel et al., 2020) was chosen alongside additional structural and topographic metrics for this study, in order to best evaluate differences among the four classes of snag structural characteristics. We focused on lidar metrics previously shown to be effective indicators of forest biomass across different forest types (e.g., Vogeler et al., 2013; Bouvier et al., 2015) and those which would have specific utility for individual snags, as compared to individual live tree or plot-level analyses (Table 4.2).

Random Forest model development

To analyze whether airborne lidar metrics could be used to discriminate between snag classes, we conducted random forest (RF) classification using the R environment and with the packages randomForest (Liaw and Wiener, 2002) and caret (Kuhn et al., 2021). For our response variables, we focused on two aspects from field inventory data for each snag: diameter and intactness. We divided the candidate snags into two categories for each of these variables, in order to have distinct groups to compare lidar metrics against. Snag diameter was divided into small (DBH less than 40 cm) and large (DBH greater than or equal to 40 cm) groups, based on literature suggesting these are ecologically relevant distinctions (Davis,

1983), as well as important for ALS detectability (Martinuzzi et al., 2009a). Snag intactness was divided into intact (where the snag bole still had a visible top) and broken (where at least part of the bole had broken off) groups. We therefore had four snag classes for our response variable (Figure 4.2): “small intact” (SI), “small broken” (SB), “large intact” (LI), and “large broken” (LB). In total, there were 198 snags evaluated across all snag classes (Table 4.3).

The thirteen lidar-derived metrics (Table 4.2) were used as predictor variables for classification into one of the four snag classes (SI, SB, LI, or LB). The number of RF trees to grow was set to 1000, and the number of predictor variables performing data partitioning at each node (mtry) was set to 13. Pearson’s correlation (r) was used to determine whether any predictor variables were highly correlated ($r > 0.9$; see Appendix A Table A2 Pearson’s correlations among predictor variables). As there was a high correlation found between percent of first returns (P1stRN) and percent of second returns (P2ndRN; $r = 0.97$), a multicollinearity test was performed, and no predictors were found to be collinear. As this study was conducted to investigate how return number metrics interact with snags, we kept both P1stRn and P2ndRN as predictor variables in our RF models. We would recommend that analysis using multivariate models other than RF (e.g., regression) should exclude P1stRN as a variable, as such models may be less resistant to multicollinearity.

For validation purposes, RF models were run within a bootstrap with 20 iterations. For each iteration, we drew 60% of the snags ($n_{train} = 118$) from the total available snag population ($n_{total} = 198$) to train the RF model. The remaining snags not drawn per iteration ($n_{test} = 80$) were used for independent validation of the RF model. For each bootstrap iteration, confusion matrices of observed versus predicted classifications were used to calculate overall accuracy and the kappa statistic (a coefficient ranging from 0 to 1, where 0 is equated with random chance and 1 is perfect concordance; Cohen, 1960), as well as producer’s accuracy (inverse of omission error) and user’s accuracy (inverse of commission error) for each class.

In addition to the confusion matrix, an evaluation of predictor variable importance was reported for the top RF model (RF_{ALL}) in terms of mean decrease in the Gini Index (a measure of the decrease in node impurity; Liaw and Wiener, 2002; Breiman, 2001). To

evaluate the importance of each predictor relative to one another among the four snag classes (and across models), the class- specific variable importance scores were standardized using the Model Improvement Ration (MIR; Evans and Cushman, 2009), whereby all raw variable importance scores were divided by the maximum.

Modeling subset by diameter

We conducted additional RF modeling on subsets of the snags by diameter, modeling only small snags (n_{total} = 82) and only large snags (n_{total} = 116) against the same suite of predictor variables and using the same RF parameters and validation methods. The only change was that classification was reduced from the four snag classes to only two based on snag intactness (intact versus broken top) for each model. The confusion matrix and predictor variable importance tables for the top RF models (small snags = RF_{SM}; large snags = RF_{LG}) let us further evaluate which of the 13 variables were most important for each size class.

Results

Model performance across all four snag classes

Across the 20 iterations of RF models classifying all snags into four classes by diameter and intactness, the top model (RF_{ALL}) had an overall accuracy of 50%, with a kappa statistic of 0.29 (Table 4.4a). Performance accuracies were highly variable by snag class, with large broken top snags having the highest producer's accuracy, small intact snags having the highest user's accuracy, and large intact snags having the lowest accuracy for both (Table 4.4a). The most important overall predictor variables for RF_{ALL} (based on mean decrease in Gini) were percent of third returns (P3rdRN), coefficient of variation in Leaf Area Density (LADcv), elevation (ELEV), and Vegetation Area Index (VAI; Table 4.5a). Three of these top variables were the most important predictors for the individual snag classes (Table 4.5a). The most important variable for both small intact and small broken snags was ELEV; for large intact snags it was VAI, and for large broken snags it was P3rdRN. LADcv was distinct from the other top variables in not being the most important for any given snag class (Table 4.5a).

Model performance subset by diameter

When snags were subset by diameter, RF model performance improved for each subset as compared to the top model for all snags (Table 4.4). For small snags only, across the 20 iterations of RF models classifying snags into two groups by intactness, the overall accuracy of the top model (RF_{SM}) increased by 26% over RF_{ALL}. The confusion matrix for RF_{SM} (Table 4.4b) showed much higher performance accuracies across both classes. Out of the top three overall predictor variables from RF_{ALL}, only LADcv remained in the top three overall for RF_{SM} (Table 4.5b).

For large snags only, across the 20 iterations of RF models classifying snags into two groups by intactness, the overall accuracy of the top model (RF_{LG}) increased by 27% over RF_{ALL}. The confusion matrix for RF_{LG} showed improved performance accuracies across each class except for (large) broken snags; producer's accuracy had the lowest value of the snag subsets (50% for broken tops), but also the highest value (93% for intact tops; Table 4.4c). Out of the top three overall predictor variables from RF_{ALL}, once again LADcv remained in the top three overall for RF_{LG}, as well as P3rdRN (Table 4.5c).

Discussion

Advancing our understanding of where broken-top snags occur within a closed-canopy forest has the potential to benefit habitat management for multiple wildlife species. Our goal was to explore whether ALS data could be used to differentiate tree top intactness of snags with known structural characteristics of value to wildlife. To our knowledge, this was the first study to use ALS data to focus on structural differences among snags, particularly in closed-canopy conifer forests.

The accuracy of our overall RF model for classifying snags by diameter and intactness was relatively low, suggesting there may not have been clear enough distinctions among the four snag classes to accurately distinguish all of them at the individual tree level with airborne lidar alone. Inclusion of additional information provided by other sensors, such as very-high-resolution satellite or airborne (including unmanned aircraft systems or UAS) imagery, could improve discrimination capability. Adjusting the modeling strategy also has

potential for improvement. When our models were subset by diameter to examine intactness among only small snags and only large snags separately, the overall model accuracies and kappa statistics both improved to above 75% and 0.45, respectively. These findings suggested there is potential for improved applications given further refinement, especially when focused more narrowly on one or two snag classes.

One factor that is important to consider with ALS applications relative to snag detection and characterization of snag characteristics is the ALS point density. Higher point densities are generally associated with high levels of accuracy. For instance, Krzystek et al. (2020) were able to characterize snags via lidar metrics and 3D shape from an ALS dataset with excellent accuracy (> 90%), but with a much greater point density (55 points/m^2) than available for our study. The snags studied were primarily pest-infected, and thus had accumulated in larger groups (Krzystek et al., 2020), which represented a much different context than our study of using ALS to classify individual snags across a closed-canopy forest. Other studies also had relatively high accuracies associated with ALS applications of snags with relatively high point densities (Yao et al., 2012; Vauhkonen et al., 2011; Kim et al., 2009; Bright et al., 2013; Wing et al., 2015; Casas et al., 2016).

In order to place our point densities within a broader standardized framework, we used the Topographic Data Quality Levels (QLs) as defined by the United States Geological Survey (USGS) 3D Elevation Program (USGS, 2021) to evaluate the quality of our ALS datasets. We focused on three QLs (based on points per meter squared): QL1 (≥8), QL2 (2–7.9), and QL3 (0.5–1.9). The overall point density across both sitewide lidar acquisitions in our study was 4.2 points/m^2 (placing it within the QL2 category), but point densities of individual snags varied a great deal, and spanned all three QLs. Even within the same survey plot, point densities could be highly variable. For example, one plot with 12 snags had point densities that ranged from 1.7 to 20.4 points/m^2, spanning all three QLs (Figure 4.3). We found the lower limit of point densities required to properly calculate the lidar metrics of interest around individual snags was 1 point/m^2.

There were no strong drivers affecting point densities universally, though elevation did show weak negative associations (higher elevations had lower point densities across

sites). Two additional factors that likely contributed to variable QLs around individual snags were scan angle and surrounding live crown proximity. Scan angle showed no strong relationship with point density but may still have played important albeit disparate roles in reflecting snag returns: returns close to nadir may have better reflected the tops of snags surrounded by dense taller canopies and differentiated them from a true gap, while shallower view pulse angles were more likely to reflect a greater number of returns from snag boles, especially at the edge of gaps. Surrounding live crown proximity likely affected QLs as well; live tree canopy returns within the 5-m diameter point cloud around a given snag would be counted toward snag point density, falsely raising QL. This is an expected challenge when looking for lone snags in a dense closed-canopy forest; many of the snags we surveyed were found at the edge of a gap, with some partially or almost completely underneath surrounding live canopy, especially broken-top snags. All of these factors combined suggested that the relatively low point densities in our ALS data likely contributed to a limited ability to classify tree intactness when small snags were included in the data sets.

Our finding that larger DBH snags were identified with higher classification accuracies was consistent with previous snag-detection work. Prior work in mapping snag presence or absence has shown DBH to be a strong predictor of snag-detection probability (Martinuzzi et al., 2009a; Wing et al., 2015), where the likelihood of detecting snags increased with diameter. Our results were consistent with these findings, even though we were investigating the ability of ALS to classify snag characteristics, as opposed to detecting snags.

It is important to note that the ecological context of remote-sensing studies focused on snag detection can vary widely. Much of the previous work in mapping snags has been carried out where one type of massive tree die-off event has occurred, such as a wildfire or beetle kill/outbreak (Yao et al., 2012; Kim et al., 2009; Bright et al., 2013; Casas et al., 2016; Krzystek et al., 2020). While such results certainly provide opportunities to evaluate the power of remote sensing to address snag-related questions of distribution and biomass, the structural characteristics of the snags themselves have not typically been the focus of wildlife-related investigations, although the role of these snags for wildlife use has been well documented (Vogeler et al., 2014; Saab et al., 2009).

Of particular interest to us, though, are individual snags that are embedded within dense live conifer forests that provide a valuable resource for many wildlife species. Our focus on the structural characteristics of broken versus intact tops of snags has important relevance for many wildlife species of management interest. For instance, the federally listed northern spotted owl (*Strix occidentalis caurina*; USFWS, 2021) uses snags as platforms for nesting, as do multiple other species of management interest, such as the Northern goshawk and great gray owl (Squires and Reynolds, 1997; Wu et al., 2015; IDFG, 2021; Bull et al., 1997). These species also require forests with high canopy closure for foraging and protection from predators (North et al., 1999; Squires and Reynolds, 1997; Wu et al., 2015; USFWS, 2021). Further, the importance of broken tops for wildlife is not limited to direct nesting or roosting use; broken tops also serve as an indicator of additional use by wildlife, particularly in the form of woodpecker cavity excavation (McClelland and McClelland, 1999). Nests excavated by woodpeckers (primarily in snags) can support entire networks of cavity-reliant bird and mammal species within conifer-dominated forests (Martin et al., 2004; Aitken and Martin, 2007; Blanc and Walters, 2008), lending added importance to the value of identifying broken-top snags amongst closed-canopy forests for wildlife management efforts.

This individual tree approach was meant as a case study to better inform workflows at broader extents. We sought to improve parameterization for individual structural elements, in order to improve upon search patterns applied across entire landscapes. Viewing these results as one step within a broader stepwise approach for forest characterization via ALS-derived lidar metrics lends greater weight to our findings. A prerequisite first step could be to refine RF modeling at the plot or stand level to differentiate live trees from snags (e.g., Casas et al., 2016) prior to RF modeling at the individual tree level, to evaluate within-group differences among live tree and snag characteristics separately. While our study was novel in attempting to differentiate structural differences among snags, there is a great deal of value in looking at how this methodology compares to and can be combined with pre-existing methods in snag modeling (e.g., via intensity and height-based metrics: Martinuzzi et al., 2009a; Kim et al., 2009; Wing et al., 2015; Casas et al., 2016; Krzystek et al. 2020).

Going forward, we would suggest that those wishing to apply some aspect of these methods do the following to yield better results: focus on metrics for one class at a time (e.g., large broken-top snags only), and raise the height cutoff to 5 or 10 m above ground. Additionally, if calibrated ALS intensity data (or very-high-resolution imagery) are available, it would certainly be worth incorporating, either into RF models or for other methods of snag characterization. Further, higher-density point clouds (QL1) would undoubtedly improve model performance, and likely better distinguish among groups. Thankfully, the structural features of snags on which we focused (based on benefit to wildlife) were positively correlated with characterization via ALS, which suggested there is value in focusing more closely on just those snag classes that hold the greatest benefits for wildlife: larger-diameter snags, as well as broken-top snags (Michel and Winter, 2009; Basile et al., 2020; Bull et al., 1997). By limiting the focus of snag detection or modeling efforts to the binary of presence/absence for large broken snags only, the focus can shift to lidar (or spectral) metrics most strongly correlated with this class (e.g., LADcv, ENTmid, and P3rdRN).

Conclusions

While we used ALS alone in this study, the next step would be to focus on multisensor or data-fusion approaches (such as incorporating multi- or hyperspectral lidar data, satellite imagery, and/or photogrammetry), which could lead to far more robust predictions resulting from a greater diversity of spatial, spectral, and temporal resolutions that add complementary dimensions of information (Wing et al., 2015; Casas et al., 2016; Boucher et al., 2020). Employing modeling methods other than RF (such as imputation [Hudak et al., 2008], gradient boosting [Zhang et al., 2019], or artificial neural networks [Neuville et al., 2021]) may also lead to improved results and uncover useful predictors of forest structures not previously applied. As open-access data sets continue to be more widely accessible, the concepts discussed become more readily applicable; applying novel methods to broader swaths of data becomes more feasible, incorporating multiple sources of data becomes easier, and comparisons of competing methodologies can be tested more rigorously. We encourage continued investigation of ways in which new and upcoming tools can be used

to better characterize forest structures remotely, across a variety of landscapes, especially with respect to snags and other wildlife habitat features.

Literature Cited

Aitken, K. E. H., & Martin, K. (2007). The importance of excavators in hole-nesting communities: availability and use of natural tree holes in old mixed forests of western Canada. *Journal of Ornithology, 148*(S2), 425–434. https://doi.org/10.1007/s10336-007-0166-9

Asbeck, T., Basile, M., Stitt, J., Bauhus, J., Storch, I., & Vierling, K. T. (2020). Tree-related microhabitats are similar in mountain forests of Europe and North America and their occurrence may be explained by tree functional groups. *Trees, 34*(6), 1453–1466. https://doi.org/10.1007/s00468-020-02017-3

Basile, M., Asbeck, T., Pacioni, C., Mikusiński, G., & Storch, I. (2020). Woodpecker cavity establishment in managed forests: relative rather than absolute tree size matters. *Wildlife Biology, 2020*(1). https://doi.org/10.2981/wlb.00564

Bater, C. W., Coops, N. C., Gergel, S. E., LeMay, V., & Collins, D. (2009). Estimation of standing dead tree class distributions in northwest coastal forests using lidar remote sensing. *Canadian Journal of Forest Research, 39*(6), 1080–1091. https://doi.org/10.1139/x09-030

Blanc, L. A., & Walters, J. R. (2008). Cavity excavation and enlargement as mechanisms for indirect interactions in an avian community. *Ecology 89*(2), 506–514. https://doi.org/10.1890/07-0219.1

Boucher, P. B., Hancock, S., Orwig, D. A., Duncanson, L., Armston, J., Tang, H., Krause, K., Cook, B., Paynter, I., Li, Z., Elmes, A., & Schaaf, C. (2020). Detecting change in forest structure with simulated GEDI lidar waveforms: A case study of the hemlock woolly adelgid (HWA; *Adelges tsugae*) infestation. *Remote Sensing, 12*(8), 1304. https://doi.org/10.3390/rs12081304

Bouvier, M., Durrieu, S., Fournier, R. A., & Renaud, J. P. (2015). Generalizing predictive models of forest inventory attributes using an area-based approach with airborne LiDAR data. *Remote Sensing of Environment, 156*, 322–334. https://doi.org/10.1016/j.rse.2014.10.004

Breiman, L. (2001). Random Forests. *Machine Learning, 45*(1), 5–32. https://doi.org/10.1023/A:1010933404324

Bright, B. C., Hudak, A. T., McGaughey, R., Andersen, H. E., & Negrón, J. (2013). Predicting live and dead tree basal area of bark beetle affected forests from discrete-return lidar. *Canadian Journal of Remote Sensing, 39*, S99–S111. https://doi.org/10.5589/m13-027

Bull, E. L., Parks, C. G., & Torgersen, T. R. (1997). Trees and logs important to wildlife in the Interior Columbia River Basin (PNW-GTR-391). U.S. Department of Agriculture,

Forest Service, Pacific Northwest Research Station. https://doi.org/10.2737/PNW-GTR-391

Casas, Á., García, M., Siegel, R. B., Koltunov, A., Ramírez, C., & Ustin, S. (2016). Burned forest characterization at single-tree level with airborne laser scanning for assessing wildlife habitat. *Remote Sensing of Environment, 175*, 231–241. https://doi.org/10.1016/j.rse.2015.12.044

Cohen, J. (1960). A coefficient of agreement for nominal scales. *Educational and Psychological Measurement, 20*(1), 37–46. https://doi.org/10.1177/001316446002000104

Conner, R. N., Miller, O. K., & Adkisson, C. S. (1976). Woodpecker dependence on trees infected by fungal heart rots. *The Wilson Bulletin, 88*(4), 575–581. http://www.jstor.org/stable/4160827

Davies, A. B., & Asner, G. P. (2014). Advances in animal ecology from 3D-LiDAR ecosystem mapping. *Trends in Ecology & Evolution, 29*(12), 681–691. https://doi.org/10.1016/j.tree.2014.10.005

Davis, J. W. (1983). Snags are for wildlife. In Proceedings of the Symposium on Snag Habitat Management. USDA Forest Service General Technical Report RM-99 4–9.

Dudley, J. G. (2003). A field protocol to monitor cavity-nesting birds. United States Department of Agriculture, Forest Service, Rocky Mountain Research Station.

Evans, J. S., & Cushman, S. A. (2009). Gradient modeling of conifer species using random forests. *Landscape Ecology, 24*(5), 673–683. https://doi.org/10.1007/s10980-009-9341-0

Fekety, P. A., Falkowski, M. J., Hudak, A. T., Jain, T. B., & Evans, J. S. (2018). Transferability of lidar-derived basal area and stem density models within a northern Idaho ecoregion. *Canadian Journal of Remote Sensing, 44*(2), 131–143. https://doi.org/10.1080/07038992.2018.1461557

Fielder, P. C., & Starkey, R. G. (1986). Bald eagle perch-sites in eastern Washington. *Northwest Science, 60,* 186–190.

Hudak, A. T., Crookston, N. L., Evans, J. S., Hall, D. E., & Falkowski, M. J. (2008). Nearest neighbor imputation of species-level, plot-scale forest structure attributes from LiDAR data. *Remote Sensing of Environment, 112*(5), 2232–2245. https://doi.org/10.1016/j.rse.2007.10.009

Idaho Department of Fish and Game (IDFG). (2016). Species of Greatest Conservation Need. https://idfg.idaho.gov/species/taxa/list/sgcn

Jung, K., Kaiser, S., Böhm, S., Nieschulze, J., & Kalko, E. K. V. (2012). Moving in three dimensions: Effects of structural complexity on occurrence and activity of insectivorous bats in managed forest stands. *The Journal of Applied Ecology, 49*(2), 523–531. https://doi.org/10.1111/j.1365-2664.2012.02116.x

Kim, Y., Yang, Z., Cohen, W. B., Pflugmacher, D., Lauver, C. L., & Vankat, J. L. (2009). Distinguishing between live and dead standing tree biomass on the North Rim of

Grand Canyon National Park, USA using small-footprint lidar data. *Remote Sensing of Environment, 113*(11), 2499–2510. https://doi.org/10.1016/j.rse.2009.07.010

Kuhn, M., Wing, J., Weston, S., Williams, A., Keefer, C., Engelhardt, A., Cooper, T., Mayer, Z., Kenkel, B., & Others. (2020). Caret: classification and regression training. R Package Version 6.0-86. https://cran.r-project.org/web/packages/caret/caret.pdf

Larrieu, L., Paillet, Y., Winter, S., Bütler, R., Kraus, D., Krumm, F., Lachat, T., Michel, A. K., Regnery, B., & Vandekerkhove, K. (2018). Tree related microhabitats in temperate and Mediterranean European forests: A hierarchical typology for inventory standardization. *Ecological Indicators, 84,* 194–207. https://doi.org/10.1016/j.ecolind.2017.08.051

LaRue, E. A., Wagner, F. W., Fei, S., Atkins, J. W., Fahey, R. T., Gough, C. M., & Hardiman, B. S. (2020). Compatibility of aerial and terrestrial LiDAR for quantifying forest structural diversity. *Remote Sensing, 12*(9), 1407. https://doi.org/10.3390/rs12091407

Liaw, A., & Wiener, M. (2002). Classification and regression by randomForest. *R News, 2*(3), 18–22.

Lorenz, T. J., Vierling, K. T., Johnson, T. R., & Fischer, P. C. (2015). The role of wood hardness in limiting nest site selection in avian cavity excavators. *Ecological Applications, 25*(4), 1016–1033. https://doi.org/10.1890/14-1042.1

MacArthur, R. H., & MacArthur, J. W. (1961). On bird species diversity. *Ecology, 42*(3), 594–598. https://doi.org/10.2307/1932254

Martin, K., Aitken, K. E. H., & Wiebe, K. L. (2004). Nest sites and nest webs for cavity-nesting communities in interior British Columbia, Canada: Nest characteristics and niche partitioning. *The Condor*. https://doi.org/10.1650/7482

Martinuzzi, S., Vierling, L. A., Gould, W. A., Falkowski, M. J., Evans, J. S., Hudak, A. T., & Vierling, K. T. (2009a). Mapping snags and understory shrubs for a LiDAR-based assessment of wildlife habitat suitability. *Remote Sensing of Environment, 113*(12), 2533–2546. https://doi.org/10.1016/j.rse.2009.07.002

Martinuzzi, S., Vierling, L. A., Gould, W. A., & Vierling, K. T. (2009b). Improving the characterization and mapping of wildlife habitats with lidar data: Measurement priorities for the inland northwest, USA. *Gap Analysis Bulletin, 16,* 1–8.

McClelland, B. R., & McClelland, P. T. (1999). Pileated woodpecker nest and roost trees in Montana: Links with old-growth and forest "health." *Wildlife Society Bulletin, 27*(3), 846–857. http://www.jstor.org/stable/3784108

Michel, A. K., & Winter, S. (2009). Tree microhabitat structures as indicators of biodiversity in Douglas-fir forests of different stand ages and management histories in the Pacific Northwest, U.S.A. *Forest Ecology and Management, 257*(6), 1453–1464. https://doi.org/10.1016/j.foreco.2008.11.027

Miller, E., & Miller, D. R. (1980). Snag use by birds. Management for Non-Game Birds. Gen. Tech. Rep. INT-GTR-86. Ogden, UT: Intermountain Forest and Range Experiment Station, Forest Service, US Department of Agriculture, 337–356.

Neuville, R., Bates, J. S., & Jonard, F. (2021). Estimating forest structure from UAV-mounted LiDAR point cloud using machine learning. *Remote Sensing, 13*(3), 352. https://doi.org/10.3390/rs13030352

North, M. P., Franklin, J. F., Carey, A. B., Forsman, E. D., & Hamer, T. (1999). Forest stand structure of the northern spotted owl's foraging habitat. *Forest Science, 45*(4), 520–527. https://doi.org/10.1093/forestscience/45.4.520

Pesonen, A., Maltamo, M., Eerikäinen, K., & Packalèn, P. (2008). Airborne laser scanning-based prediction of coarse woody debris volumes in a conservation area. *Forest Ecology and Management, 255*(8), 3288–3296. https://doi.org/10.1016/j.foreco.2008.02.017

Pretzsch, H. (2009). Description and analysis of stand structures. In Forest Dynamics, Growth and Yield: From Measurement to Model (pp. 223–289). Springer, Berlin Heidelberg. https://doi.org/10.1007/978-3-540-88307-4_7

Rayner, A. D. M., & Boddy, L. (1988). Fungal decomposition of wood: Its biology and ecology. John Wiley & Sons Ltd, Chicheste.

Reitberger, J., Krzystek, P., & Stilla, U. (2008). 3D segmentation and classification of single trees with full waveform LIDAR data. *Proceedings of SilviLaser, 8,* 216–226.

Roussel, J. R., Auty, D., Coops, N. C., Tompalski, P., Goodbody, T. R. H., Meador, A. S., Bourdon, J. F., de Boissieu, F., & Achim, A. (2020). lidR: An R package for analysis of Airborne Laser Scanning (ALS) data. *Remote Sensing of Environment, 251,* 112061. https://doi.org/10.1016/j.rse.2020.112061

Sadoti, G., Pollock, M. G., Vierling, K. T., & Albright, T. P. (2014). Variogram models reveal habitat gradients predicting patterns of territory occupancy and nest survival among vesper sparrows. *Wildlife Biology, 20*(2), 97–107. https://doi.org/10.2981/wlb.13056

Squires, J. R., & Reynolds, R. T. (1997). Northern goshawk (*Accipiter gentilis*). In The Birds of North America. Washington, DC: The Academy of Natural Sciences, Philadelphia, PA.

Staniaszek-Kik, M., Chmura, D., & Żarnowiec, J. (2019). What factors influence colonization of lichens, liverworts, mosses and vascular plants on snags? *Biologia, 74*(4), 375–384. https://doi.org/10.2478/s11756-019-00191-5

Stitt, J. M., Hudak, A. T., Silva, C. A., Vierling, L. A., & Vierling, K. T. (2021). Characterizing individual tree-level snags using airborne lidar-derived forest canopy gaps within closed-canopy conifer forests. *Methods in Ecology and Evolution, 13,* 473–484. https://doi.org/10.1111/2041-210x.13752

Tews, J., Brose, U., Grimm, V., Tielbörger, K., Wichmann, M. C., Schwager, M., & Jeltsch, F. (2004). Animal species diversity driven by habitat heterogeneity/diversity: the importance of keystone structures: Animal species diversity driven by habitat heterogeneity. *Journal of Biogeography, 31(1),* 79–92. https://doi.org/10.1046/j.0305-0270.2003.00994.x

U.S. Fish & Wildlife Service (US FWS). (2021). FWS-Listed U.S. Species by Taxonomic Group - All Animals. https://ecos.fws.gov/ecp/report/species-listings-by-tax-group?statusCategory=Listed&groupName=All%20Animals

van Ewijk, K. Y., Treitz, P. M., & Scott, N. A. (2011). Characterizing forest succession in central Ontario using lidar-derived indices. *Photogrammetric Engineering & Remote Sensing, 77*(3), 261–269. https://doi.org/10.14358/PERS.77.3.261

Vauhkonen, J., Ene, L., Gupta, S., Heinzel, J., Holmgren, J., Pitkänen, J., Solberg, S., Wang, Y., Weinacker, H., Hauglin, K. M., Lien, V., Packalén, P., Gobakken, T., Koch, B., Næsset, E., Tokola, T., & Maltamo, M. (2011). Comparative testing of single-tree detection algorithms under different types of forest. *Forestry, 85*(1), 27–40. https://doi.org/10.1093/forestry/cpr051

Vogeler, J. C., Hudak, A. T., Vierling, L. A., & Vierling, K. T. (2013). Lidar-derived canopy architecture predicts brown creeper occupancy of two western coniferous forests. *The Condor, 115*(3), 614–622. https://doi.org/10.1525/cond.2013.110082

Wing, B. M., Ritchie, M. W., Boston, K., Cohen, W. B., & Olsen, M. J. (2015). Individual snag detection using neighborhood attribute filtered airborne lidar data. *Remote Sensing of Environment, 163*, 165–179. https://doi.org/10.1016/j.rse.2015.03.013

Wu, J. X., Siegel, R. B., Loffland, H. L., Tingley, M. W., Stock, S. L., Roberts, K. N., Keane, J. J., Medley, J. R., Bridgman, R., & Stermer, C. (2015). Diversity of great gray owl nest sites and nesting habitats in California. *The Journal of Wildlife Management, 79*(6), 937–947. https://doi.org/10.1002/jwmg.910

Yao, W., Krzystek, P., & Heurich, M. (2012). Identifying standing dead trees in forest areas based on 3D single tree detection from full waveform lidar data. *ISPRS Annals of the Protogrammetry.*

Zellweger, F., Braunisch, V., Baltensweiler, A., & Bollmann, K. (2013). Remotely sensed forest structural complexity predicts multi-species occurrence at the landscape scale. *Forest Ecology and Management, 307*, 303–312. https://doi.org/10.1016/j.foreco.2013.07.023

Zhang, J., Lu, C., Xu, H., & Wang, G. (2019). Estimating aboveground biomass of *Pinus densata*-dominated forests using Landsat time series and permanent sample plot data. *Journal of Forest Economics, 30*(5), 1689–1706. https://doi.org/10.1007/s11676-018-0713-7

Tables

Table 4.1 Lidar acquisition parameters.

The discrete-return airborne lidar (also airborne laser scanning, ALS) data from the two study sites (based on IPNF Ranger Districts: Coeur d'Alene River, CdA; Saint Joe, StJ) were part of a larger acquisition carried out by USFS RMRS in 2016 (see Fekety et al. [2018] for more details).

Parameter	Specification
Date collected	12 October 2016
Vendor	Atlantic Group, LLC
Sensor	Leica ALS70-HP
Flight altitude	1965 m above ground level
Flight speed	110 kts
Pulse frequency	278 kHz
Scan frequency	41 Hz
Scan angle	± 30º
Swath width	1098 m
Swath overlap	50%
Laser wavelength	1064 nm
Laser beam divergence	0.22 mrad
Vertical accuracy	5.9 cm
Footprint diameter	43 cm
Nominal pulse density	4.2 pulses/m^2

Table 4.2 Airborne lidar-derived metrics used as predictor variables

Airborne lidar-derived metrics used as predictor variables in RF models to classify snag characteristics of snags measured in Idaho coniferous forests. For additional information on equations and ecological significance of each predictor variable, please see Appendix A Table A3 Airborne-lidar-derived metrics used as predictor variables in random forest (RF) models..

Variable	Description
PTDEN	Point density; number of total returns per meter
P1stRN	Percent of first returns (out of total returns)
P2ndRN	Percent of second returns (out of total returns)
P3rdRN	Percent of third returns (out of total returns)
GFPmid	Gap Fraction Profile (GFP), calculated only for midcanopy heights (every 1 m between 5 m and 20 m above ground)
LADcv	Leaf Area Density (LAD) coefficient of variance; derived from measures every 2 m across all canopy heights
RUMPLE	Rumple index; roughness of a surface based on ratio between surface area and projected area on the ground
ENTmid	Entropy, calculated only for midcanopy heights (between 5 m and 20 m above ground); normalized Shannon diversity and evenness index
VAI	Vegetation Area Index (VAI); sum of LAD values, derived from measures every 2 m across all canopy heights
VCI	Vertical Complexity Index (VCI); fixed normalization of entropy across heights, derived from measures every 2 m across all canopy heights
ELEV	Elevation (in meters), averaged across the 25-m radius reference plot
SLOPE	Slope (in degrees), averaged across the 25-m radius reference plot
TRASP	Transformed aspect (in degrees), averaged across the 25-m radius reference plot

Table 4.3 Summary statistics by snag class

Summary statistics by snag class across all snags (n = 198) measured in conifer forests in Idaho, USA. A breakdown of airborne lidar point density (total returns/area) per snag point cloud is included, with mean (μ) and standard deviation (sd) for each snag class. Snags split by study site are not shown, but overall there were more snags at CdA (n = 141) than StJ (n = 63), driven primarily by a greater number of broken top snags in both size classes.

Diameter	Intactness	Number of Snags	Point Density (μ ± sd)
Small (< 40 cm)	Intact	35	13.2 ± 7
	Broken	48	11.2 ± 5
Large (≥ 40 cm)	Intact	44	12.4 ± 5
	Broken	77	12.4 ± 7

Table 4.4 Confusion matrices from top random forest models

Confusion matrices from the top random forest models for classifying snags within conifer forests in Idaho, USA. RF classification used ALS lidar metrics to split snags into groups across known characteristics. There were three RF models used across the full dataset: **(a)** all snags (split into four classes: "small intact" (SI), "small broken" (SB), "large intact" (LI), and "large broken" (LB); n_{train} = 118, n_{test} = 80); **(b)** small-diameter snags only (using intactness as a binary class; n_{train} = 49, n_{test} = 33); and **(c)** large-diameter snags only (using intactness as a binary class; n_{train} = 69, n_{test} = 47). In each table, the matrix on the left shows the number of correct and incorrect classifications per snag class; correct classifications are those where the predicted matched the observed snag class, highlighted in grey on the diagonal. On the right, the accuracy metrics per class are shown in grey: producer's accuracy (correct / observed sum) and user's accuracy (correct / predicted sum). Overall accuracy and the kappa statistic are listed in the bottom-left corner of each table; on the bottom-right are the top three predictor variables for the model (ranked by mean decrease in Gini).

(a) All snags

		Observed						
	Class	**SI**	**SB**	**LI**	**LB**	*Sum*	Producer's accuracy (%)	User's accuracy (%)
Predicted	**SI**	6	1	1	0	*8*	35.3	75.0
	SB	7	8	3	2	*20*	50.0	40.0
	LI	1	1	3	5	*10*	17.7	30.0
	LB	3	6	10	23	*42*	76.7	54.8
	Sum	*17*	*16*	*17*	*30*	*80*		

Overall accuracy = 50%; kappa = 0.29 — Top predictors: P3rdRN, LADcv, ELEV

(b) Small snags only

		Observed				
	Class	**Intact**	**Broken**	*Sum*	Producer's accuracy (%)	User's accuracy (%)
Predicted	**Intact**	17	3	*20*	77.3	85.0
	Broken	5	8	*13*	72.7	61.5
	Sum	*22*	*11*	*33*		

Overall accuracy = 76%; kappa = 0.49 — Top predictors: LADcv, PTDEN, ENTmid

(c) Large snags only

		Observed				
	Class	**Intact**	**Broken**	*Sum*	Producer's accuracy (%)	User's accuracy (%)
Predicted	**Intact**	27	9	*36*	93.1	75.0
	Broken	2	9	*11*	50.0	81.8
	Sum	*29*	*18*	*47*		

Overall accuracy = 77%; kappa = 0.47 — Top predictors: LADcv, ENTmid, P3rdRN

Table 4.5 Predictor variable importance from top random forest models

Predictor variable importance from the top random forest models for classifying snags within conifer forests in Idaho, USA. There were three RF models used across the full dataset: **(a)** all snags (with four classes: "small intact" (SI), "small broken" (SB), "large intact" (LI), and "large broken" (LB)); **(b)** small-diameter snags only (using intactness as a binary class); and **(c)** large-diameter snags only (using intactness as a binary class). For the class-specific columns, all scores for each class were adjusted via MIR, where each value was divided by the largest absolute value as a means of standardization across models (Evans and Cushman, 2009). The mean decrease in Gini (MDGini) refers to the total decrease in node impurities from splitting on that variable averaged over all RF trees (Liaw and Wiener, 2002). All rows are sorted by MDGini (indicated by the small down arrow), as this was used to rank predictor variables in terms of overall variable importance.

a) All snags

Variable	SI	SB	LI	LB	MDGini ↓
P3rdRN	−0.53	0.25	−0.13	1.00	9.513
LADcv	0.06	−0.41	−0.21	0.36	8.105
ELEV	0.46	0.43	0.07	−0.11	7.636
VAI	0.01	−0.21	0.51	−0.07	7.445
VCI	−0.25	−0.04	−0.08	0.47	7.365
ENTmid	−0.24	−0.34	0.18	0.14	7.113
RUMPLE	0.00	0.07	0.01	−0.27	6.804
GFPmid	0.03	−0.24	−0.09	−0.10	6.022
SLOPE	0.28	0.30	0.00	0.09	5.964
PTDEN	−0.44	−0.35	−0.26	0.10	5.827
P1stRN	−0.28	−0.10	0.05	0.17	4.900
P2ndRN	−0.17	−0.26	−0.24	0.35	4.536
TRASP	−0.22	−0.42	0.17	−0.06	4.028

(b) Small snags only

Variable	Intact	Broken	MDGini ↓
LADcv	0.94	0.39	3.60
PTDEN	0.98	0.64	3.12
ENTmid	−0.99	−0.34	2.41
GFPmid	−0.52	−1.00	2.29
ELEV	0.72	−0.11	1.90
SLOPE	−0.14	−0.51	1.81
P1stRN	0.04	−0.15	1.78
P3rdRN	−0.42	−0.04	1.57
VAI	0.37	−0.38	1.56
TRASP	−0.51	−0.06	1.19
VCI	−0.57	−0.47	1.04
RUMPLE	−0.97	−0.44	0.94
P2ndRN	−0.93	−0.47	0.82

(c) Large snags only

Variable	Intact	Broken	MDGini ↓
LADcv	−0.61	0.02	5.34
ENTmid	−0.31	0.01	3.43
P3rdRN	−0.64	0.27	2.90
PTDEN	−0.45	−0.01	2.37
ELEV	−0.32	−0.23	2.25
RUMPLE	−0.47	0.22	2.19
VCI	−0.69	−0.10	2.15
GFPmid	−1.00	−0.48	2.15
VAI	−0.72	−0.38	2.01
TRASP	−0.35	−0.15	1.97
SLOPE	−0.27	0.37	1.89
P2ndRN	−0.55	0.18	1.47
P1stRN	−0.66	0.29	1.16

Figures

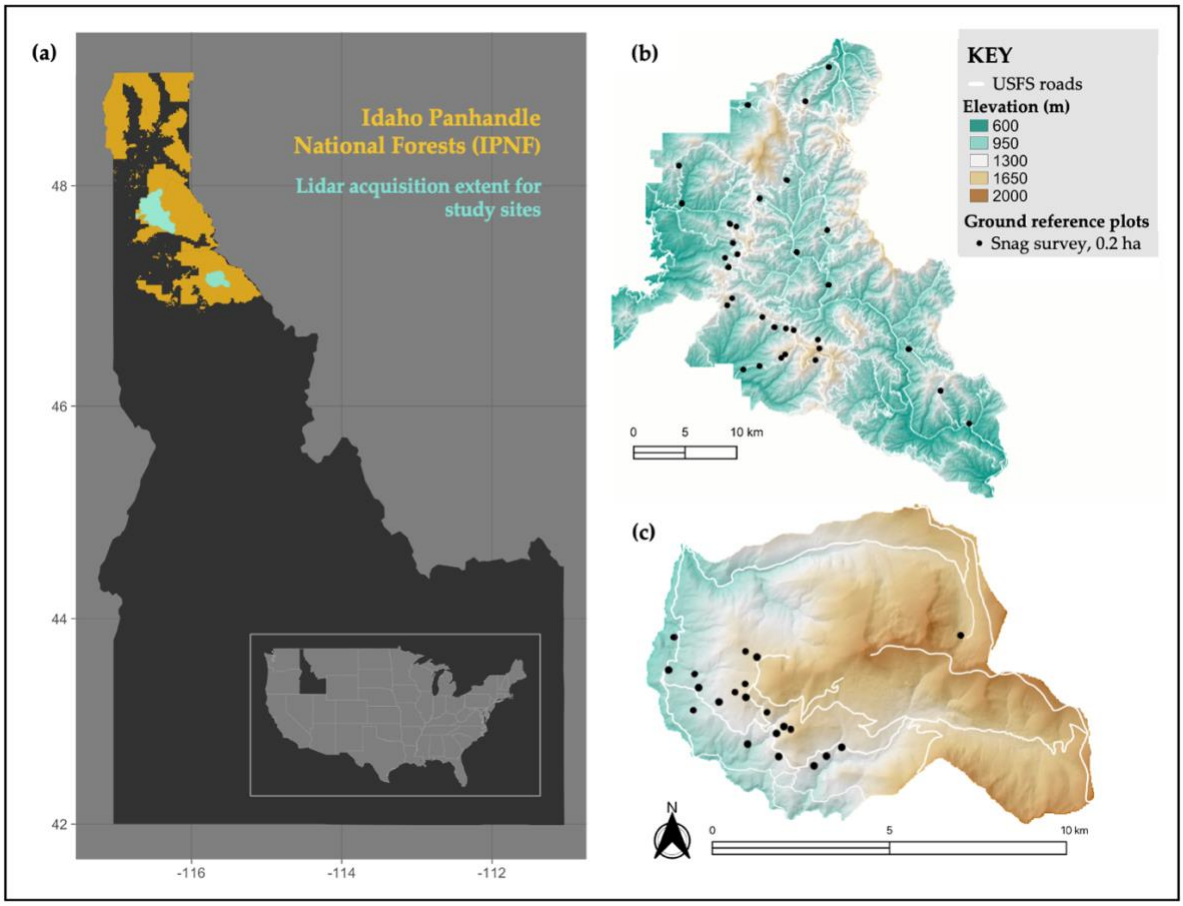

Figure 4.1 Map of the study area

(a) Study area within Idaho Panhandle National Forests (IPNF) in northern Idaho, United States of America. There were two lidar acquisitions in the IPNF where all ground reference survey data were collected: within the **(b)** Coeur d'Alene River (CdA) and **(c)** Saint Joe (StJ) Ranger Districts. Please note the different scales for each site. Across the two sites there were a total of 53 25-m radius ground reference plots (0.2 ha; black circles) where the 198 snags included in this study were surveyed. This figure has been adapted from Stitt et al. (2021).

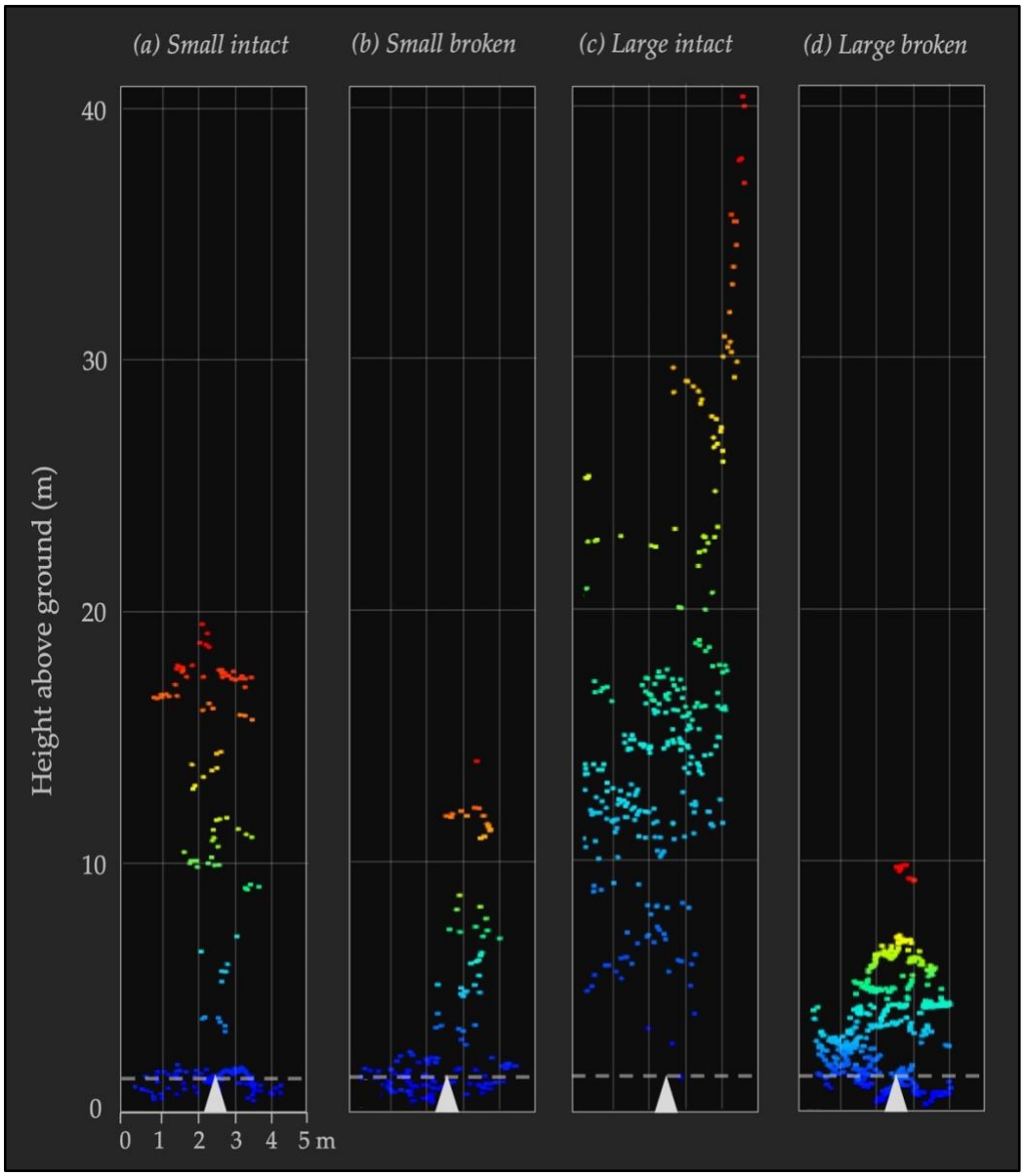

Figure 4.2 Sample lidar point clouds by snag class

Representative ALS point clouds for each snag class are viewed from ground level as 2.5 m-radius circular clips around snag center coordinates (marked by white triangles). Lidar returns are colored by height above ground. The dashed horizontal line represents the height at which snag diameter was measured (1.37 m above ground). The four snag classes shown illustrate the differences across diameter (small [<40 cm DBH] vs. large [≥40 cm DBH]) and intactness (intact vs. broken top): **(a)** a representative "small intact" (SI) snag; **(b)** a representative "small broken" (SB) snag; **(c)** a representative "large intact" (LI) snag; **(d)** a representative "large broken" (LB) snag.

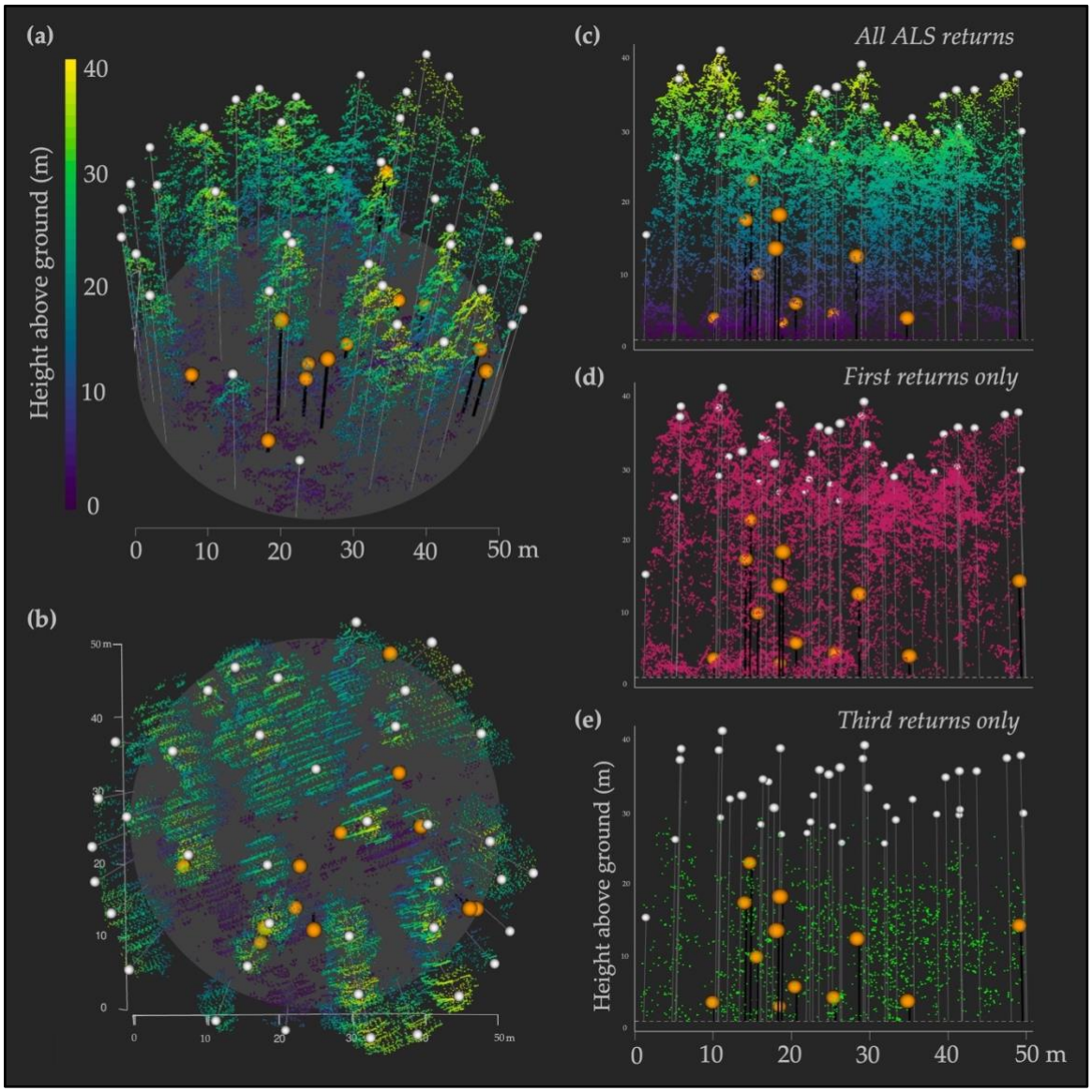

Figure 4.3 Example of a 50-m diameter IPNF survey plot illustrating variability in point densities

Snags and live trees are overlaid on the ALS point cloud of a representative survey plot (with points below 1.37 m omitted), where orange circles with black lines represent snag locations and heights, and white circles with white lines represent live tree locations and heights. Multiple views of the same point cloud are shown to illustrate different aspects of interest: **(a)** plot viewed from an angle to best show stand structure and individual tree canopies and spacing; **(b)** plot viewed from directly above (at nadir) to best show parallel scan angles, variations in point density, snag and gap distributions, and the absence of returns around multiple snags; **(c–e)** plot viewed from ground level to best show tree heights and ALS returns across three versions, where **(c)** includes all returns (colored by height) to highlight a relatively uniform point distribution across vertical heights, as well as show that nearly all live trees were in the upper strata of heights relative to snags; **(d)** includes first returns only to highlight the notably greater first return densities in the upper canopy; and **(e)** includes third returns only to highlight that the majority of third returns fell within the midcanopy range, below live tree crowns.

Chapter 5: Conclusion

This dissertation focused on exploring new ways lidar data can be incorporated to measure biodiversity indicators via assessing two keystone structures found in closed-canopy conifer forest: snags and cavities. Chapter 1 provided an overview of the concepts, and Chapters 2–4 delved into specific methodologies. While the methodology chapters of this dissertation centered analysis on the individual tree-level, each served as a proof of concept for implementation in broader scale applications.

Chapter 2 evaluated the accuracy of smartphone lidar to measure tree cavity dimensions from afar to differentiate among woodpecker species. Even in the time since publication of the chapter, advances in handheld lidar technology have improved greatly, making this approach even more feasible and widely accessible. While this method requires time-intensive field surveys and manual inspection of snags, it may enable more robust mapping for wildlife than currently exists, especially for cavity nest web species. While most cavities found will not be from the current year, being able to assess the number and distributions of cavity entrance sizes present on a landscape will allow for rough mapping of both woodpecker species occurrence (and co-occurrence) and obligate secondary cavity user species occurrence based on body size.

Chapters 3 and 4 investigated whether airborne lidar could be used to improve snag characterization. Both were valuable in confirming the baseline assumptions needed for further efforts: Chapter 3 confirmed that snags do in fact have greater gap fractions surrounding them than live trees do and that fraction is more variable across heights; Chapter 4 confirmed that individual snag features can be distinguished via ALS. How these differences in individual tree-scale analysis translate to landscape-scale analysis is yet unknown. The next step I propose is to establish a stepwise snag mapping workflow, based on processing airborne lidar datasets at the landscape scale, to generate topographic, structural, height, and possibly intensity metrics for use in predicting probable locations and characteristics of snags across a forested system (for a conceptual diagram, please see Appendix B Figure B2).

The aim of this theoretical snag mapping workflow is for it to be carried out with just an airborne lidar dataset, accompanied by lidar validation via ground reference surveys for calibrating the data and training snag models. I intend to build this workflow fully within the R environment, as R is open-source and widely accessible, and there already exist many robust and well-documented lidar processing packages, such as lidR and rLiDAR.

With the assumption that I am beginning with an unprocessed airborne lidar (also airborne laser scanning or ALS) dataset, the first step would be to pre-process the point cloud with snag mapping in mind. This would mean that noise filtration should be done carefully and conservatively so as not to remove snag returns alongside other sources of noise. For example, intact western white pines (*Pinus monticola*) were emergent in some plots, standing 10 m taller than the live tree crowns; however, these boles may register as only a handful of scattered ALS returns, likely above maximum canopy height (J. Stitt, personal observation), and thus these snags may be omitted during routine noise filtering processes.

Once I have a conservatively-filtered point cloud, the next steps would be to generate multiple products to accomplish separate tasks: 1) a digital elevation model based on the ground returns for use in calculating topographic metrics of interest, such as slope, aspect, and elevation; 2) a height-normalized canopy height model (CHM) for use in mapping both probable live tree crowns (via Individual Tree Detection or ITD methods) and canopy gaps; 3) the height-normalized point cloud itself for use in calculating "grid" metrics, which are lidar-derived metrics calculated a given grid scale (e.g., 5 m × 5 m squares) across an entire area, including structural, height, and intensity (if calibrated) metrics relevant to snag characterization.

With the data processed and metrics derived across the landscape scale, I believe the key component for snag mapping will be to evaluate both the spaces where trees are present and where they are absent. For the purpose of this methodology, there are three forest canopy categories that a given space (e.g., a square in a 5 m × 5 m grid) can be characterized as: live tree crown, snag, or true gap (defined here as canopy gaps that extend all the way to the ground level, or 2 m). Disentangling snags from live tree crowns is a distinct task from disentangling snags from true gaps.

For differentiating snags and live trees, my method leans into the challenges of mapping snags via ITD, namely that snags often are not detected as individual trees through traditional methods. I will add the caveat that there are myriad ITD methods currently available, including some that use the ALS point cloud directly versus others using the derived CHM; further delving into altering the parameters of any given ITD method to best include or exclude snags is certainly an undertaking worthy of further evaluation, but each instance will be highly sensitive to forest composition and ALS quality. One possible extension of the use of ITD is to then omit spaces characterized as live tree crown from further analysis; this would serve to greatly reduce the overall amount of data to be processed and theoretically leave only snag and true gaps spaces left to differentiate.

Fully differentiating snags from true gaps is challenging since one useful element of mapping snags via ALS can be a lack of returns, which can be conflated with true gaps. In this dissertation, Chapter 3 discussed the use of ALS to characterize canopy gaps around snags relative to live trees. There were significantly more canopy gaps around snags relative to live trees, especially at midcanopy heights (~20 m above-ground). This information would prove useful in the snag mapping workflow to assess snag presence or absence across a forest stand. Incorporating canopy gap analysis to detect snags may be of added benefit when airborne lidar datasets are of lower density; attempting to discern between true gaps and snags may be a pathway of less resistance than attempting to discern between snags and live trees, though likely incorporating both pathways may improve accuracy most.

In scaling up from the individual-tree scale to the landscape scale of my snag mapping workflow, identifying canopy gap size and shape may help focus efforts to identify probable snag locations. For example, determining whether snag locations are strongly correlated with canopy gap size may be of interest, and delving further into spatial analysis to evaluate snag location relative to canopy gap edge versus interior would also shed light on both snag and gap dynamics. Another direction to go in teasing apart live tree canopy, snag, and true gap spaces would be to employ random forest modeling. This first will require that I determine the best predictor variables from the lidar (training and testing models using data on known snag, gap and live tree locations), but bringing together ITD and canopy gap mapping with additional ALS-derived metrics may also prove powerful in mapping snags.

Attempting snag classification after identifying probable snag locations in my stepwise snag mapping workflow may help highlight snags with more abundant microhabitat features valuable to wildlife. Chapter 4 explored whether ALS could discern differences in structural characteristics among snags that are important for wildlife. Random forest techniques were only marginally successful in this, but this effort represents a first step (and only known attempt to date) to delineate among snag types. Working with higher density lidar data or including an even larger sample size of snag point clouds will no doubt improve model outcomes, as would focusing on just one snag type (e.g., large diameter broken top snags).

The conclusions of Chapter 3 and 4 both suggest that airborne lidar data should not be used in isolation, but rather implemented alongside other remote sensing datasets. Incorporating data from additional sensors such as satellite imagery, photogrammetry, and hyperspectral lidar would strengthen analyses by picking up on different components of the forest canopy to further refine snag mapping efforts. Moving beyond ALS in my snag mapping workflow will be beneficial for both snag location and classification. Pulling in spectral data to evaluate probable snag locations will help strengthen random forest modeling efforts. Bringing in temporal components such as repeated satellite imagery to see when and where snag occurrence changes over time is also becoming more attainable as imagery resolution improves. The scale of the grid applied is also fluid, and multiple scales can be applied at different steps in the process. For example, to incorporate spaceborne lidar data in modeling efforts (i.e., NASA GEDI waveform lidar) it may be useful to evaluate ALS metrics at a comparable scale, such as using a 30 m × 30 m grid instead of 5 m × 5 m grid.

Should this theoretical workflow be accurate enough to predict snag, gap, and live tree canopy with high probabilities across a landscape, such a map would be greatly beneficial for wildlife modeling efforts, including occupancy modeling and habitat mapping for single species or at the community level. If focusing on just cavity nest web wildlife (which includes woodpeckers that excavate cavities in snags, plus the birds and mammals that further depend on those cavities for nesting and roosting), being able to evaluate spatial patterns in tree crown, snag, and gap locations could expose maps of connectivity and pathways previously obscured. Having a gap map can highlight where travel corridors for

birds and bats may exist within the canopy. Knowing probable snag densities and distributions would not only provide a foundation for where cavity nest webs can occur across the landscape, it may also help delineate territories of given species and highlight where greater numbers of microhabitats can be found to support additional species.

While a fully remote methodology is enticing, it can only go so far. Having ground survey data for any given site is always important and can provide additional information not attainable from the sky. Thankfully, finer-scale remote sensing technologies are also continuing to advance, with UAV, terrestrial, and handheld lidar tools available and being tested for wildlife implications as well. Building a greater database of ground-derived characteristics of a forest adds additional avenues to refine wildlife monitoring and management efforts, in particular to help in identifying useful indicator variables.

My hope in explaining these methods and their possible implementations is to bring increased awareness to novel uses of existing datasets, enabling users to glean additional information and apply that knowledge to improve our understanding of forested systems and processes. The importance of biodiversity and ecosystem functioning are continuing to be realized in a growing number of fields, and I hope that my contributions outlined in this dissertation will aid others in better evaluating indicators of biodiversity, in order to best serve wildlife modeling, monitoring, and management efforts.

Appendix A - Supplemental Tables

Table A1 Minimum cavity entrance size requirements for both cavity excavators and secondary cavity nesters that may coexist in western North America

Minimum cavity entrance size requirements for both cavity excavators and secondary cavity nesters that may coexist in western North America, based on the smallest entrance area observed being used by each cavity nesting species (data from Dudley and Saab, 2003; Martin et al., 2004). Included in this appendix are references for species of conservation concern, which correspond with the footnotes.

Cavity nesting species	Scientific name	Minimum cavity entrance area used (cm^2)
Cavity excavators		
Downy woodpecker	*Dryobates pubescens*	6.5
Black-backed woodpecker[c,d,e]	*Picoides arcticus*	15.2
Hairy woodpecker	*Dryobates villosus*	17.0
White-headed woodpecker[a,b,d,e]	*Picoides albolarvatus*	18.8
Northern flicker	*Colaptes auratus*	26.2
Lewis' woodpecker[a,b,c,d,e]	*Melanerpes lewis*	28.3
Pileated woodpecker[c,d,e]	*Dryocopus pileatus*	69.1
Secondary cavity nesters		
Northern flying squirrel	*Glaucomys sabrinus*	0.0
Red squirrel	*Tamiasciurus hudsonicus*	4.9
Mountain chickadee	*Poecile gambeli*	5.6
Bushy-tailed woodrat	*Neotoma cinerea*	6.2
Tree swallow	*Tachycineta bicolor*	8.2
Mountain bluebird	*Sialia currucoides*	14.8
Flammulated owl[a,c,d,e]	*Psiloscops flammeolus*	16.9
European starling	*Sturnus vulgaris*	20.2
American kestrel	*Falco sparverius*	20.6
Northern saw-whet owl[a]	*Aegolius acadicus*	25.0
Bufflehead	*Bucephala albeola*	26.0
Deer mouse	*Peromyscus maniculatus*	29.2
Barrow's goldeneye[a]	*Bucephala islandica*	33.0
Chipmunk	*Tamias spp.*	41.1

[a] Species at Risk, British Columbia; COSEWIC 2017
[b] Species of Greatest Conservation Need, Idaho; IDFG 2016
[c] Species of Concern, Montana; MFWP 2017
[d] Species of Greatest Conservation Need, Oregon; ODFW 2016
[e] Species of Concern, Washington; WDFW 2013

a. Committee on the Status of Endangered Wildlife in Canada (COSEWIC). (2017). COSEWIC, Ottawa, Canada. https://www.canada.ca/en/environment-climate-change/services/committee-status-endangered-wildlife.html

b. Idaho Department of Fish and Game (IDFG). (2016). Idaho species of greatest conservation need. Idaho Department of Fish and Game, Boise, Idaho. https://idfg.idaho.gov/species/taxa/list/sgcn

c. Montana Fish, Wildlife, and Parks (MFWP). (2017). Montana's species of concern. Montana Fish, Wildlife, and Parks, Helena, MT. http://fwp.mt.gov/fishAndWildlife/species/speciesOfConcern

d. Oregon Department of Fish and Wildlife (ODFW). (2016). Oregon Conservation Strategy. Oregon Department of Fish and Wildlife, Salem, Oregon. http://www.oregonconservationstrategy.org

e. Washington Department of Fish and Wildlife (WDFW). (2013). Threatened and endangered wildlife in Washington: 2012 Annual Report. Listing and recovery section, wildlife program. Washington Department of Fish and Wildlife, Olympia, Washington.

Table A2 Pearson's correlations among predictor variables

A correlation table showing all pairwise Pearson's (r) correlation scores across the 13 predictor variables used for modeling snag classifications. A list of the predictor variable descriptions can be found in Table 4.2. Scores with an absolute value of $r \geq 0.9$ were considered "strongly correlated" and are highlighted in grey. Positive scores suggest a relationship where a pair changes value in the same direction, while negative scores indicate a relationship where a pair changes value in opposite directions.

	PTDEN	**P1stRN**	**P2ndRN**	**P3rdRN**	**GFPmid**	**LADcv**	**RUMPLE**	**ENTmid**	**VAI**	**VCI**	**ELEV**	**TRASP**	**SLOPE**
PTDEN		-0.34	0.34	0.24	-0.14	0.04	-0.01	0.25	0.40	0.45	-0.33	0.02	-0.03
P1stRN	-0.34		-0.97	-0.83	0.02	-0.16	-0.10	-0.45	-0.30	-0.66	0.13	0.17	0.07
P2ndRN	0.34	-0.97		0.68	-0.05	0.15	0.11	0.39	0.32	0.62	-0.21	-0.13	-0.09
P3rdRN	0.24	-0.83	0.68		0.05	0.15	0.05	0.48	0.17	0.56	0.07	-0.22	0.02
GFPmid	-0.14	0.02	-0.05	0.05		-0.32	0.33	0.35	-0.47	-0.01	0.11	-0.12	-0.02
LADcv	0.04	-0.16	0.15	0.15	-0.32		-0.42	0.07	0.20	0.21	0.07	0.00	0.06
RUMPLE	-0.01	-0.10	0.11	0.05	0.33	-0.42		0.15	-0.30	0.28	-0.03	-0.05	-0.04
ENTmid	0.25	-0.45	0.39	0.48	0.35	0.07	0.15		-0.02	0.54	0.04	-0.26	0.00
VAI	0.40	-0.30	0.32	0.17	-0.47	0.20	-0.30	-0.02		0.30	-0.12	0.04	-0.14
VCI	0.45	-0.66	0.62	0.56	-0.01	0.21	0.28	0.54	0.30		-0.13	-0.18	-0.07
ELEV	-0.33	0.13	-0.21	0.07	0.11	0.07	-0.03	0.04	-0.12	-0.13		-0.13	0.18
TRASP	0.02	0.17	-0.13	-0.22	-0.12	0.00	-0.05	-0.26	0.04	-0.18	-0.13		-0.44
SLOPE	-0.03	0.07	-0.09	0.02	-0.02	0.06	-0.04	0.00	-0.14	-0.07	0.18	-0.44	

Table A3 Airborne-lidar-derived metrics used as predictor variables in random forest (RF) models.

Explanations of each of the lidar-derived predictor variables selected for analysis within the RF models are provided. All of these predictors were included in model selection to predict one of four snag classes, modeled across two field-derived characteristics: diameter (small [<40 cm DBH] vs. large [≥40 cm DBH]) and intactness of the bole (intact vs. broken). Airborne lidar metrics were derived from point clouds of 2.5 m circular radius (~20 m^2) clipped around known snag locations determined from the field. Each variable is listed with its abbreviation, description of the calculation, and the ecological significance for this model.

Variable	Equation	Ecological significance
PTDEN	*All returns (> 1.37 m)] / total area (19.63 m^2)*	Relative number of all returns (greater than 1.37 m above ground level, a.g.l.) can reflect the total amount of surface area present to interact with in the canopy, in the form of the snag bole and branches
P1stRN	*(First returns / all returns) * 100*	Higher percentages of first returns (returns that reflect directly back to sensor) suggest a greater proportion of "external" hits, where lidar has not penetrated the canopy; this may indicate more intact crown features remain
P2ndRN	*(Second returns / all returns) * 100*	Higher percentages of second returns (returns that bounce once before returning to sensor) suggests a more "porous" snag crown that allows for more pulses to penetrate the canopy
P3rdRN	*(Third returns / all returns) * 100*	Higher percentages of third returns (returns that bounce twice before returning to sensor) suggests a greater amount of openness mixed with structures within the canopy that allows for pulses to bounce more than once within and still return to the sensor; indicates greater physical complexity
GFPmid	*Gap Fraction (GF) = N_z / ($N_{total} - N_{z+dz}$); N = number of returns, total = across all heights (z), dz = height bin width (1 m); Gap Fraction Profile (GFP) = mean GF across heights; mid = only 5m – 20m a.g.l.*	Gap fraction is calculated as a ratio of the number of points within a given layer versus those that passed through the layer; the relative proportion of canopy gaps within the midcanopy (5–20 m a.g.l.) helps to quantify the total amount of open space present in the lidar footprint at heights where snag crowns will vary, while reducing input from the "gaps" above treetops (Bouvier et al., 2015)
LADcv	*Leaf Area Density (LAD) = -ln(GF) / (k * dz); k = extinction coefficient (0.5), dz = height bin width (2 m); $LAD_{cv} = LAD_{\mu} / LAD_{sd}$*	This serves as an indicator of vertical stratification and subdominant structure presence by measuring the homogeneity of vertical strata across all height bins; lower values indicate a more even distribution of vegetation across strata (Bouvier et al., 2015)
RUMPLE	*Surface area of returns (as a convex hull) / projected area of returns on ground*	Higher scores on this index indicate a rougher canopy surface (in terms of heights varying more from one pixel to the next), suggesting greater structural complexity (Bouvier et al., 2015)

ENTmid	*Shannon entropy index (H') =* $-\sum p_z * log(p_z)$*;* p_z *= proportion of heights (z), mid = only 5m – 20m a.g.l.*	The evenness of midcanopy heights (5–20 m a.g.l.) may indicate how closed the canopy is; more evenness may suggest an intact dominant canopy, while less evenness may suggest disturbances, such as gaps, subdominant structures such as snags or saplings, or other deviations (Pretzsch, 2009)
VAI	*Vegetation Area Index (VAI) =* $\sum LAD$	By summing LAD values, this index reports total vegetation coverage in the vertical column; since footprint area is held constant here, this index can be used as a relative measure, where higher scores suggest more canopy, possibly in the form of snag branches and dead needles, or else as encroaching live vegetation (surrounding mature tree crown or sapling; LaRue et al., 2020)
VCI	*Vertical Complexity Index (VCI) =* $(-\sum(p_z * ln(p_z))) / ln(HB)$*;* p_z *= proportion of heights (z), HB = total number of height bins (dz = 1)*	Similar to ENTmid (but including *all* heights), this index measures evenness in terms of proportion of returns by height in the canopy and allows a set maximum height, which can standardize variable snag tops; high scores suggest more even distributions of returns and a higher maximum canopy height, which may mean an intact top (van Ewijk et al., 2011)
ELEV	–	Relative elevation will play a role in forest species composition; as our site was in the Northern Rockies, this can affect tree growth and/or decomposition patterns, as well as affect exposure to higher or lower temperature extremes
SLOPE	–	Relative flatness or steepness under a snag may subject it to different disturbance risk levels and types (e.g., steeper slope may have higher winds, leading to more bole break potential)
TRASP	–	Relative sun angle interacting with a snag may subject it to different temperature and moisture levels at a microhabitat scale, leading to differing rates of decomposition

Appendix B - Supplemental Figures

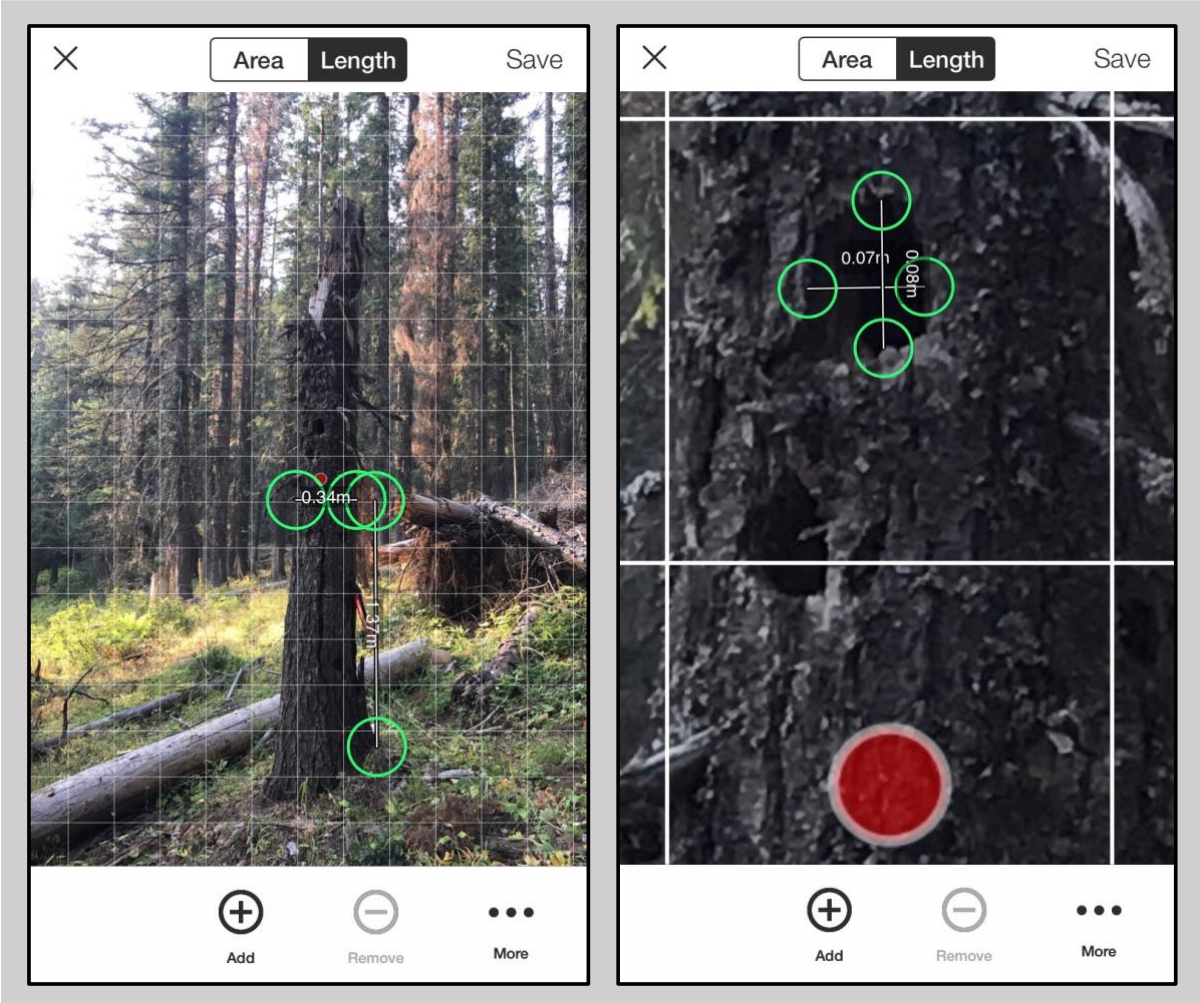

Figure B1 Visualizations of handheld photo measurements

Screenshots (from the smartphone app) of photo measurements taken with the Spike handheld LIDAR device in the field to measure tree diameter and cavity dimensions, as detailed in Chapter 2.

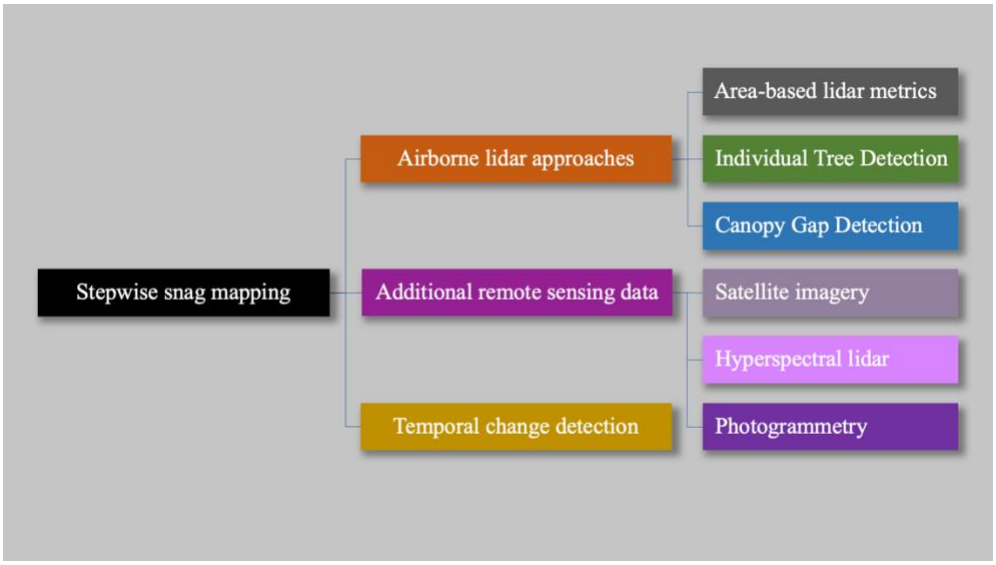

Figure B2 Conceptual workflow diagram for stepwise snag mapping method

An overview of the proposed datasets and analysis methods to include for a stepwise method of mapping snags in closed-canopy conifer forests using Random Forest, as proposed in Chapter 5. A more detailed explanation of the "Airborne lidar approaches" can be found in the diagrams below.

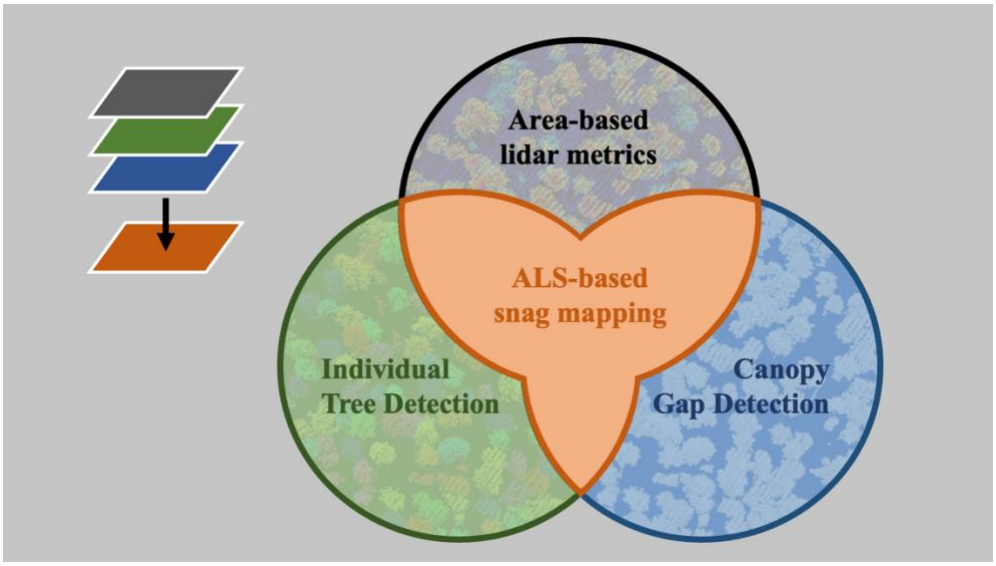

Figure B2 *(continued)* Venn diagram for the "Airborne lidar approaches" to snag mapping

A Venn diagram showing how three separate ALS-based methods for quantifying forest elements can be combined to improve snag mapping. This figure is color-coded based on the above workflow diagram. Explanations for each of the three methods are described in greater detail in the diagram below, based on the proposal in Chapter 5. For each step, a gridded approach to lidar processing has been taken to calculate relevant predictor variables for Random Forest models, shown below for the same 30 m x 30 m grid cell.

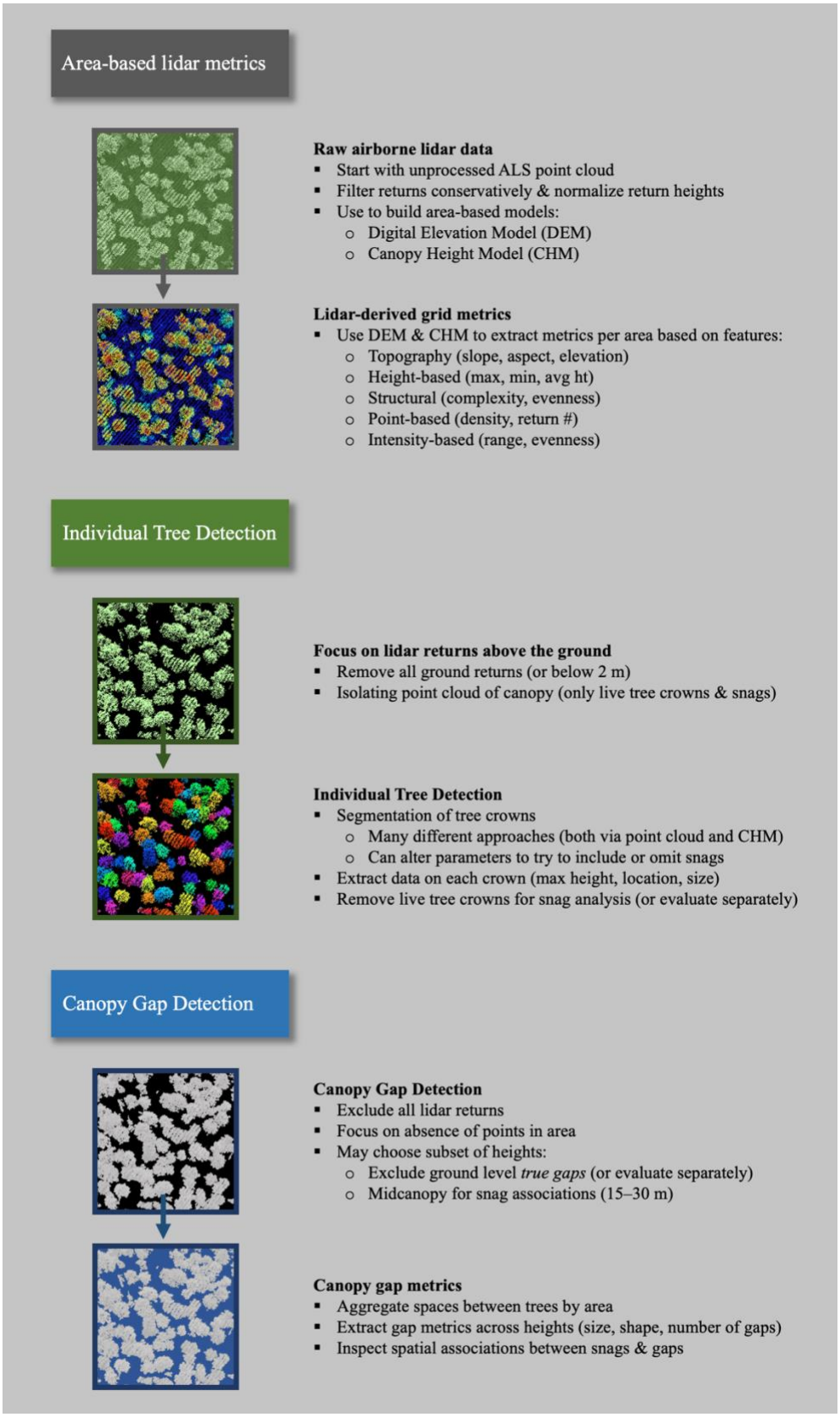

Figure B2 *(continued)* Detailed explanations of the three airborne lidar approaches to snag mapping